

STUDIES IN TIME-RESOLVED OPTOACOUSTIC SPECTROSCOPY

By

EDWARD G. VOIGTMAN JR.

A DISSERTATION PRESENTED TO THE GRADUATE COUNCIL OF THE  
UNIVERSITY OF FLORIDA  
IN PARTIAL FULFILLMENT OF THE REQUIREMENTS FOR THE  
DEGREE OF DOCTOR OF PHILOSOPHY

UNIVERSITY OF FLORIDA

1979

## ACKNOWLEDGMENTS

I would like to acknowledge Dr. Martin Vala for his help and encouragement throughout these exasperating experiments. His constant optimism and enthusiasm were of incalculable value in seeing the experiments through.

I would like to thank my wife Janiece Leach, whose love and understanding were my only joy. Without her faith in me and her personal sacrifices, nothing would have been accomplished.

I would also like to thank my fellow graduate students, Joe Baiardo (who helped with the FFT subroutine translation), Bob Brittain, Rodger Capps, and Dave Powell (who goaded me into lengthening the dye laser cavity to effect tuning). Their fellowship was crucial to maintaining my sanity in the face of unrelenting artifact production by the TROAS apparatus. I would also like to thank Ed Whitehead for his excellent machining and Rudy Strohschein for his expert glassblowing. In addition, I would like to thank the staff of the departmental electronics shop (Joe Miller, Russ Pierce, and Bill Wells) and Dr. J. D. Winefordner, Jr., for the loan of various necessary pieces of equipment and laser dye. I also would like to thank Dr. J. Eyler for the loan of Laser Dye 473.

The words of Mercury are harsh after the songs of Apollo.

Love's Labor Lost

# TABLE OF CONTENTS

CHAPTER		PAGE
	ACKNOWLEDGMENTS . . . . .	ii
	PREFACE . . . . .	iii
	LIST OF TABLES. . . . .	vi
	LIST OF FIGURES . . . . .	vii
	ABSTRACT. . . . .	ix
ONE	INTRODUCTION. . . . .	1
TWO	THEORETICAL CONSIDERATIONS. . . . .	19
	Introduction and Direction. . . . .	19
	The Extended Solution of the Heat-Flow Model. . . . .	20
	Excitation Source Selection . . . . .	26
	Sample Cell Construction. . . . .	27
	Sample Selection. . . . .	32
	Pressure Transducer Selection . . . . .	33
	Pressure Transducer Electronics . . . . .	38
THREE	THE EXPERIMENTAL APPARATUS. . . . .	41
	The Dye Laser System. . . . .	41
	Sample Cells and the Vacuum System. . . . .	47
	Pressure Transducers and their Associated Electronics . . . . .	56
	Pressure Transducer Electronics . . . . .	61
	Microcomputer Interface Electronics . . . . .	64
	The Microcomputer System. . . . .	67
FOUR	SAMPLE SELECTION. . . . .	69
FIVE	EXPERIMENTAL ARRANGEMENTS . . . . .	77
SIX	RESULTS . . . . .	108
SEVEN	SINGLET TIME-RESOLVED OPTOACOUSTIC SPECTROSCOPY . . . .	122

## APPENDICES

ONE	RELEVANT OAS RESULTS. . . . .	126
TWO	TROAS NOISE EQUIVALENT POWER. . . . .	132
THREE	CAPACITANCE MICROPHONE PREAMPLIFIER NOISE MODEL . . .	134
FOUR	MICROCOMPUTER PROGRAM AND I/O LOCATIONS . . . . .	141
	REFERENCES. . . . .	150
	BIOGRAPHICAL SKETCH . . . . .	156

# LIST OF TABLES

TABLE		PAGE
1	A comparison of light sources considered for use in TROAS experiments . . . . .	28
2	Pressure transducers which may be used in TROAS experiments. . . . .	35
3	Capacitance microphones considered for use in TROAS experiments. . . . .	36
4	Performance characteristics of the Candela dye laser system . . . . .	46
5	Sample cells. . . . .	48
6	Capacitance microphone comparison . . . . .	60
7	Relevant triplet properties of the compounds studied by triplet TROAS . . . . .	72
8	A summary of the TROAS experiments performed. . . . .	78
9	Peripheral systems memory locations . . . . .	148

# LIST OF FIGURES

FIGURE		PAGE
1	Electronic states and rate constants typically of importance in the photophysics of polyatomic molecules . . . . .	7
2	The idealized TROAS spectrum resulting from direct triplet excitation. . . . .	12
3	Schematic representation of a typical TROAS apparatus . . . . .	14
4	Schematic representation of a versatile OAS apparatus with dye laser excitation . . . . .	17
5	Optocoupled trigger circuit for the Candela dye laser . . . . .	44
6	TROAS sample cell number 2 . . . . .	51
7	TROAS sample cell number 3 . . . . .	53
8	TROAS sample cell number 4 . . . . .	55
9	TROAS sample cell number 7 . . . . .	58
10	Pressure transducer impedance conversion circuit . . .	63
11	Schematic representation of the microcomputer interface system and electronic subsystems used in the TROAS experiments . . . . .	66
12	Structures of the sample substances used in the TROAS experiments . . . . .	74
13	The TROAS spectrum of dithione obtained with a Phase-R DL-1200 dye laser, Rhodamine 6G dye lasing broadband, and a capacitance electret microphone . . . .	82
14	The TROAS spectrum of dithione obtained with a Xe flashlamp (unfiltered) and a capacitance electret microphone . . . . .	85

15	The TROAS spectra of naphthaline in helium (upper trace) and in air (lower trace) . . . . .	90
16	The TROAS spectrum of iodine at 25. C in air at atmospheric pressure. . . . .	94
17	The TROAS spectrum of 9-bromoanthracene in air at atmospheric pressure with the piezoelectric transducer used to detect the signal. . . . .	96
18	An artifact TROAS spectrum obtained with air at 25. C and atmospheric pressure in the sample cell . . . .	99
19	The output of a piezoelectric transducer directly exposed to a laser light pulse of high intensity. .	102
20	The TROAS spectrum obtained with an empty ( $10^{-4}$ torr) cell. . . . .	110
21	A voltage preamplifier and externally polarized capacitance microphone circuit. . . . .	136
22	The voltage preamplifier and externally polarized capacitance microphone circuit of Figure 21 with appropriate noise sources added . . . . .	138



Abstract of Dissertation Presented to the Graduate Council  
of the University of Florida in Partial Fulfillment of the  
Requirements for the Degree of Doctor of Philosophy

STUDIES IN TIME-RESOLVED OPTOACOUSTIC SPECTROSCOPY

By

Edward G. Voigtman Jr.

March 1979

Chairman: Martin T. Vala  
Major Department: Chemistry

The approach of time-resolved optoacoustic spectroscopy is applied to the study of the radiationless decay processes of electronically excited polyatomic molecules in the gas phase. The loss-free theory of time-resolved optoacoustic spectroscopy (TROAS) is extended by the addition of the two major model-independent energy loss mechanisms (viscosity and thermal conductivity) so that acoustic mode amplitudes, mode amplitude ratios, and noise equivalent power may be calculated for TROAS experiments.

Restrictions on design of experimental apparatus imposed by the theory of TROAS are considered, and the necessary properties of experimental apparatus sufficient to yield TROAS spectra are deduced. Limitations on sample selection are also considered and lead to the decision to study the following compounds: biacetyl, naphthalene, 2-chloronaphthalene, anthracene, 1-chloroanthracene, 9-bromoanthracene, iodine, nitrogen dioxide, and 2,2,4,4-tetramethyl-1,3-cyclobutanedithione (dithione).

A microcomputer-based apparatus was designed and constructed in concordance with the theoretical constraints imposed by the theory of TROAS and numerous experiments were performed. The predicted pressure

rise was partially observed as were the predicted radial and longitudinal acoustic modes, but no triplet yield information could be obtained by direct triplet excitation of the sample compounds due to the existence of irremovable, mimicking artifacts produced by the sample cell upon exposure to the highly intense (5 megawatts maximum) dye laser excitation source pulses. Additional experiments determined the nature of the four types of artifacts concomitant with direct triplet excitation TROAS. The possibility of obtaining triplet yield information by singlet excitation TROAS is examined and found to afford excellent prospects for polyatomic molecules in the gas phase, without interference from the mimicking artifacts of triplet TROAS.

## CHAPTER ONE INTRODUCTION

The optoacoustic effect was discovered in 1880 by Bell [1] when he observed that a great variety of substances emitted audible sounds when exposed to periodically fluctuating illumination in their absorption regions. Bell's spectrophone was based on the observation that the sound intensity was proportional to the sample's absorptivity. He hoped it would find some use in absorption measurements, particularly in the infrared region. Though a number of Bell's contemporaries studied the effect [2-5], interest waned until 1938 when Veingerov [6] rediscovered the effect and employed it in the study of IR absorption by gases. Despite a few scattered uses [7-10] for such applications as IR gas analysis, IR detection instrumentation, and microwave detection, it was largely neglected until 1946 when Gorelik [11] noted that the spectrophone could be used to measure the vibrational relaxation times of gases. Again the technique lay dormant until Kaiser [12] and Delaney [13] in 1959 proposed a reaction kinetics-based model for the optoacoustic effect. Also in 1959, Gerlovin [14] applied the spectrophone technique in the visible and UV.

It will be useful for our later discussion to note the more important contributions to the development of the optoacoustic technique over the last two decades. In 1963, White [15] observed that elastic waves are produced in solids following absorption of pulsed light. Several other investigators have made similar observations [16-17].

In 1967, Hey [18], using broadband illumination and the spectrophone technique, measured the relaxation rates of dyes in solution. In 1969, Seybold et al. [19], using steady state illumination and a capillary rise technique, made similar studies. Also in 1969, Callis et al. [20], using broadband pulsed illumination and capacitance microphone volume change detection, were able to determine triplet yields of anthracene in ethanol. In 1971, Kreuzer [21] greatly improved the spectrophone technique, as it applies to gas phase absorbance measurements, by employing a laser as the illumination source. Since then, the technique has found wide use in such applications as air pollutant detection [22-24], in situ aerosol absorbance measurements [25], and the study of photochemical reaction mechanisms in the gas phase [26-27]. In 1977, Patel and Kerl [28] achieved absorptivities of  $10^{-9}$  to  $10^{-10}$   $\text{cm}^{-1}$  for the gas NO. Significantly increased sensitivities may also be achieved by placing the spectrophone inside a laser cavity [29].

Since 1973, the gas phase optoacoustic effect has also been used in the study of  $\text{NO}_2$  and  $\text{SO}_2$  [30], the quenching of iodine atoms by oxygen [31], and in investigations of radiationless transitions in biacetyl [32] and the azabenzenes [33]. The quenching of the first vibrational level of the lowest excited oxygen singlet has been studied by Parker and Ritke [34-35]. Hunter and coworkers [36-37] have also used the spectrophone technique in the study of electronically excited benzene and biacetyl. These studies were significant for several reasons. First, important information was obtained which would have been difficult, if not impossible, to obtain by other techniques. Secondly, a variety of auxiliary techniques were developed and led to an

increase in the usefulness of the basic spectrophone. Among these were lock-in amplifier signal detection, carrier-modulated pressure detectors, and dual excitation source techniques [38].

The source of the heat in a simple (IR source) spectrophone experiment is collisionally-induced vibrational to translational relaxation [39]. For condensed phases the mechanism is substantially more complex. In 1973, Parker [40] observed that the glass windows on his optoacoustic sample cell generated an in-phase signal when illuminated even though the gas in the cell (Ne, N<sub>2</sub>, O<sub>2</sub>) was transparent to the excitation wavelengths used. With the aid of a thermal diffusion model of the window and adjacent gas, he established that the signal he had observed was produced by thermal diffusion from the window into an adjacent boundary gas layer. At about this time, Rosencwaig and others, using capacitance microphone detection, extended the spectrophone technique to include solids, liquids, smears, gels, and biological materials [41-43]. In 1976, Rosencwaig and Gersho [44] developed the "thermal piston" model to explain the optoacoustic effect exhibited by condensed phase materials. These authors suggested that diffusion of heat into the surrounding gas (to a depth of the thermal diffusion length) causes the boundary layer to fluctuate and thereby drive the remainder of the gas. Hence, chopped source illumination could be expected to produce fluctuations at the same frequency in the boundary layer. Comparison of their theory with experimental results suggested that this was the primary source of sounds produced by condensed phases. In 1978, McDonald and Wetsel [45] extended the theory (the composite piston model) by including the effect of the expansion and contraction of the condensed phase. They proposed that the boundary layer was mechanically

driven, thereby generating sound. As noted previously, however, elastic waves may also be produced in condensed phases by the absorption of intensity-modulated light. These elastic waves may be detected directly [46] using piezoelectric transducers. Thus, three mechanisms have been proposed to account for the production of sounds by condensed phases in "the" optoacoustic effect: the thermal piston model, the mechanical piston model, and light-generated elastic waves.

With a few notable exceptions (*vide infra*), recent work on the optoacoustic effect applied to chemical systems has dealt with the spectral distribution of the released heat and not with the kinetics of the release process. Work in this laboratory was begun a number of years ago to develop a theory of time-resolved optoacoustic spectroscopy which was capable of describing the kinetics of radiationless decay processes (heat release) after electronic excitation in polyatomic molecules. The theory was developed by Wrobel [47]. It was motivated by the need for detailed information concerning nonradiative deactivation pathways in electronically excited polyatomic molecules under approximately collision-free conditions. In general, phosphorimetry and fluorimetry are incapable of providing all the data necessary to obtain accurate triplet yields, without which it is impossible to test the various theories of radiationless processes in polyatomic molecules. Time-resolved optoacoustic spectroscopy (TROAS) is intended to complement these other techniques, particularly for species with low radiative yields, and thereby lessen the need for the motley assortment of ingenious methods which have been devised to furnish triplet yields [48-56].

To understand the need for a complementary technique, it is helpful to consider the various pathways of deactivation available to an electronically excited molecule. Irradiation of a molecule results in its excitation from its ground state ( $S_0$ ) to a vibrational level of some excited singlet state,  $S_x$ . With few exceptions, rapid radiationless relaxation ensues populating the lowest vibrational level ( $v = 0$ ) of the lowest excited singlet,  $S_1^0$  (the superscript denotes vibrational level and the subscript electronic state). Three deactivation processes may now occur which depopulate  $S_1^0$  (see Figure 1): fluorescence with a rate  $k_f$ , radiationless decay with a rate  $k_S$ , and intersystem crossing to the triplet with a rate  $k_{ISC}$ . The triplet vibrational level so populated may relax directly to  $S_0$  via radiationless decay with a rate  $k_{T_1^v}$ , or it may relax via rapid radiationless decay to  $T_1^0$  with a rate  $k_{T_1^v, T_1^0}$ . Intersystem crossing back to  $S_1^0$  is negligible. Finally,  $T_1^0$  may relax by phosphorescence with a rate  $k_p$  or by radiationless decay with a rate  $k_T$ . Since decay directly from the vibrational manifold of  $T_1$  to  $S_0$  is not usually possible (Kasha's rule),  $k_{T_1^v}$  may be neglected. In addition, vibrational relaxation in  $T_1$  is usually fast relative to  $k_T$  and  $k_p$ .

The five remaining rate constants ( $k_f$ ,  $k_S$ ,  $k_{ISC}$ ,  $k_p$ ,  $k_T$ ) may be used to define the fluorescence quantum yield  $\phi_f$ , the phosphorescence quantum yield  $\phi_p$ , and the triplet yield  $\phi_t$  as follows:

$$\phi_f = k_f/k_f^* \quad \text{where } k_f^* = k_f + k_S + k_{ISC} \text{ is the observed}$$

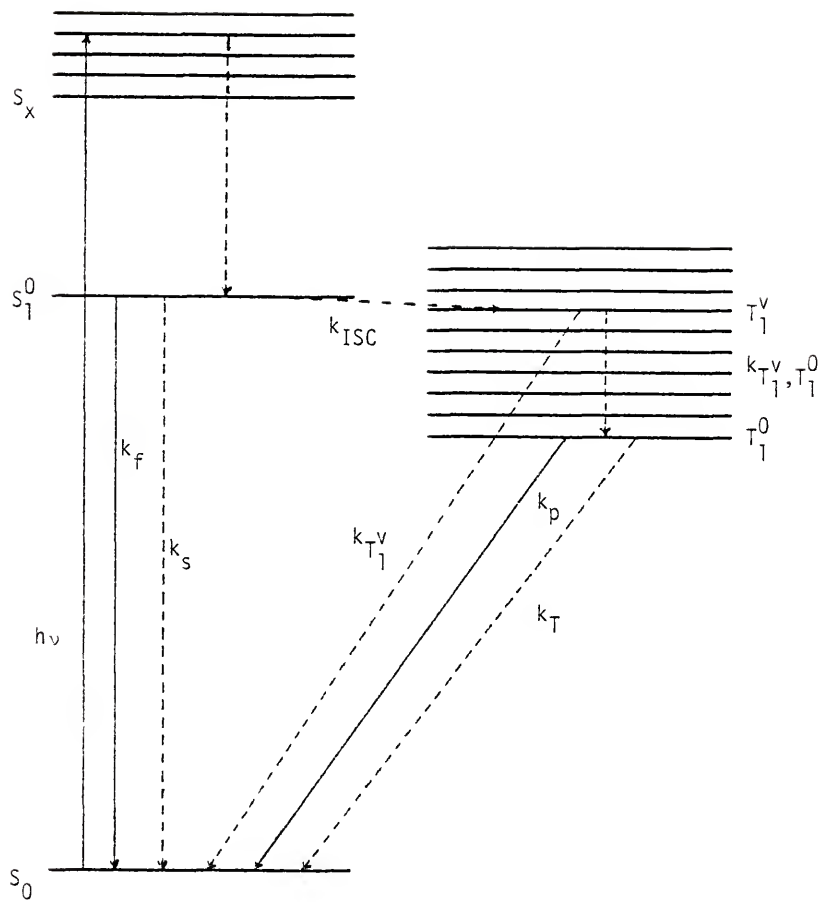
fluorescence rate,

$$\phi_p = k_p/k_p^* \quad \text{where } k_p^* = k_p + k_T \text{ is the observed phosphorescence}$$

rate, and

Figure 1. Electronic states and rate constants typically of importance in the photophysics of polyatomic molecules.





$$\phi_t = k_{ISC}/k_f^*.$$

Thus, fluorimetry and phosphorimetry experiments yield the four quantities  $\phi_f$ ,  $\phi_p$ ,  $(k_f^*)^{-1}$  the observed fluorescence lifetime, and  $(k_p^*)^{-1}$  the observed phosphorescence lifetime, but these are obviously insufficient to determine the five rate constants noted above.

Clearly, then, another independent experimental quantity is necessary. Although a number of techniques have been developed to meet this need [48-56], each such technique possesses certain disadvantages which prevent it from being a practical complementary technique to fluorimetry and phosphorimetry. In fact, it is common to simply assume  $k_S$  is negligible (Kasha's intersystem crossing rule [57]), although there is no unassailable basis for such an assumption. Consequently, it is desirable to find a general technique which is easily capable of providing the requisite independent quantity and which preferably does so by measurement of the radiationless rate constants. A clue as to the nature of this desired technique is provided by noting that radiationless processes are accompanied by the release of heat. Therefore, the general technique should ideally involve monitoring the heat released during radiationless decay processes subsequent to excitation of the sample. This is the basis of optoacoustic spectroscopy.

In 1974, Wrobel [47] developed the theory of gas phase optoacoustic spectroscopy which was specifically designed to accommodate tunable pulsed dye laser excitation of the electronic states of polyatomic molecules. In this theory, the pressure fluctuations produced in the sample vapor were determined from the conservation equations (mass, momentum, and energy), the equation of state, and the rate equations

associated with a selected multielectronic state model ( $S_0, T_1^V$  or  $S_0, T_1^V, S_1^{V'}$ ). The fundamental result of TROAS (valid for the simple  $S_0, T_1^V$  model) is the following relation between the pressure fluctuations expected to occur in the gas phase and the nonradiative rate constants:

$$P'_{0,0} = (\gamma - 1)q_{0,0}\bar{n}_{T_1^V}^0 [k_{T_1^0}k_{T_1^V, T_1^0}h\nu_{T_1^0} (1 - e^{-(k_p^*)t}) /$$

$$(k_{T_1^V} + k_{T_1^V, T_1^0} - k_p^*)(k_p^*)$$

$$+ (k_{T_1^V, T_1^0}h\nu_{T_1^V, T_1^0} / (k_{T_1^V, T_1^0} + k_{T_1^V}))$$

$$- k_{T_1^0}h\nu_{T_1^0} / (k_{T_1^V} + k_{T_1^V, T_1^0} - k_p^*)(1 - e^{-(k_{T_1^V, T_1^0} + k_{T_1^V})t})]$$

where  $\gamma$  is the heat capacity ratio,  $\bar{n}_{T_1^V}^0$  is the cell-averaged initial number density of molecules excited into  $T_1^V$ ,  $q_{0,0}$  is an expansion coefficient dependent on the model-specific heat source term, and  $P'_{0,0}$  is the amplitude of the pressure rise expected to occur.

Normally, the vibrational relaxation rate  $k_{T_1^V, T_1^0}$  is much larger than the triplet deactivation rate  $k_p^*$ . The above equation then simplifies to

$$P'_{0,0} = (\gamma - 1)q_{0,0}\bar{n}_{T_1^V}^0 [\phi_{T_1^V}^{IC}h\nu_{T_1^V, T_1^0} (1 - e^{-(k_{T_1^V, T_1^0} + k_{T_1^V})t})$$

$$+ \phi_{T_1^V}^{IC}\phi_{T_1^0}^{ISC}h\nu_{T_1^0} (1 - e^{-k_p^*t})]$$

where  $\phi_{T_1}^{ISC}$  is the intersystem crossing yield  $k_T/k_p^*$ , and  $\phi_{T_1}^{IC}$  is the internal conversion yield  $k_{T_1}^{v,T_1^0}/(k_{T_1}^{v,T_1^0} + k_{T_1}^{v,T_1^0})$ . Thus, the expected pressure rise is the sum of two exponentially rising components with different amplitudes. Note, however, that  $k_{T_1}^{v,T_1^0}$  is much larger than  $k_p^*$ . Hence, the pressure rise will appear to be a step rise with an exponential rise building upon it. This situation is depicted in Figure 2 [47]. If the amplitude of the slow rise is denoted  $p'_s$  and that of the fast rise is denoted  $p'_f$ , then from Figure 2 the following equation is obtained:

$$\phi_{T_1}^{ISC} = (h\nu_{T_1}^{v,T_1^0}/h\nu_{T_1}^{v,T_1^0}) p'_s/p'_f .$$

Since  $k_p^*$  is obtained experimentally from the time constant of the slow rise, the radiationless rate constant  $k_T$  may be obtained directly and independently of phosphorimetry and fluorimetry experiments. Unfortunately, Wrobel [47] was not able to experimentally determine the validity of this result, so additional experiments have proven necessary.

Figure 3 illustrates schematically the experimental setup of a TROAS apparatus. A light pulse from a flashlamp-pumped tunable dye laser passes through the cylindrical sample cell and strikes the laser energy detector. Absorbed energy converted to heat via radiationless decay processes heats the sample gas mixture (molecular vapor plus carrier gas) producing a pressure jump and acoustic oscillations. These pressure variations are converted to electrical signals by a sensitive broadband pressure transducer. The electrical signals are amplified and acquired by a microcomputer-controlled transient waveform recorder. The microcomputer also synchronizes data acquisition by controlling

Figure 2. The idealized TROAS spectrum resulting from direct triplet excitation.

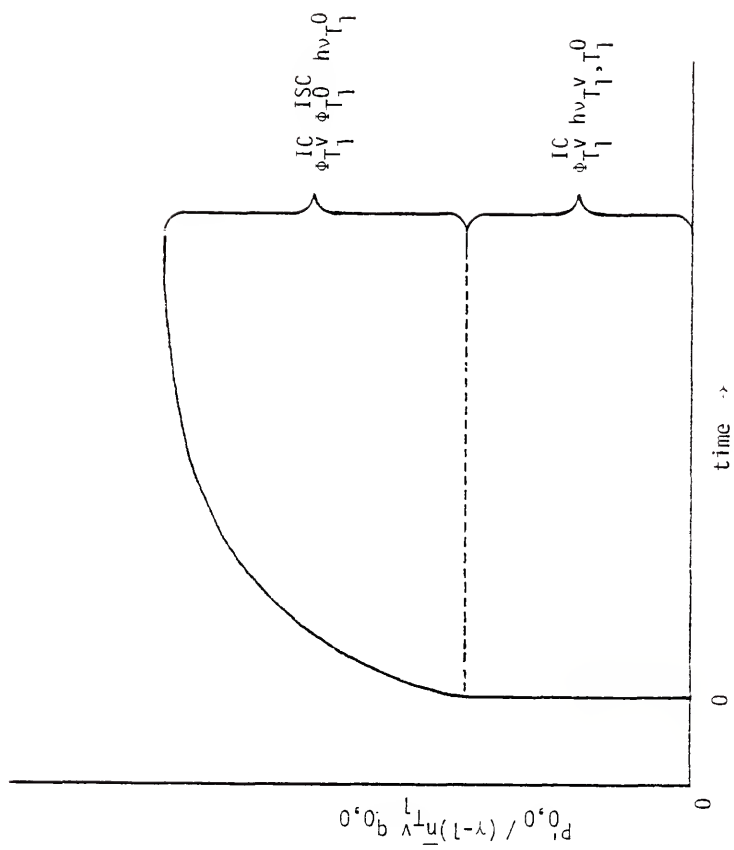
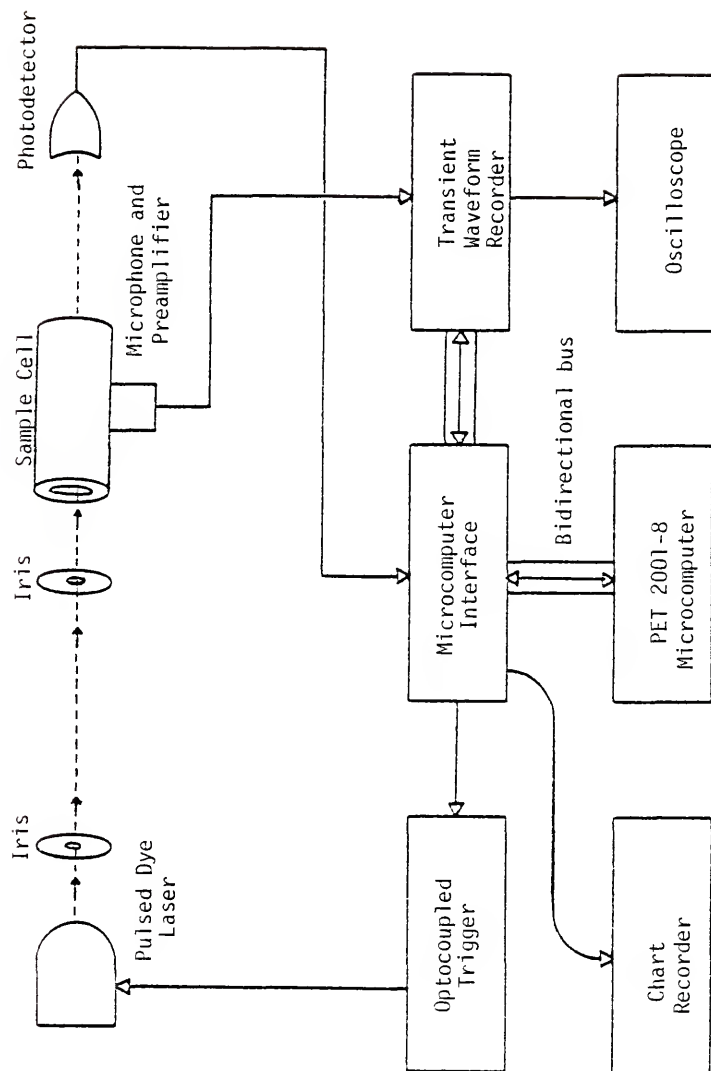


Figure 3. Schematic representation of a typical TROAS apparatus.





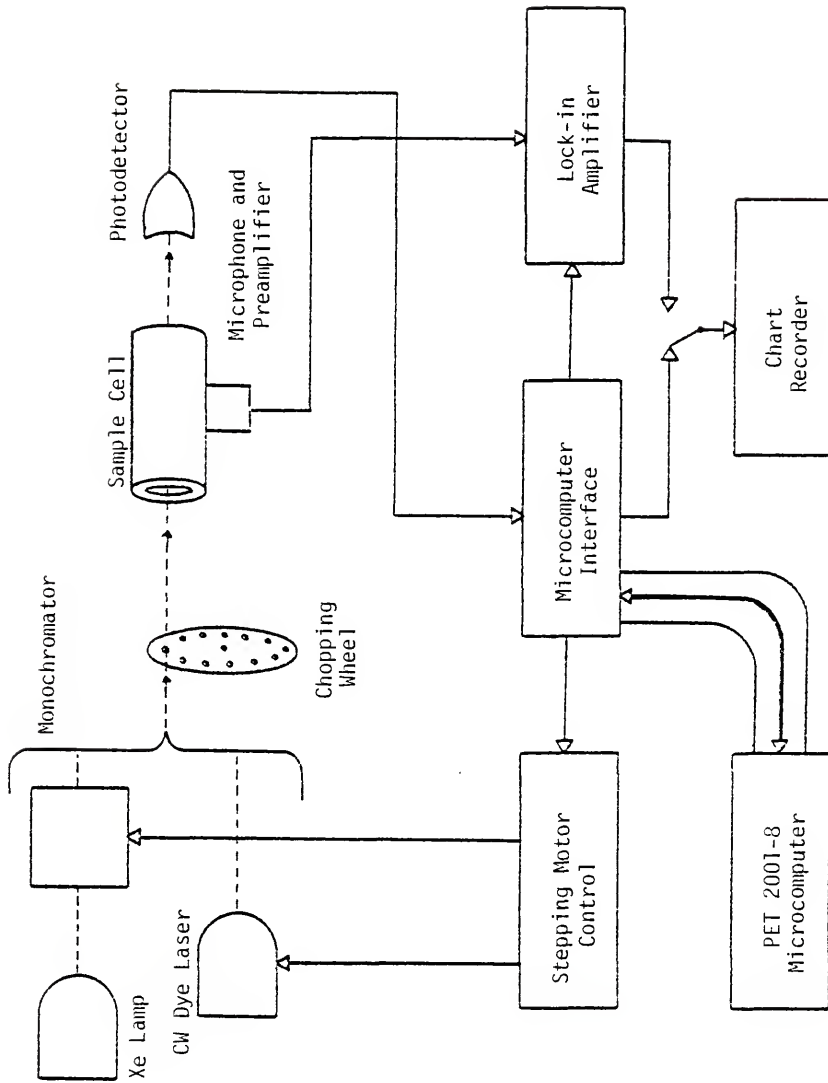
laser firing, light pulse peak-detector reset, etc. It also performs data processing tasks (such as Fast Fourier Transforms) and outputs data to a chart recorder as necessary. The oscilloscope displays acquired data prior to processing.

This experimental arrangement differs markedly from that of conventional optoacoustic spectroscopy (OAS) as shown in Figure 4. The excitation light source is usually a monochromator and Xe lamp combination with light modulation provided by a rotating slotted disk. Alternatively, a tunable continuous wave (CW) dye laser and either an acousto-optic modulator or chopping wheel provides the requisite modulated source intensity. In any event, the spectrum obtained must be corrected for variations of source intensity as a function of source wavelength. The second major difference between OAS and TROAS is the use of a lock-in amplifier to amplify and detect the pressure transducer signal (after the preamplifier stage, of course). The resulting extremely narrow equivalent noise bandwidth allows the use of OAS in the detection of signals in extraordinarily dilute samples [28]. An especially good collection of research papers concerning all relevant aspects of OAS has recently been published [58].

In OAS, accurate waveform information is not necessary; in fact, a lock-in amplifier provides only amplitude and phase shift information in the usual case. This is adequate for sample detection purposes but not well suited for the study of such processes as triplet deactivation pathways. Further details concerning this use of OAS may be found in [32].

The theory of TROAS was developed by Wrobel [47] and, therefore, will not be repeated here, although Chapter Two concerns certain

Figure 4. Schematic representation of a versatile OAS apparatus with dye laser excitation.



extensions and corrections to the loss-free theory. Chapter Three describes the experimental apparatus used in this research. In Chapter Four, the sample selection criteria developed in Chapter Two are used to select promising polyatomic molecules for study. Chapter Five details the numerous experimental arrangements and modifications used. Chapter Six discusses the obtained results, and Chapter Seven contains a discussion of singlet TROAS and its advantages.

## CHAPTER TWO THEORETICAL CONSIDERATIONS

### Introduction and Direction

Several papers have appeared in which pulsed light sources were combined with the optoacoustic effect in order to study various vibrational and electronic state properties of polyatomic molecules. Although the pulsed optoacoustic effect is certainly shown in the works of Parker [34], Aoki and Katayama [59], and Grabiner et al. [60], the interpretations provided are either of limited scope or unnecessarily complex. The theory of TROAS is intended to bring together these diverse observations in a relatively simple and coherent manner.

Unfortunately, the particular solutions given in Wrobel [47] for radiationless decay from the lowest singlet and triplet states of polyatomic molecules are incomplete due to neglect of all energy loss mechanisms, exclusive of those incorporated in the model-specific source term, in the sample gas mixture and sample cell. The most important of these dissipative processes are viscosity and thermal conductivity losses [61]. By inclusion of these two loss mechanisms, it is possible to calculate realistic acoustic mode amplitudes, mode amplitude ratios, and an important figure of merit, the noise equivalent power (NEP). Restrictions imposed by the extended theory are then applied to sample cell design, selection of appropriate pressure transducers, and excitation light source requirements.

# The Extended Solution of the Heat-Flow Model

Consider a molecular vapor at equilibrium in a cylindrical sample cell of length  $L$  and radius  $A$ . The equilibrium density, pressure, and temperature are  $\rho_0$ ,  $p_0$ , and  $T_0$ . Radiationless relaxation processes following excitation of the vapor in an absorption region cause fluctuations in  $\rho$ ,  $p$ ,  $T$  and cause the vapor to assume an acoustic velocity  $\bar{v}(\bar{r}, t)$ . The conservation equations and equation of state constrain the behavior of the vapor

$$p = \frac{R}{M} \rho T \quad \text{equation of state,}$$

$$\frac{d\rho}{dt} = -\rho \nabla \cdot \bar{v} \quad \text{conservation of mass,}$$

$$\rho \frac{d\bar{v}}{dt} = -\nabla \cdot \vec{p} \quad \text{conservation of momentum,}$$

$$\rho \frac{du}{dt} = -p_{ij} \frac{\partial v_i}{\partial x_j} - \nabla \cdot (\bar{I} + \bar{I}_R) \quad \text{conservation of energy,}$$

where  $R$  is the ideal gas constant,  $M$  is the molecular weight of the sample,  $u$  is the internal energy per gram of sample,  $\vec{p}$  is the pressure tensor,  $\bar{I}$  is the nonradiative energy flux vector,  $\bar{I}_R$  is the radiative energy flux vector, the convective derivative is given by

$$\frac{d}{dt} \equiv \frac{\partial}{\partial t} + (\bar{v} \cdot \nabla)$$

and the Einstein summation convention is used.

This solvable system of equations may be simplified by noting that the fluctuations induced by released heat are small relative to the

equilibrium values. This acoustic approximation "linearizes" the system of equations and hence avoids the possibility of shock waves [62]. Thus,  $\rho = \rho' + \rho_0$ ,  $p = p' + p_0$ ,  $T = T' + T_0$ , and  $\bar{v}$  is small. Products of primed quantities are neglected. If viscosity and thermal conductivity are also neglected, the system of equations simplifies to yield a single separable equation [47,63]

$$\frac{\partial^2 p'}{\partial t^2} - c^2 \nabla^2 p' = (\gamma - 1) \frac{\partial H}{\partial t} \quad (2.1)$$

where the heat source term  $H$  is given by

$$H \equiv -\nabla \cdot \bar{T}_R - \rho_0 \frac{du_e}{dt} \quad (2.2)$$

and  $u_e$  is the energy per gram stored in electronically excited molecules.

The heat source term is given explicitly only when the physical model (e.g., a simple two-state model of triplet decay) is selected. With appropriate heat source terms, equation (2.1) underlies both OAS and TROAS. As stated previously, the loss-free solutions of (2.1) are inadequate for the calculation of mode amplitudes, etc. Appendix One contains a brief summary of Kreuzer's approach [63] which includes the two major energy loss mechanisms--viscosity and thermal conductivity. These results will be used as needed to complete the treatment of TROAS.

The fundamental effect of including viscosity and thermal conductivity is the introduction of a finite quality factor  $Q_j$  for each acoustic resonance  $\omega_j$ . The use of a Fourier Transform technique to effect a solution of (2.1) is natural for OAS since the frequency parameter  $\omega$  may represent the frequency at which the illumination source is

modulated. It may be, for instance, the number of pulses per second (times two pi) delivered by a simple chopping wheel interposed between illumination source and sample cell. If the analysis of Kreuzer [63] is to be carried over to TROAS, it must be possible to identify a suitable  $\omega$ .

It is assumed in the theory of TROAS that the illumination source is an energy pulse of negligible duration. This situation is approximately met when the light pulse duration is much less than the smallest relevant time constant in the physical model. As a practical matter, it is satisfactory to have the light pulse duration,  $t_p$ , substantially less than the nonradiative lifetime of the spin-forbidden processes being examined. Such spin-forbidden processes will almost always be involved due to intersystem crossing even if only an excited singlet state were initially excited. In the event no "slow" (e.g., forbidden) states lie below the desired "fast" (e.g., allowed) state, the system is probably better treated by conventional spectroscopic methods. The time constant,  $t_T$ , of the thermal damping subsequent to pulse excitation and relaxation will, for reasonable physical models, always be much greater than  $t_p$ .

The high modulation frequency case for OAS is given by the condition [63]

$$\omega t_T \gg 1. \quad (2.3)$$

For the simple chopping wheel type of intensity modulation, the light pulse duration is

$$\omega^{-1/2}$$



assuming a 50% duty cycle for the chopping wheel. Hence,

$$\omega t_t \gg 1 \quad \text{implies} \quad t_T \gg \omega^{-1} > \omega^{-1}/2$$

so the light pulse duration is short relative to the thermal damping time. Precisely this situation occurs in TROAS. A reasonable estimate for  $\omega$  in TROAS is, therefore, given by  $t_p^{-1}$ . More accurately,  $\omega$  will be assumed to be the spectral bandwidth required to encompass most of the spectral energy in the Fourier Transform of the light pulse [38]. For example, assume the light pulse to be a rectangular pulse of duration  $t_p$  centered at  $t = 0$ . Then the Fourier Transform is proportional to [64]

$$t_p \operatorname{sinc}(\omega t_p/2\pi).$$

The significant portion of the spectrum is in the range  $|\omega/2\pi| < t_p^{-1}$ . Hence,  $\omega \approx 2\pi t_p^{-1}$ . With an estimated frequency, it is possible to calculate acoustic mode quality factors  $Q_j$ , mode amplitudes  $A_j(\omega)$ , and NEP for TROAS. Expressions for  $Q_j$  and  $A_j(\omega)$  are given in Appendix One and an expression for NEP is derived in Appendix Two.

One possible complication arises in the quantity for the absorbance,  $\alpha$ . The relation between absorbed light pulse intensity  $I$  and resultant heat produced  $H$  is

$$H(\vec{r}, t) = \alpha I(\vec{r}, t) \quad (2.4)$$

if the intensity is not high enough to saturate the absorbance and if the time variation of  $I$  is slow relative to the rate of relaxation. The second condition is usually violated in the study of triplet

relaxation via TROAS. Hence, in a more realistic fashion, the relation between  $H$  and  $I$  should be [63]

$$H(\vec{r}, \omega) = \alpha(\omega) I(\vec{r}, \omega). \quad (2.5)$$

The only immediate effect of this for TROAS is that the heat produced lags the light intensity variation. This will not be considered further.

Combining the above relation with the expression for corrected acoustic mode amplitudes (A1.20) from Appendix One yields

$$A_j(\omega) = \frac{-i\omega(\gamma-1)}{V_c \omega_j^2} \frac{\int p_j^*(\vec{r}, \omega) \alpha(\omega) I(\vec{r}, \omega) dV}{[1 - (\omega/\omega_j)^2 - i(\omega/\omega_j) Q_j]} \quad (2.6)$$

The integral determines the coupling between the normal acoustic modes and the beam intensity since  $I(\vec{r}, \omega)$  may be expanded in the same orthonormal set of functions used to express the pressure  $p(\vec{r}, \omega)$ . Hence, the orthogonality equation (A1.7) from Appendix One implies that a normal mode can be excited if and only if the intensity has a corresponding nonvanishing component. Intuitively, one expects longitudinal modes to be excited if significant attenuation of the beam occurs in passage through the cell. In a uniformly illuminated cell (e.g., intracavity in a dye laser) longitudinal modes should not be excited. It is also reasonable to suppose that radial modes will be least strongly pumped in the uniform illumination case. The former expectation is verified by calculator simulations by Wrobel [47] while Kamm [61] has explicitly given the relationship between excitation beam width ( $a$ ) and acoustic mode excitation:

$$p(r,t) = \sum_j \frac{(-i\omega)^2}{\omega_j^2} \frac{\gamma-1}{(1 - \omega^2/\omega_j^2 - i\omega/\omega_j Q_j)} \frac{P}{V_c} \frac{e^{-\mu_j}}{J_0^2(\alpha_{1,j})} J_0(\alpha_{1,j} r/A) e^{-i\omega_j t} \quad (2.7)$$

where

$$\mu_j \equiv \left(\frac{a}{A}\right)^2 (2\alpha_{1,j})^{-2} \quad (2.8)$$

For the lowest frequency radial mode ( $j=1$ ) excited at  $\omega_1$ , the above equation simplifies to

$$A_1(\omega_1) = \frac{(\gamma-1)Q_1}{\omega_1} \frac{P}{V_c} \frac{e^{-\mu_1}}{J_0^2(\alpha_{1,1})} J_0(\alpha_{1,1} r/A) . \quad (2.9)$$

Note that the radial dependence of the amplitude of the lowest radial mode is relatively weak, residing solely in  $\mu_1$ .

In TROAS, the pressure rise mode ( $j=0$ ) contains the significant information. The other acoustic modes obscure the pressure rise and waste energy that would preferably be pumped solely into the  $j=0$  mode. Examination of (2.9) above indicates that the radial modes will be minimally pumped when  $e^{-\mu_1}$  is minimized. This occurs at  $a=A$ , i.e., when the excitation beam width equals the sample cell radius.

Although other dissipative mechanisms external to the source term, such as wave reflection, wave scattering, microphone conversion, and volumetric losses, are present [61], they are of minor importance in comparison with viscosity and thermal conductivity effects. Consequently, we are now in position to consider the characteristics required of each component of a TROAS experiment. The modified TROAS theory restricts the selection of various components of the apparatus and also determines to a large extent just what substances may be studied.

Excitation Source Selection

The "ideal" illumination source for TROAS should have the following properties:

- (1) high constant energy per output pulse (preferably greater than 100 mJ),
- (2) short, stable pulse duration  $t_p$  (such that  $t_p$  is much less than other significant system time constants),
- (3) high pulse repetition rate (for possible signal averaging purposes),
- (4) low beam divergence (for efficient energy coupling to the cylindrical sample cell),
- (5) moderately large beam width (0.5-3.0 cm typically),
- (6) nearly monochromatic light output (no more than several Angstroms spectral bandwidth to enable excitation of a single state),
- (7) tunable operation in the visible and near ultraviolet (to excite electronic states),
- (8) ease of alignment,
- (9) reliable operation over more than  $10^4$  high energy pulses (higher if signal averaging is used).

These conditions are only met by tunable pulsed dye lasers. A compromise between conditions 1 and 3 must be made in the selection of a suitable dye laser system since the optical pumping sources have limited duty cycles, pumping capacities, or heat dissipation capabilities. Since the desired pressure rise mode is proportional to pulse energy, high pulse energy is especially desirable; a coaxial flashlamp-pumped dye laser will

provide energies of several Joules per pulse. Unfortunately, the repetition rate for this type of laser is approximately 0.1 Hz so signal averaging is laborious. In fact, the rather limited tube life (something above  $10^4$  shots), tube expense (approximately \$500.), tube failure mode (rapid disintegration), and photo-decomposition of the dye solutions after a few score shots effectively rule out signal averaging. Linear flashlamp-pumped dye lasers have repetition rates up to 30 Hz and pulse energies of 100 mJ maximum. Nitrogen laser-pumped dye lasers have similar repetition rates but significantly less energetic output pulses. They are not recommended for TROAS in the general case. See Table 1 for a comparison of the above three dye laser types and the monochromator and Xe lamp combination.

#### Sample Cell Construction

The sample cell should be an inert, high heat capacity, isothermal cylinder having transparent end windows and several inlets for pressure transducer(s), pump-out ports, sample admission, etc. A cylindrical geometry is chosen to provide maximum coupling between excitation beam and sample vapor. As previously shown, the desired pressure rise mode ( $j=0$ ) is maximally pumped when the excitation beam width equals the cell radius. The inlets should be as small as possible to avoid excessive wave reflection losses. If one pressure transducer is used, it is probably best positioned midway between the end windows since the solution of the equations of TROAS is greatly facilitated for such a choice [47] and beats in longitudinal modes are eliminated. The end windows present a problem in that they should have high thermal conductivity and yet be at the same temperature as the body of the cell. The

Table 1. A comparison of light sources considered for use in TROAS experiments.

Desired property	Xe lamp and monochromator	Coaxial flashlamp-pumped dye laser	Linear flashlamp-pumped dye laser	N <sub>2</sub> laser pumped dye laser
Energy/pulse	10-100 mJ	5 J max.	100 mJ max.	10 mJ
Pulse width	5 $\mu$ sec	0.5 $\mu$ sec	0.5 $\mu$ sec	10 nsec
Repetition rate	>30 Hz	0.1 Hz	30 Hz	30 Hz
Beam divergence	high (>> 1 mR)	low (<1 mR)	<1 mR	<1 mR
Beam width	large (1" typ.)	large (1" typ.)	small (1/4" typ.)	small (1/4" typ.)
Monochromaticity	10. nm	0.1 nm	0.1 nm	0.1 nm
Tuning range	900. nm-300. nm	750. nm-350. nm	750. nm-350. nm	750. nm-350. nm
Alignment ease	best (CW)	fair	fair	fair
Reliability	best	fair	fair	fair

high thermal conductivity is necessary so that the windows can dissipate any heat produced by adsorbed substances. Otherwise, this heat will pump spurious longitudinal modes [65] despite the windows being at nodes of these modes [66]. If the windows cool significantly, condensation may occur and the previous problem is greatly exacerbated. Sapphire is an excellent choice of window material though expensive. Double windows of Suprasil or Pyrex are satisfactory if light intensity can be compromised approximately 8%. The double windows must have an adequate dead air space between them, and they must be parallel to avoid scattering light onto the cell walls and pressure transducer.

In the absence of thermal conduction, the expected pressure rise term is given by Wrobel [47]:

$$p'_{0,0}|_{t \rightarrow \infty} = (\gamma - 1) k_T (k_p^*)^{-1} (1 - e^{-\alpha L}) E / V_c \quad (2.10)$$

where  $k_T (k_p^*)^{-1}$  is the nonradiative yield,  $\alpha$  is the sample absorbance,  $L$  is the cell length,  $E$  is the excitation source energy per pulse, and  $V_c$  is the cell volume. As a practical matter,  $\alpha$  will be small since all samples should be run at as low a pressure as possible (consistent with the continuum model of sound conduction) to minimize the quenching effect of collisions. For  $\alpha$  small,  $1 - e^{-\alpha L}$  is approximately equal to  $\alpha L$ . Thus, equation (2.10) simplifies to

$$p'_{0,0}|_{t \rightarrow \infty} \propto \alpha L / \pi A^2 L = \alpha / \pi A^2 \quad (2.11)$$

where  $A$  is the cell radius. Thus, the pressure rise is independent of cell length but inversely proportional to  $A^2$ . Nevertheless,  $L$  should be as short as possible to lessen scattered light problems and to allow

placement of the cell in the sample compartment of a UV-visible spectrophotometer for in situ gas phase absorbance measurements.

Cell radius is much more important for a variety of reasons. Pressure rise amplitude is proportional to  $A^{-2}$  so the cell radius should be minimized. The lower limit on radius is the excitation beam width. The NEP is also proportional to  $A$  so again the radius should be minimized. Three time constants also depend on cell radius; these are designated  $t_T$ ,  $t_d$ , and  $t_w$  and are described below.

The time constant for the thermal reequilibration following release of heat in the cell is approximately given by

$$t_T \cong A^2/\kappa \quad (2.12)$$

where  $\kappa$  is the thermal diffusivity. This upper time limit is not critical and usually is of the order of 1 to 10 seconds.

The acoustic delay time  $t_d$  is the time required for sound waves to reach the pressure transducer from the nearest illuminated sample region. It is a lower time limit given by

$$t_d = (A - a)/c \quad (2.13)$$

Note that  $t_d = 0$  for  $a = A$ .

The "mean free path time"  $t_w$  is the time required for collisional deactivation at the cell wall (ignoring deactivation at the windows). This is given approximately by

$$t_w \cong A^2/\xi c \quad (2.14)$$

where  $\xi$  is the mean free path in the sample gas mixture. This is an important upper time limit.



The time limits defined by these time constants may be modified in several ways. First, since both  $t_d$  and  $t_w$  are inversely proportional to the speed of sound in the sample gas, it is possible to add a transparent carrier gas such as He, Ar,  $\text{SF}_6$  or a freon to the sample to change the speed of sound in the mixture. The speed of sound in an ideal gas mixture is

$$c = (\gamma RT/M)^{1/2} \quad (2.15)$$

where  $M$  is the average molecular weight of the sample mixture. Thus, by employing a heavy carrier gas (e.g.  $\text{SF}_6$ ) the speed of sound can be decreased and the upper limit due to the "mean free path time,"  $t_w$ , increased. Unfortunately, at the same time the lower limit due to the acoustic time delay,  $t_d$ , is also increased. Thus, it is necessary to choose the carrier gas with care to select the upper and lower time limits which are most convenient for study of the molecule under consideration.

The second possibility is to use the fact that both  $\kappa$  and  $\xi$  are inversely proportional to pressure [47]. Note, however, that the pressure rise amplitude is proportional to the partial pressure of the absorbing species and that collisional deactivation processes such as triplet-triplet annihilation become more important at higher pressures. The use of an inert monatomic carrier gas also increases the signal amplitude through the heat capacity ratio term. A sample calculation is given in Chapter Four.

### Sample Selection

The pressure rise which occurs after radiationless decay is given approximately by [47]

$$p' \approx (\gamma - 1) k_T (k_p^*)^{-1} E \tilde{\epsilon} p_0 / \pi A^2 RT \quad (2.16)$$

where  $E$  is the pulse energy,  $k_T (k_p^*)^{-1}$  is the nonradiative yield,  $\tilde{\epsilon}$  is the molar absorption coefficient, and  $p_0$  is the sample partial pressure. It is assumed that  $\alpha$  is small so that the following relation is valid:

$$1 - e^{-\alpha L} \approx \alpha L = \tilde{\epsilon} p_0 L / RT. \quad (2.17)$$

Equation (2.16) is the principal constraint on sample selection. A well-chosen sample should have a high vapor pressure at room temperature, a high singlet-triplet absorption coefficient, and a low radiative yield. The laser output pulse energy must be high in the triplet absorption region, the cell radius relatively small, and an inert monatomic carrier gas should be used to increase the  $\gamma - 1$  term and to insure that the acoustic approximation is valid.

In addition, the sample should not be readily quenched by collisions (especially with the carrier gas), should not readily decompose, and should not undergo any sort of photochemistry. It should also have triplet and singlet manifolds well separated relative to the spectral bandwidth of the excitation light source. The triplet lifetime must also fit in the time window given by

$$t_d < t < \text{minimum of } (t_T, t_W). \quad (2.18)$$

Another limitation is imposed by the frequency response of the pressure transducer and associated electronics. An upper time limit

due to low frequency roll-off of the pressure detection system response (typically 6 db per octave) may limit observation times to substantially less than the thermal damping time  $t_T$  unless care is taken in the design of the pressure detection system. Even worse is the lower time limit given approximately by

$$t_d \approx (2f_h)^{-1} \quad (2.19)$$

where  $f_h$  is the -3 db high frequency cut-point. High frequency roll-off for a capacitance microphone is typically 12 db per octave [67]. Since the desired pressure rise is actually a sum of two disparate exponential rises followed by the thermal reequilibration exponential decay, it is necessary to have high frequency response. Otherwise, the pressure detection system will be rise-time limited and thus unable to distinguish "fast" heat from "slow." Thus, the triplet lifetime is constrained by another time window; it must, therefore, fit into the intersection of the allowed time frames.

#### Pressure Transducer Selection

The "ideal" pressure transducer for TROAS should have the following properties:

- (1) high acoustic sensitivity (preferably above 1 mV/Pa),
- (2) high, flat frequency response including dc (to facilitate static pressure calibration),
- (3) low acoustic impedance (concordant with gas phase acoustics),
- (4) high immunity to elastic waves in the mounting substrate (e.g., vibrations and light-induced artifacts in the substrate),

- (5) immunity to stray light,
- (6) linear response to absolute pressure changes,
- (7) low output impedance (for high noise immunity and ease of amplification),
- (8) long-term output stability,
- (9) wide operating temperature range and low temperature drift,
- (10) small, rugged, chemically inert construction (for ease of mounting),
- (11) low output drift in reactive environments,
- (12) ability to withstand vacuum pump-down,
- (13) relatively low cost.

No single pressure transducer available meets all of these conditions or even the first dozen of them. In the previous TROAS study [47], the pressure transducer was a Pitran<sup>TM</sup> (pressure sensitive transistor) developed and marketed by Stolab, Inc. Several different pressure transducer types were used in the present study: capacitance microphones, piezoelectric disks, and piezoelectric cylinders. These types of transducers are compared with respect to the above properties in Table 2. A more detailed comparison of capacitance microphones is presented in Table 3. Properties not listed are similar for the various microphone types.

Although capacitance microphones are well suited to gas phase acoustics applications in general, they have several disadvantages relative to TROAS applications. First, it is usually necessary to exclude oxygen from the sample cell to avoid triplet quenching. This is achieved by pump-down of the cell and refill with sample and carrier

Table 2. Pressure transducers which may be used in TROAS experiments.

Desired property	Pitran	Piezoelectric ceramic	Capacitance microphone
Acoustic sensitivity	370 $\mu\text{V}/\text{Pa}$	30 $\mu\text{V}/\text{Pa}$	0.5-60 mV/Pa
Frequency response	dc - 1 MHz	$10^2 - 10^7$ Hz	10 Hz - $5 \times 10^4$ Hz
Acoustic impedance	high	high	low
Vibrational immunity	low	low	moderate
Light immunity	?	low	low
Linearity	differential mode only	high	high
Output impedance	low ( $<10^3$ ohms)	very high ( $>10^8$ ohms)	very high ( $>10^8$ ohms)
Output stability	fair	fair	very good
Operating temp. range	120 C	400 C	250 C
Ruggedness	easily damaged	rugged	rugged
Reactive environment drift	moderate	low	moderate
Vacuum tolerance	yes	yes	usually no

Table 3. Capacitance microphones considered for use in TROAS experiments.

Microphone	Commercial (externally polarized)	Commercial (electret polarized)	Lab.-made (externally polarized)	Lab.-made (electret polarized)
Acoustic sensitivity	highest 60. mV/Pa typ.	high 20. mV/Pa typ.	moderate 0.1-10. mV/Pa typ.	moderate 0.1-10. mV/Pa typ.
Frequency response	best 3 Hz-200 KHz	good 10 Hz-25 KHz	fair 20 Hz-10 KHz	fair 20 Hz-10 KHz
Vacuum tolerance	usually no	usually no	yes	yes

gas. Well-designed capacitance microphones, however, have a trapped gas volume beneath the metallized diaphragm and a deliberate slow leak to the external environment. For optimum sensitivity the restoring force on the diaphragm due to the compliance of the trapped volume should equal that due to tension in the diaphragm [67]. The second disadvantage is operating temperature range. Although externally polarized microphones may tolerate operating temperatures of several hundred degrees C, electret elements depolarize at elevated temperatures [68].

Piezoelectric transducers are not well suited to gas phase acoustics because of their severe acoustic impedance mismatch with gases. The acoustic impedance  $Z_a$  of a medium is the product of the sound velocity and the density of the medium. Typical values for solids are in the range  $10^7$  to  $10^8$   $\text{kg m}^{-2}\text{sec}^{-1}$ ; for gases, about  $5 \times 10^2$   $\text{kg m}^{-2}\text{sec}^{-1}$  [69]. As noted by Farrow et al. [69], the acoustic transmission coefficient  $a_t$  is given by

$$a_t = (4Z_{a1} Z_{a2}) / [(Z_{a1} + Z_{a2})^2] \quad (2.20)$$

where  $Z_{ai}$  is the acoustic impedance of medium  $i$  with sound waves normally incident at the media boundary. The transmission coefficient ( $a_t$ ) is the ratio of transmitted wave amplitude to reflected wave amplitude; gas-solid interfaces have typical values of  $3 \times 10^{-5}$  while solid-solid interfaces may be close to unity (0.9) [69]. Thus, piezoelectric transducers are susceptible to vibrations and shocks in the mounting substrate and are relatively insensitive to gas phase sound waves.

### Pressure Transducer Electronics

The output signal of the pressure transducer must be amplified and possibly conditioned before being further processed. The two primary pressure transducer choices are capacitance microphones and piezo-electric ceramics both of which have extremely high output impedances (greater than  $10^8$  ohms). If a voltage preamplifier is used, it must be located as close to the transducer as possible to avoid power line noise and cable microphonics. Since the sample cell (and transducer) may need to be heated to produce an adequate sample partial pressure, the pre-amplifier must have good temperature stability, wide operating temperature range, and low thermal noise.

Methods which allow use of a connecting cable between transducer and preamplifier are generally deficient in other aspects. Charge preamplifiers are usually noisier (*ceteris paribus*) than voltage preamplifiers [70]. Parametric amplification of audio frequencies is too complex to justify the minimal improvement in noise performance expected. Carrier current or carrier voltage modulation schemes such as AM, FM, and pulse frequency modulation are all usable if properly designed and well implemented [71-72]. These schemes are usually, however, difficult to implement. Voltage preamplification is, therefore, generally the simplest and most practical method to use.

The actual preamplifier circuit configuration is less important than the "front end." It is crucial that the front end provide high gain and add as little noise as possible [64]. The field effect transistor (FET) is preferred for voltage amplifiers driven from source impedances above approximately  $10^4$  ohms due to the extremely low input



current noise typical of FETs ( $10^{-13}$ - $10^{-16}$  A/Hz $^{1/2}$ ). The so-called  $1/f$  noise of junction FETs (JFETs) is substantially lower than that of MOSFETs for ultrasonic frequencies below approximately 1 MHz [73]. Discrete low-noise JFETs are also quieter than JFETs in IC op amps [74]. The dominant noise parameter for a JFET is input noise current  $I_n$  with input noise voltage  $V_n$  of secondary importance. The optimum source impedance is  $V_n/I_n$ . Noise performance will be degraded if nonreactive components are used to match source impedance to the above optimum source impedance.

The dominant noise sources in a JFET are channel generated thermal noise, gate leakage current shot noise, and generation-recombination surface effect noise [75]. The dominant noise source for high frequency operation is the thermal noise [75]

$$V_n^2 = 4kTB/g_{fs} \quad (2.21)$$

where  $B$  is bandwidth and  $g_{fs}$  is forward transconductance. Low noise JFETs, therefore, have low leakage and high gain.

The most convenient circuit configuration is probably the simple source follower. This circuit provides extremely high selectable input impedance, low output impedance, and high, flat frequency response. If the input is capacitively coupled, a rather long time constant results which may, in some circumstances, limit the upper time limit of observation of the transducer output. This RC time constant is particularly important for piezoelectric transducers [62].

The effect of the preamplifier input impedance is interesting. Total noise voltage decreases with increasing input resistance if the

input resistance is above approximately  $5 \times 10^8$  ohms and if the JFET input noise current  $I_n$  is below about  $2 \times 10^{-14}$  A/Hz<sup>1/2</sup>. This result is based on microcomputer calculations based on a composite noise source model. Details are found in Appendix Three.

### CHAPTER THREE THE EXPERIMENTAL APPARATUS

The apparatus used in the present research may be divided into five subsystems:

- (1) a pulsed, tunable dye laser system with photodetector,
- (2) sample cells and vacuum system,
- (3) pressure transducers and associated electronics,
- (4) microcomputer interface electronics and transient waveform recorder,
- (5) a microcomputer system with adequate software.

The subsystems have been listed in decreasing order of importance. Previous TROAS studies [47] were unsuccessful primarily due to shortcomings in the dye laser system although inadequacies in the remaining subsystems were sufficient to compel a complete redesign of the apparatus. The subsystems adopted for this study are described below in detail.

#### The Dye Laser System

The dye laser system chosen was a Candela Corporation ED 625-U flashlamp driver unit and CL 625 coaxial flashlamp. A Phase-R Corporation high voltage supply (25 KV maximum) provided the 18-22 KV necessary to fire the flashlamp and cause lasing in the dye. The laser mirror mount and grating mount were also Phase-R products. The dye solutions were turbulently pumped by a Micropump (Model 10-84-316-852)

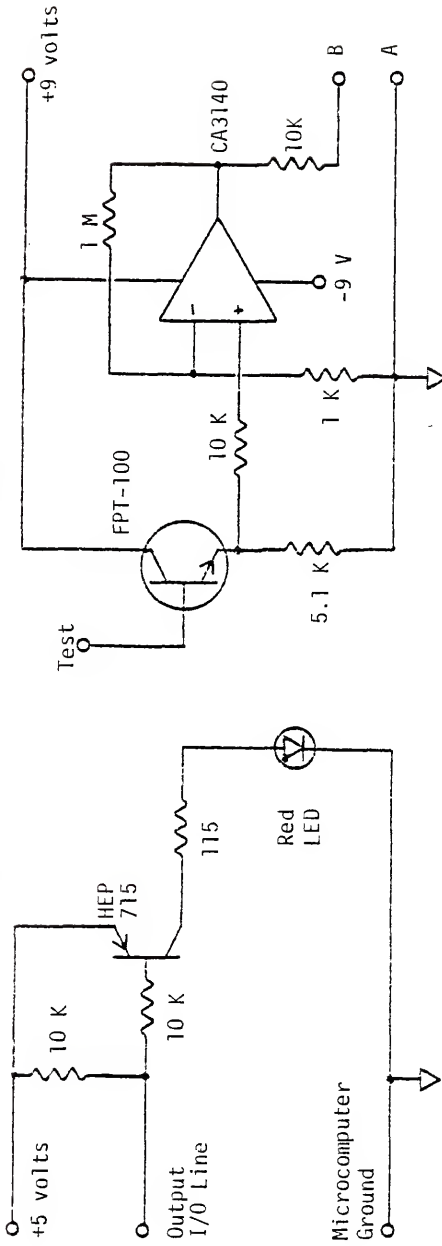
high flow centrifugal pump and filtered and bubble trapped by a Pall filter assembly (resin-free polypropylene 0.45  $\mu\text{m}$  filter cartridge and polypropylene housing). Tuning was effected using an inexpensive Edmund Scientific diffraction grating (5000  $\text{\AA}$  blaze, 600 1/mm) and a 40% reflectivity (420 nm - 650 nm) front reflector from Candela. The dye reservoir was a machined stainless steel tank not equipped with heat exchange coils. The windows on the coaxial flashlamp were antireflection coated in the visible on the outer faces only. The laser cavity length was approximately 2 meters. The system will lase broadband (70-100  $\text{\AA}$ ) and not tune if the cavity is shortened by a factor of three.

The dye solutions were prepared from laser grade dyes supplied by the Exciton Corporation. Concentrations of  $10^{-4}$  -  $10^{-3}$  M were used with 200 proof ethanol or Spectro-grade methanol as the solvent. Solution volume was one liter. Dyes used successfully were, in Exciton's nomenclature, Rhodamines 6G, B, and 110; Coumarins 540, 480, 450, 440; Fluorol 555; Kiton Red S; and Laser Dye 473.

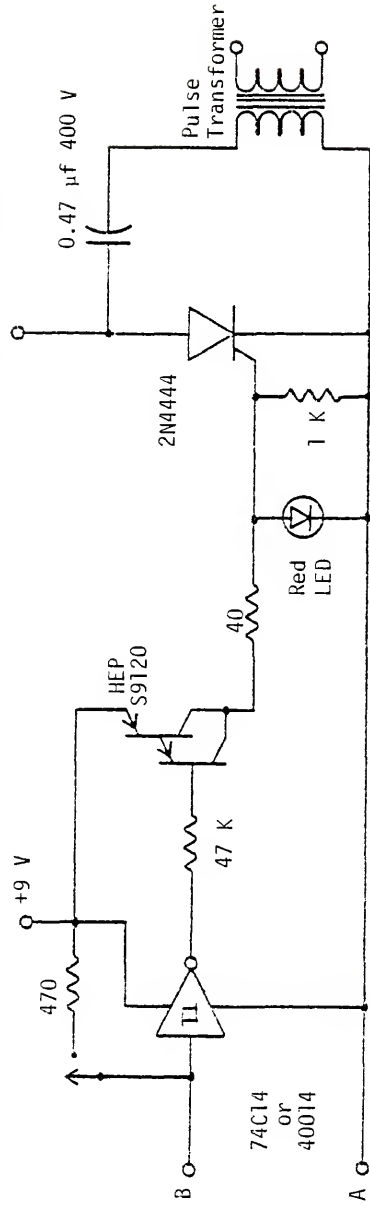
The spark gap trigger in the flashlamp driver unit was pressurized with He or dry  $\text{N}_2$  at 8-12 psi. The laser driver unit could be triggered either under manual pushbutton control or via an optocoupler circuit under microcomputer control. The circuit used is shown in Figure 5. A commercial optocoupler was not used because of their relatively low (less than 7500 V) breakdown voltages. No significant EMI or RFI was produced by a laser firing sequence.

Alignment of the optical cavity was achieved with the aid of an adjustable aperture and a He-Ne alignment laser. The aperture was used to coaxially align the dye laser optics, dye cavity, and sample cell. Three passes of the He-Ne 6328.  $\text{\AA}$  beam through the system are

Figure 5. Optocoupled trigger circuit for the Candela dye laser. The circuit protects the microcomputer system and electronics from laser malfunctions.



Current limited output ( $I_0 < 5 \text{ ma}$ ) from a full wave rectifier and isolation transformer



sufficient to produce excellent alignment. The He-Ne laser is approximately 5 meters in front of the dye laser cavity. Fine adjustment, if necessary, is accomplished by use of the micrometers on the optics mounts. Performance characteristics of the dye laser system are shown in Table 4.

Several comments on this dye laser system are in order. First, the system would lase under very poor conditions; the cavity may be a cheap mirror and a Suprasil window. An energy meter must be used to optimize system performance. Second, the dye solution heats up when turbulently pumped and pulse energy falls about 20%; the dye reservoir should have heat exchanging coils for optimum performance. Third, the power density is high enough (almost  $1 \text{ MW/cm}^2$ ) to "burn" the diffraction grating so inexpensive 600 l/mm grating replicas are recommended. Fourth, fresh dye solutions should be used whenever possible because the first few score of shots are the most energetic. When the system is almost perfectly aligned and fresh dye is used, a sharp, snapping sound accompanies the laser pulse. The grating will most likely be damaged when this excellent lasing occurs. Finally, if the laser did not lase when aligned, it was realigned once or twice. This required no more than ten minutes. If it still did not lase, the dye solution was changed. Flushing the system with 190 proof ethanol followed by one flush with 200 proof ethanol eliminates dye contamination problems.

The laser power was monitored with a silicon PIN photodiode (MRD-501) with a current limited, regulated 22.5 volt bias supply and 3.01 K ohm photocurrent conversion resistor. With the aid of machined Teflon attenuators, the detector system was used to detect pulse intensities as high as 5. MW. In addition, a Gen-Tec ED-200 joulemeter was used to obtain accurate pulse energies for comparison purposes.

Table 4. Performance characteristics of the Candela dye laser system.

Property	Achieved performance
Pulse energy	2.5 J
Pulse duration	$5 \times 10^{-7}$ sec
Pulse repetition rate	0.1 Hz
Spectral bandwidth	0.2 nm
Tuning range	410. nm to 640. nm



### Sample Cells and the Vacuum System

Six different sample cells were constructed for use in the present TROAS studies. In addition, the sample cell used by Wrobel [47] was altered and used in the initial experiments. The salient features of these cells are given in Table 5. Initial attempts to comply with the constraints imposed by the theory of TROAS were loosened in later cell designs when consistent results could not be obtained. Specific information concerning each cell is given below.

Cell #1 was the aluminum cell used by Wrobel [47]. The cell was modified to accept a capacitance microphone and a copper tube was cold soldered inside (with gallium) to increase corrosion resistance. It was not vacuum-tight after the modifications and was inconvenient to heat.

Cell #2 was the primary sample cell used. It was machined from a 9.5" long, 2.5" diameter rod of stainless steel which was drilled, reamed, and ballized to 1.002" inner diameter. The ends were machined for "O"-ring seals and 2" diameter, 1/8" thick Suprasil windows. Pump-out ports 1" from each end were Cajun Ultratorr connectors stainless steel-soldered into the cell. Two pressure transducer ports were milled into the cell to allow use of one while improvements were tested on the other port.

The cell was temperature controlled to  $\pm 0.1$  C by an Oven Industries, Incorporated, proportional temperature controller driving a doubly insulated heating tape. Feedback output was provided by a thermistor mounted in a reamed hole 0.050" from the inner cell wall. Cell temperatures were measured with a thermometer when necessary.

Table 5. Sample cells.

Sample cell number	Composition	Length and radius (cm)	Vacuum integrity	Suitable pressure transducers
1	aluminum with Suprasil windows	L = 16.5 A = 0.64	He leak tight	Pitran, capacitance microphone
2	stainless steel with Suprasil windows	L = 23.45 A = 1.27	He leak tight	piezoelectric transducer, capacitance microphones
3	Pyrex tubing Teflon valve	O.D. = 0.94 I.D. = 0.61	He leak tight	piezoelectric transducer
4	Pyrex flask and side arm	A = 2.83	He leak tight	piezoelectric
5	stainless steel with Suprasil windows	L = 5.0 A = 0.36	not He leak tight	capacitance microphone, piezoelectric transducer
6	Pyrex test tube	L = 15.0 A = 0.76	not He leak tight	capacitance microphone
7	window glass and Pyrex cylinder	L = 4.80 A = 8.40	not He leak tight	capacitance microphone

The cell was rigidly mounted to a 2' by 3' by 1" thick drilled and tapped (1/4-20, 2" centers) aluminum plate which served as optical bench, mounting platform, and system ground. The cell may be isolated from ground with Teflon straps (to avoid ground loops). See Figure 6.

Cell #3 was a Pyrex and Teflon 5 mm valve with one "arm" sealed. See Figure 7. A shielded piezoelectric transducer on the outside of the glass was intended to pick up elastic waves in the glass produced by an illuminated internal sample melted or sublimed onto the inner wall of the glass tube.

Cell #4 was a Florence flask with a Pyrex and Teflon 5 mm valve and tungsten feed-through electrodes in a separate Pyrex apparatus. This cell was used for solutions and gas phase measurements with a suspended piezoelectric transducer. See Figure 8.

Cell #5 was a Cajun Ultratorr 3/8" tee with 3/8" diameter, 1/16" thick Suprasil windows in the arms of the tee and the pressure transducer in the stem. Minimal machining was required to enable the tee to accept either a capacitance microphone or a piezoelectric disk. A spring-loaded electrode was used when the piezoelectric transducer was in place and the signal was brought out through a vacuum-tight BNC bulkhead feed-through connector soldered to a brass 3/8" nut from a similar Cajun 3/8" tee. The cell was vacuum tight though without need to be evacuated.

Cell #6 was a Pyrex test tube with a Teflon tape-wrapped capacitance microphone snugly inserted into the end. The cell was illuminated perpendicular to the long axis and heated uniformly with a heat gun.

Cell #7 was a Pyrex cylinder section with 1/4" sidearm and 1/2" drilled hole for mounting the capacitance microphone. Ordinary window

Figure 6. TROAS sample cell number 2.

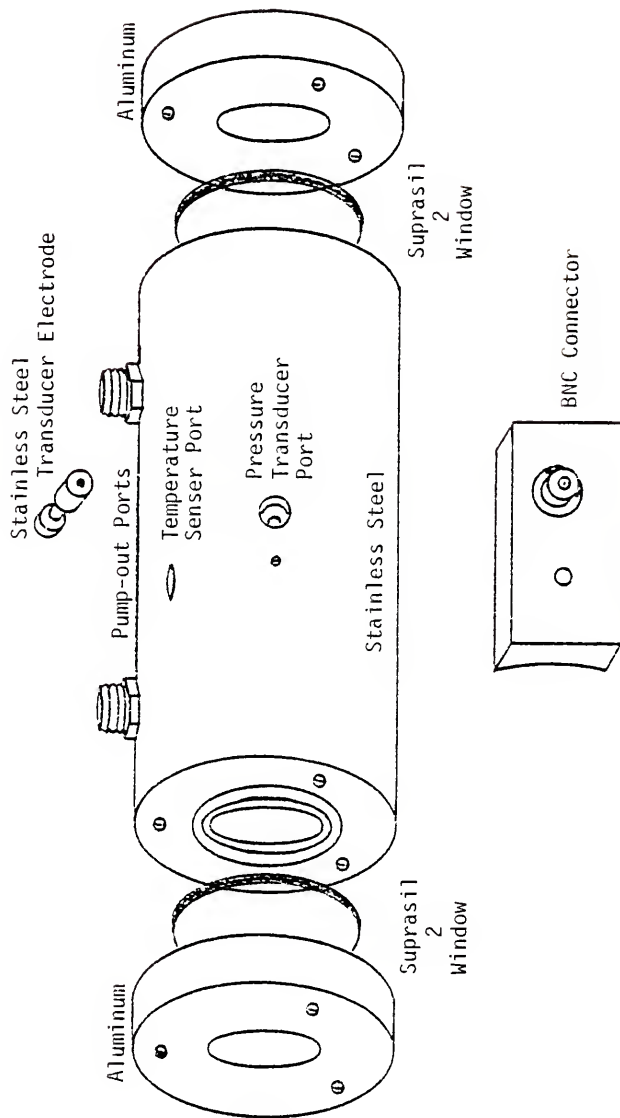


Figure 7. TROAS sample cell number 3.

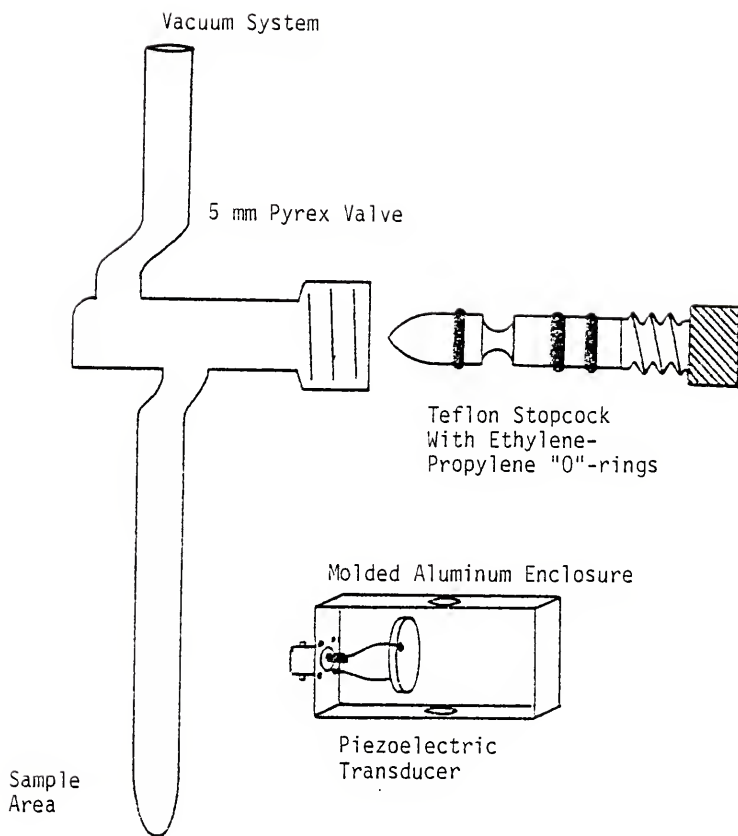
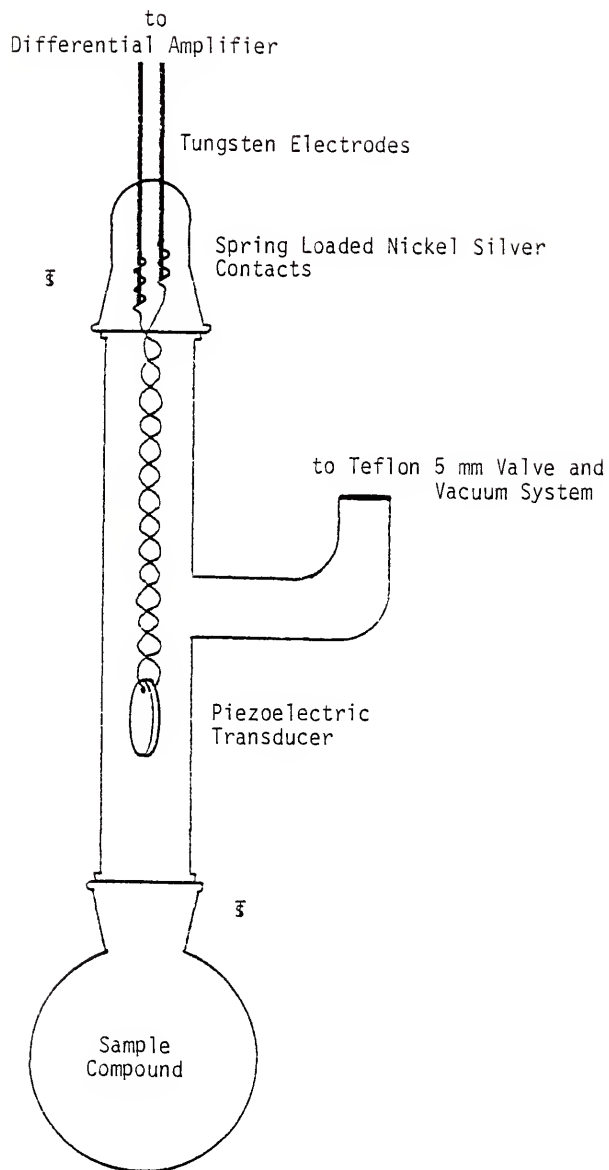


Figure 8. TROAS sample cell number 4.





glass plates were carefully epoxied onto the ends of the cylinder to produce a highly transparent cell. See Figure 9.

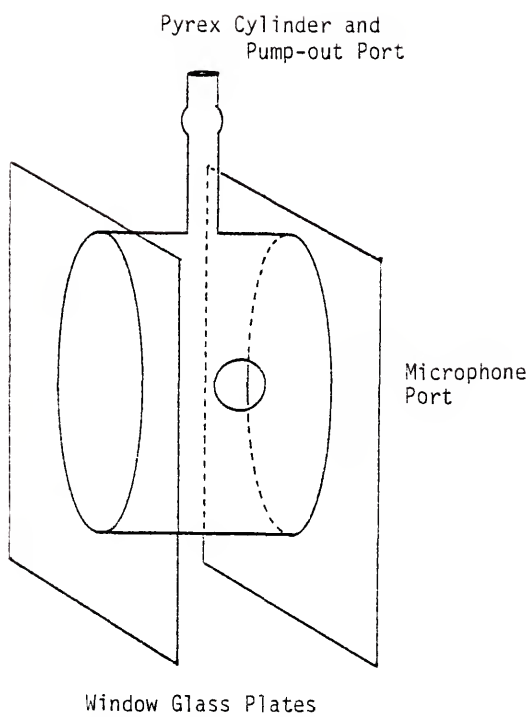
The vacuum system used must be capable of removing oxygen from the sample cell to avoid the possibility of triplet quenching. A liquid nitrogen-trapped rotary oil pump system is sufficient to attain  $10^{-4}$  torr which is adequate to exclude oxygen from liquid samples by repeated freeze-pump-thaw cycles. Solids may be deoxygenated by solution in a suitable solvent and subsequent pump-down. The system pressure was measured with a Wallace & Tiernan gauge (0-800 torr in units of 1 torr). The vacuum system was tested for leaks with a Veeco MA-2 mass spectrometer helium leak detector. Pressures to  $10^{-4}$  torr were routinely obtained in the system.

#### Pressure Transducers and their Associated Electronics

Several hundred man-hours were spent in the design and construction of improved circuitry and transducer mounting techniques. Among the techniques tried without success were laboratory-made, externally polarized capacitance microphones and FM carrier current modulation by microphone capacitance changes. The Pitran pressure sensitive transducer was rejected due to moderate sensitivity ( $380 \mu\text{V}/\text{mtorr}$ ), high temperature drift ( $400 \text{ mV}/\text{C}$ ), differential pressure mode operation, high acoustic impedance, extremely high susceptibility to damage (especially in mounting), and sensitivity to mounting substrate vibrations.

The most important parameters to be considered in selection of pressure transducers for TROAS are sensitivity, acoustic impedance, and flat, broadband frequency response. Unfortunately, these parameters are usually dependent on each other. Consider the capacitance

Figure 9. TROAS sample cell number 7.



microphone. The resonant frequency of a standard unpinned disk microphone (approximately 80% of the high frequency cut-point) is

$$f_{\text{resonant}} = (f_r/m)^{1/2} \quad (3.1)$$

where the restoring force  $f_r$  is roughly proportional to acoustic impedance and diaphragm mass  $m$  is proportional to the square of the diaphragm diameter. Thus, high frequency response requires low sensitivity and small, rigid, thin diaphragms. Two high quality microphones are compared in Table 6. The microphone actually used is also described in Table 6 [76].

Laboratory-made microphones worked, though not as well as commercial capacitance microphones, probably due to the method of construction [67]. The microphones were constructed of aluminized mylar without a trapped gas volume (to allow pump-down).

The piezoelectric transducers used were 1/2" disks of PZT-5H from Vernitron, Inc. Also used were two sizes of piezoelectric cylinders and a thin, high frequency response (5 MHz) disk also of PZT-5H. One immediate problem with piezoelectric transducers is calibration. The output voltage of the transducer is [62]

$$V_0 = \frac{i\omega\tau}{1 + i\omega\tau} \frac{K' A_p \Delta p}{C} \quad (3.2)$$

where  $K$  is the modulus of the piezoelectric,  $A_p$  is transducer area,  $C$  is the transducer and electronics shunt capacitance,  $\Delta p$  is the pressure change,  $\tau$  is the RC time constant of the transducer and amplifier, and  $\omega$  is the frequency of the pressure change. For  $\omega$  much greater than  $\tau^{-1}$ , the output voltage is proportional to pressure change. For static

Table 6. Capacitance microphone comparison.

Property	Radio Shack 33-1056	B & K 4144	Dynasciences 814
Acoustic sensitivity	3.2 mV/Pa	50. mV/Pa	0.56 mV/Pa
Resonant frequency	6. KHz	8.3 KHz	90. KHz
Frequency response	20 Hz - 12 KHz	10 Hz - about 15 KHz	50 Hz - 120 KHz
Corrosion resistance	low	low	high
References	[76]	[63]	[72]

or low frequency pressure changes this is not the case. Calibration of the piezoelectric ceramic transducer used in this research is described in Chapter Four.

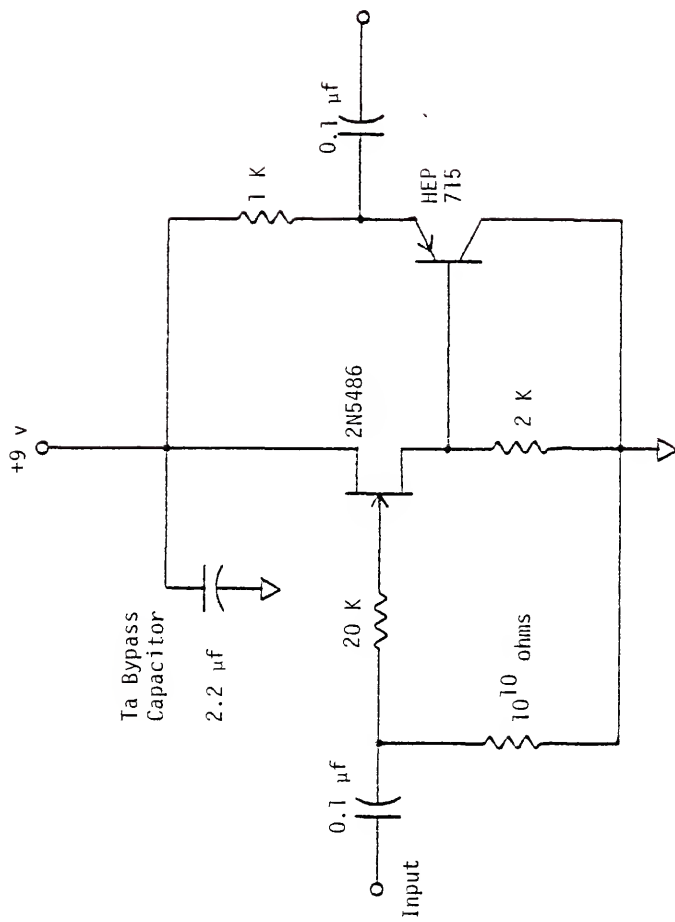
### Pressure Transducer Electronics

Many preamplifiers and amplifiers were designed, breadboarded, modified, constructed, tested, and usually rejected. These included preamplifiers with discrete JFETs, discrete bipolar transistors, and bipolar, Bi-mos, or JFET input op amps. Although the noise model (Appendix Four) indicates that the discrete JFET-input voltage follower-with-gain circuit is optimal, this circuit is not easily implemented in the vicinity of the heated cell. Unfortunately, this is necessary because of the very high output impedance of the pressure transducer. The circuit eventually adopted was a source follower ( $10^{10}$  ohms input impedance) used to provide impedance conversion. The circuit used a discrete JFET (2N5486) in an ac-coupled configuration with input time constant of  $10^3$  seconds. Voltage gain was obtained with a Tektronix Model 26A2 differential amplifier which allows switch selection of gains from  $10^2$  to  $10^5$ , adjustable bandwidth from dc to 1 MHz, and differential mode inputs. This was especially convenient when used with the data acquisition system and Fast Fourier Transform program because the bandwidth may be adjusted to avoid aliasing. Differential mode operation was necessary to eliminate power line hum pick-up. See Figure 10 for the circuit schematic.

Having selected a pressure transducer and associated preamplifier, the electrical noise of the system was measured under no-signal conditions. For the system described, this was 11.  $\mu$ V rms determined by

Figure 10. Pressure transducer impedance conversion circuit.





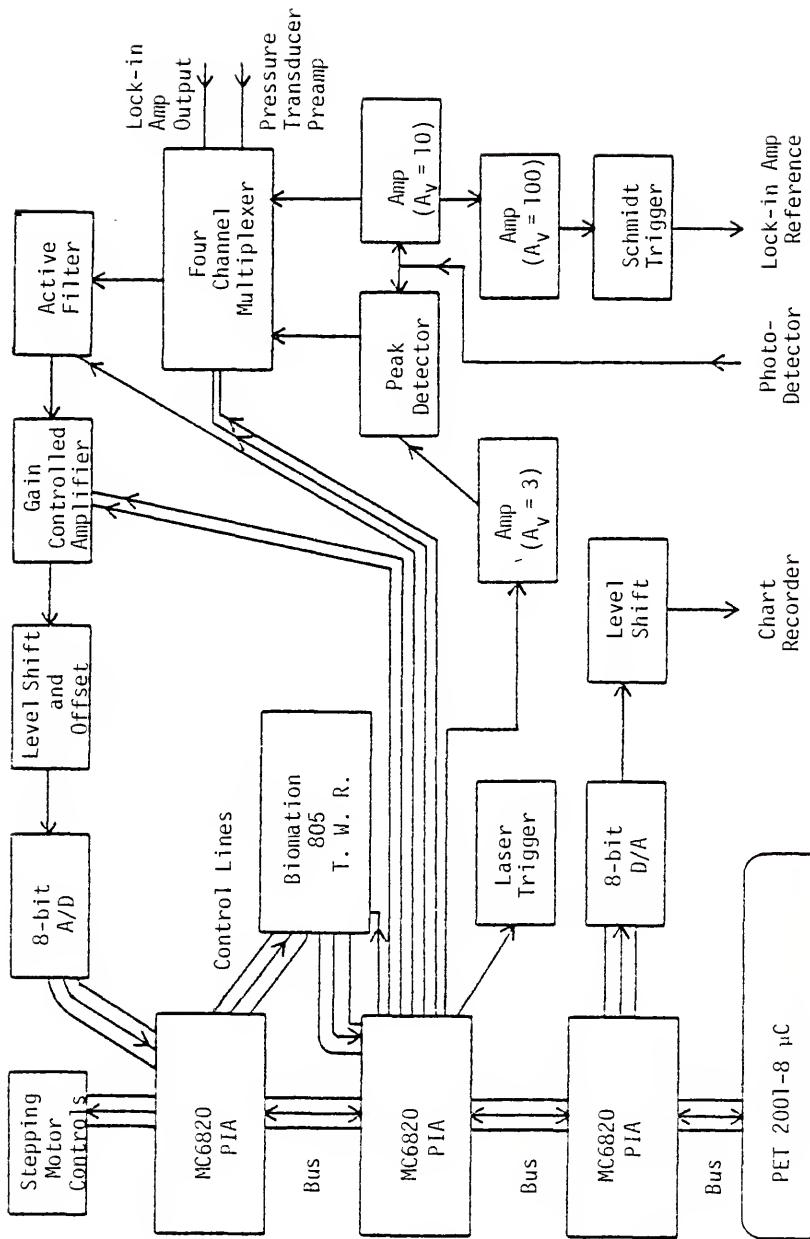
averaging 25 acquired noise spectra and assuming a crest factor of 4 [74]. The system bandwidth was 0.1 Hz to 1. MHz with shorted inputs and gain of  $5 \times 10^3$ . With the sensitivity of the Radio Shack capacitance microphone given as 3.2 mV/Pa and the conversion factor of 1 Pa = 7.50061 mtorr, the sensitivity is thus  $4.2 \times 10^{-4}$  V/mtorr. If the limit of detection is considered to be a signal to noise ratio (S/N) of unity (no signal averaging), then the pressure required to equal electrical noise is 0.20 mtorr. This pressure equivalent noise level is very important in determining the suitability of samples for TROAS studies. By direct comparison of the piezoelectric transducer with the Radio Shack capacitance microphone, the pressure equivalent noise level of the former is found to be approximately 20. mtorr. This comparison was carried out in cell #2 with  $\text{NO}_2$  (a strongly absorbing substance).

#### Microcomputer Interface Electronics

The electronics necessary to interface the microcomputer to the various amplifiers, chart recorder, peak detector, et cetera is shown in schematic form in Figure 11. The circuitry consists of relatively standard, independent subsystems interfaced to the microcomputer I/O lines which in turn are provided by Motorola 6820 Peripheral Interface Adaptor (PIA) LSI chips tied to the microcomputer address, data, and control busses. The functions of these subsystems are listed below:

- (1) chart recorder output (0-1 volts) via an 8-bit D/a converter,
- (2) four input channel multiplexer- selectable active filter- gain controlled amplifier- offset and level shifter- 8-bit A/D converter,

Figure 11. Schematic representation of the microcomputer interface system and electronic subsystems used in the TROAS experiments.



- (3) transient recorder and stepping motor control lines (LSTTL or n-MOS),
- (4) photodetector peak detector with CMOS 4016 transmission gate reset,
- (5) photodetector linear response circuit with additional CMOS 40014 Schmidt trigger optional output.

The stepping motor control lines and linear CW light detection circuitry are not used in TROAS; the circuitry was designed to allow conventional OAS with a Spectra-Physics Model 164 Argon Ion Laser and a Model 375 CW dye laser. The flashlamp-pumped dye laser, sample cell, light detector, and Spectra-Physics lasers were coaxially aligned, and the interface electronics and software facilitated rapid changeover from TROAS mode to OAS mode or vice versa.

The data acquisition system incorporated a Biomation 805 Waveform Recorder with selectable sampling rates to 5 MHz, 2048 words of 8 bits each memory storage, pretrigger recording, sensitivity to 0.1 volts full scale, and microcomputer compatible data readout. A Tracor Northern NS-570 Digital Signal Averager with 20  $\mu$ sec (minimum) dwell time per channel, 9 or 12 bit data conversion, and automatic normalization of summed spectra was used in the earliest attempts at TROAS. The signal averager was found to be too slow and susceptible to RFI generated by a laser firing sequence.

#### The Microcomputer System

The Commodore 2001-8 PET microcomputer system was chosen for use in the experiment for many reasons. The most important are hardware and software compatibility with previously used KIM-1 microcomputer

systems; 6502 microprocessor-based, efficient architecture; fast 8 K BASIC with assembly language subroutines; built-in cassette tape drive and video monitor; low cost (\$795).

The main program used in the TROAS studies is listed in Appendix Four. The listing contains no "remarks" because of memory restrictions imposed by the relatively small amount of available random access memory (8K of RAM). The program consists of independent subroutines called from the keyboard by number. These are briefly described below:

- (1) initialization and status of microcomputer interface subsystems,
- (2) data acquisition from transient recorder and control of laser firing, light peak detector readout,
- (3) chart recorder output of raw data,
- (4) data storage in named cassette files,
- (5) 256 point Fast Fourier Transform subroutine based on the Fortran version by Bell [77],
- (6) video display of numerical data concerning FFT spectral intensities and powers,
- (7) line spectrum output to chart recorder of FFT results,
- (8) assembly language subroutine to eliminate the effects of the time delay (about 100  $\mu$ sec) in the laser firing circuit optocoupler,
- (9) least squares exponential curve fit subroutine.

## CHAPTER FOUR SAMPLE SELECTION

In order to determine the validity of the theory of TROAS, suitable calibration standards must be run. These compounds should meet the conditions imposed by the theory and those arising from necessary compromises in the experimental apparatus. Previous attempts by Wrobel [47] failed to verify the fundamental two-component pressure rise expected to occur immediately after absorption of light by the sample. The observation of the pulsed optoacoustic effect by other investigators has been previously mentioned; those observations do not, however, constitute evidence for the validity of the theory of TROAS.

The first compound used in the TROAS experiments reported herein was 2,2,4,4-tetramethyl-1,3-cyclobutanedithione (dithione). Dithione is a deep red, crystalline solid with distinct camphoraceous odor. This compound and the related dione have been the objects of several theoretical and experimental investigations by Vala and coworkers [78-80]. Although the UV-visible spectrum of dithione is still without a definitive interpretation, several important facts are known. First, several definite triplet peaks at 5943 Å, 5926-5922 Å, 5836 Å, and 5738 Å are easily accessible; in fact, the dye laser output power with Rhodamine 6G dye spans these wavelengths and is highest at about 5900 Å. The second important property is a relatively high molar absorption coefficient (approximately  $1.5 \text{ l mole}^{-1} \text{ cm}^{-1}$ ). The third property is

the significant vapor pressure (approximately 0.50 torr at room temperature). These last two results are due to Powell [81].

The pressure rise expected from dithione may be calculated using equation (2.16). The expected rise  $p'$  is 24. mtorr assuming  $\tilde{\epsilon} = 1.5 \text{ l mole}^{-1} \text{ cm}^{-1}$ ,  $p_0 = 0.50 \text{ torr}$ ,  $T = 300 \text{ K}$ ,  $\gamma = 1.4$ ,  $k_p = 0$ ,  $E = 1 \text{ J}$ , and  $A = 1.27 \text{ cm}$  (for cell #2). This is much larger than the pressure equivalent noise level obtainable using the Radio Shack capacitance microphone (0.20 mtorr) and approximately equal to that of the system if a piezoelectric transducer is used (20. mtorr).

Since only the piezoelectric transducer can tolerate vacuum pump-down, a carrier gas at atmospheric pressure must be used with the dithione to avoid damaging the capacitance microphone. Helium gas is an excellent choice because of its high purity, inertness, high sound velocity, and high heat capacity ratio. The effect of trapped oxygen in the microphone would be to convert slow heat to fast heat by triplet quenching. This problem will be deferred until later.

The three time constants  $t_T$ ,  $t_d$ , and  $t_w$  may be calculated from equations (2.12) - (2.14) respectively. Under the above conditions, these are  $t_T = 0.73 \text{ sec}$ ,  $t_d = 6.6 \text{ } \mu\text{sec}$ , and  $t_w = 0.86 \text{ sec}$ . For air at STP, they are  $t_T = 2.7 \text{ sec}$ ,  $t_d = 19. \text{ } \mu\text{sec}$ , and  $t_w = 7.3 \text{ sec}$ . The acoustic delay times  $t_d$  were calculated assuming  $a = A/2 = 0.635 \text{ cm}$ . With the frequency response of the microphone given as 20. Hz to 12. KHz, the corresponding allowed time window is 42.  $\mu\text{sec}$  to 25. msec. Thus, the pressure detector limits the triplet lifetime which can be observed at both extremes. If the oxygen in the trapped volume in the microphone quenches the triplet, the result may well be solely fast heat, i.e., heat fast relative to the 42.  $\mu\text{sec}$  limit. It is also known



from previous studies [82] that the triplet lifetime of dithione is less than 1 msec. In addition, dithione definitely photochemically decomposes and also thermally decomposes to the mixed ketone and other unknown species. This decomposition to a viscous red oil occurs at temperatures below the reported decomposition temperature [83]. The dithione used in these experiments was supplied by the research laboratories of Tennessee Eastman. In general, impurities caused no problems in the TROAS experiments so that compounds were used as supplied, which was in no case less than 95% purity.

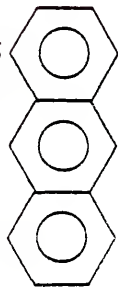
In order to overcome the problem of decomposition and to obtain known radiationless rate constants, several compounds exhibiting the internal heavy atom effect were studied. These were naphthalene, 2-chloronaphthalene, anthracene, 1-chloroanthracene, and 9-bromoanthracene. These compounds have been studied for many years and consequently several of the triplet energies, molar absorption coefficients, and radiationless rate constants are known or can be estimated reasonably accurately. The lowest triplet in naphthalene, at 77 K in a glass [84], is  $4695 \overset{\circ}{\text{A}}$ . It may be expected to shift somewhat in the gas phase. Other relevant data (and references [85-87]) are given in Table 7. Figure 12 shows the structures of the organic molecules studied. Unfortunately, the molar absorption coefficients are very small for all of these compounds. It was hoped that the relatively high vapor pressures of several of the compounds, particularly naphthalene (10 torr @ 35.8 C [85]), would compensate for the low absorptivities.

In addition to the above compounds, both  $\text{I}_2$  and  $\text{NO}_2$  were tried. Both of these substances absorb strongly throughout the visible, have been studied extensively, and have complicated spectra. Iodine has

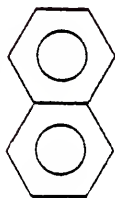
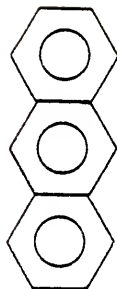
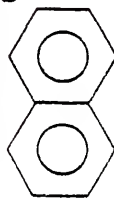
Table 7. Relevant triplet properties of the compounds studied by triplet TROAS.

Compound	Triplet wavelength (Å)	Triplet Absorption coefficient (l mole <sup>-1</sup> cm <sup>-1</sup> )	Triplet Non-radiative yield	Triplet lifetime (seconds)	Vapor pressure (torr, K)
Dithione	5943, 5926-5922, 5836, 5738 [80]	1.5 [81]	-	less than 10 <sup>-3</sup> [82]	0.50 @ 300 [81]
Biacetyl	5000 [32]	1.4x10 <sup>-7</sup> oscillator strength [87]	0.851 [32]	1.52x10 <sup>-3</sup> [32]	tens of torr @ 300 K
Naphthalene	4695 [84]	-	0.96 [86]	2.4	ln p = 19.51 - 6264/T [85]
2-chloro-naphthalene	4739-4854 [54]	10 <sup>-3</sup> [54] for 1-chloro	-	0.43 for 1-chloro [54]	-
Anthracene	6803 [84]	-	-	0.045	ln p = 20.70 - 8517/T [85]
1-chloro-anthracene	6788 [54]	-	-	-	-
9-bromo-anthracene	-	-	-	-	-

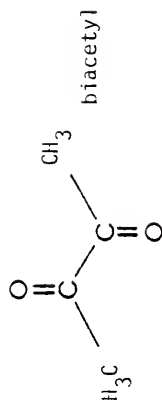
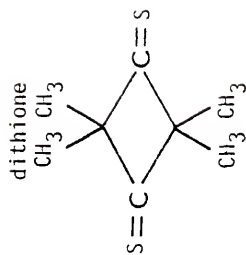
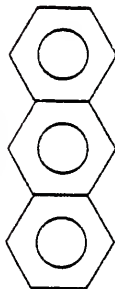
Figure 12. Structures of the sample substances used in the TROAS experiments.

1-chloroanthracene  
Cl

naphthalene

9-bromoanthracene  
Br2-chloronaphthalene  
Cl

anthracene



been studied by conventional OAS techniques with interesting results [31]. When moist, iodine attacks aluminum very rapidly and stainless steel (316) slowly. It also attacks the silver metallization on the PZT-5H piezoelectric transducers yielding silver iodide and intermittent operation. Nitrogen dioxide does not appreciably attack either aluminum or stainless steel. It was used to compare the sensitivities of the capacitance microphone and the piezoelectric transducer. Reactive substances reportedly cause drift problems with externally biased capacitance microphones [87]. It should be noted that neither iodine nor  $\text{NO}_2$  is suitable for a rigorous TROAS study because neither of them is adequately modeled by a simple two-state model.

Biacetyl ( $\text{CH}_3\text{COCOCH}_3$ ) is an excellent compound to study because of its unusual properties--high phosphorescence quantum yield (0.149) [88], low triplet energy (57 Kcal/mole), high vapor pressure, and unusual transition from small molecule behavior to large molecule behavior at an accessible wavelength (4450 Å [89], 4430 Å [32]). It is a small enough molecule to be accessible to detailed theoretical studies and relatively easy to study since both fluorescence (from  $S_1$ ) and phosphorescence (from  $T_1$ ) are readily observed and spectrally distinct. In addition, the photochemistry of biacetyl has been extensively studied [90-91] especially by Noyes and coworkers [92-94]. It is used routinely as a gas phase emission standard and as a triplet energy acceptor in the study of the photochemistry of other molecules [95]. It is also known [96] that biacetyl, at pressures below 10 torr, exhibits essentially no collisions during the lifetime of the lowest excited singlet state  $S_1$  ( $\tau = 10^{-8}$  sec).

Among the disadvantages of using biacetyl for TROAS studies are its reactivity, low  $S_0 \rightarrow T_1$  oscillator strength ( $1.4 \times 10^{-7}$  [87]), and foul odor (rancid butter). On the whole, the advantages probably outweigh the disadvantages insofar as TROAS is concerned.

## CHAPTER FIVE EXPERIMENTAL ARRANGEMENTS

The major components of the attempted TROAS experiments are presented (in concise form) in rough chronological order in Table 8. The arrangement of the components was essentially that of Figure 2 though, of course, the initial experiments were performed without the aid of either microcomputer system or transient waveform recorder. Consequently, the complexity of the experimental apparatus increased (as necessary) to obtain results and eliminate interferences.

The previous experiments had been performed in the near-UV (320-420 nm) where the performance of the Phase-R DL-1200 coaxial flashlamp-pumped dye laser was very poor, at best [47]. It was decided, therefore, to use this system in the visible region only, where dye performance is much better and alignment of the system is far easier. With Rhodamine 6G dye, the maximum output energy per pulse in the Phase-R system was guaranteed to be at least 250 mJ as opposed to the obtained maximum near-UV output of 150  $\mu$ J [47]. Poor laser performance, in general, and low pulse energy, in particular, were felt to be the primary impediments to successful completion of the previous work.

As mentioned in the previous chapter, the maximum energy output of Rhodamine 6G occurs at approximately 590. nm which is almost ideal for excitation of the lowest triplet state of dithione. In addition to favorably placed triplet bands, dithione has a molar absorption coefficient of about  $1.5 \text{ l mole}^{-1} \text{ cm}^{-1}$  and a vapor pressure of about 0.5

Table 8. A summary of the TROAS experiments performed.

Sample compound	Cell number	Excitation sources	Pressure transducers	Data acquisition system	Carrier gases
Dithione	1	Phase-R laser, N <sub>2</sub> laser-pumped dye laser	CM	Tracor Northern NS-570 digital signal averager	air
Dithione	2	Xe flashlamp	CM	NS-570	air
Dithione	2	Candela laser	CM, PT	Hewlett-Packard 181A storage osc.	air
Biacetyl	2	Candela laser, Xe flashlamp	PT	HP-181A	none
Naphthalene	2	Xe flashlamp	CM	Biomation 805 transient record.	air
Naphthalene	2	Candela laser	PT	805	none, air, He
Naphthalene	2	Candela laser	CM	805	air
Naphthalene	2	Candela laser	Lab.-made CM	805	none
Anthracene	2	Candela laser	PT	805	none, He
Iodine	2	Candela laser	PT	805	none, air, He
9-bromo- anthracene	2	Candela laser	PT	805	none, He



Table 8--Continued.

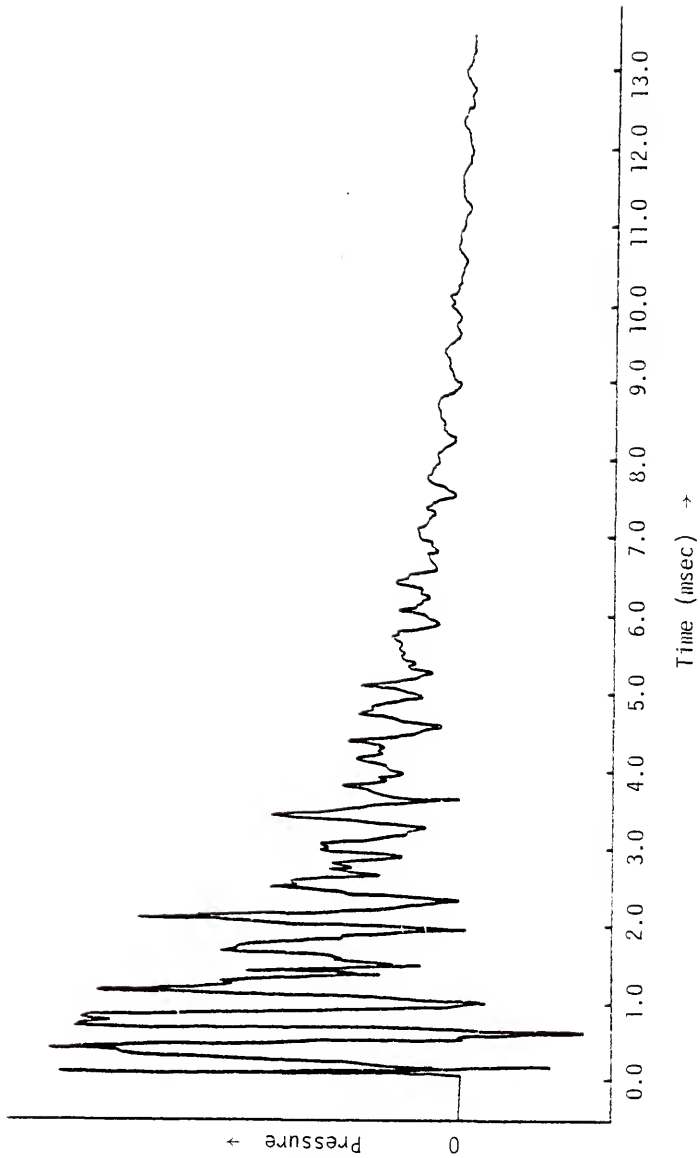
Sample compound	Cell number	Excitation sources	Pressure transducers	Data acquisition system	Carrier gases
1-chloro-anthracene	2	Candela laser	PT	805	air
2-chloro-naphthalene	2	Candela laser	PT	805	air
Anthracene	4	Candela laser, Xe flashlamp	PT	805	none
Anthracene	3	Candela laser, Xe flashlamp	PT	805	none
NO <sub>2</sub>	2	Candela laser	CM, PT	805	none
Naphthalene	5	Candela laser	CM, PT	805	air
Dithione	2	Candela laser	PT	805	none, air, He
Dithione	2	Candela laser	CM	805	air
Dithione	6	Candela laser	CM	805	air
Dithione	7	Candela laser	CM	805	air

torr at 300 K. Therefore, a small quantity of solid dithione was placed in cell #1 with the capacitance microphone (hereafter CM) connected directly to the input of the Tracor Northern NS-570 digital signal averager. Whenever possible, samples were run at room temperature first to see if a spectrum could be obtained. If no spectrum was obtained, the cell was heated via a doubly-insulated heating tape driven by a feedback controlled, fully proportional temperature controller. Dithione samples were heated as high as 85. C to increase sample partial pressure while not greatly increasing the likelihood of thermal decomposition. Temperatures were also limited to avoid thermal depolarization of the electret microphone diaphragm and to avoid significantly increasing the integral JFET preamplifier's thermal noise.

Samples were also usually run with air as a carrier gas in the initial attempts with each sample since the effects of oxygen quenching of the excited triplet would be confined to converting slow heat to fast heat. The CM was only used with air at atmospheric pressure as the carrier gas because it is not possible to pump down the CM without causing diaphragm rupture as the trapped air beneath the diaphragm expanded.

Despite these limitations, initial results were encouraging (see Figure 13). Unfortunately, the Phase-R system refused to tune or even lase narrowband; it also suffered numerous breakdowns culminating in the decision to switch to the Candela laser system. Additional problems encountered during the initial experiments included sample cell corrosion, possible oxygen quenching of the triplet (in an unexpected fashion, such as excitation of the metastable  $^1\Delta_g$  state), possibly inadequate low frequency response of the transducer and/or the digital

Figure 13. The TR0AS spectrum of dithione obtained with a Phase-R DL-1200 dye laser, Rhodamine 6G dye lasing broadband, and a capacitance electret microphone. The spectrum is the average of 32 runs. Cell temperature was 51. C.

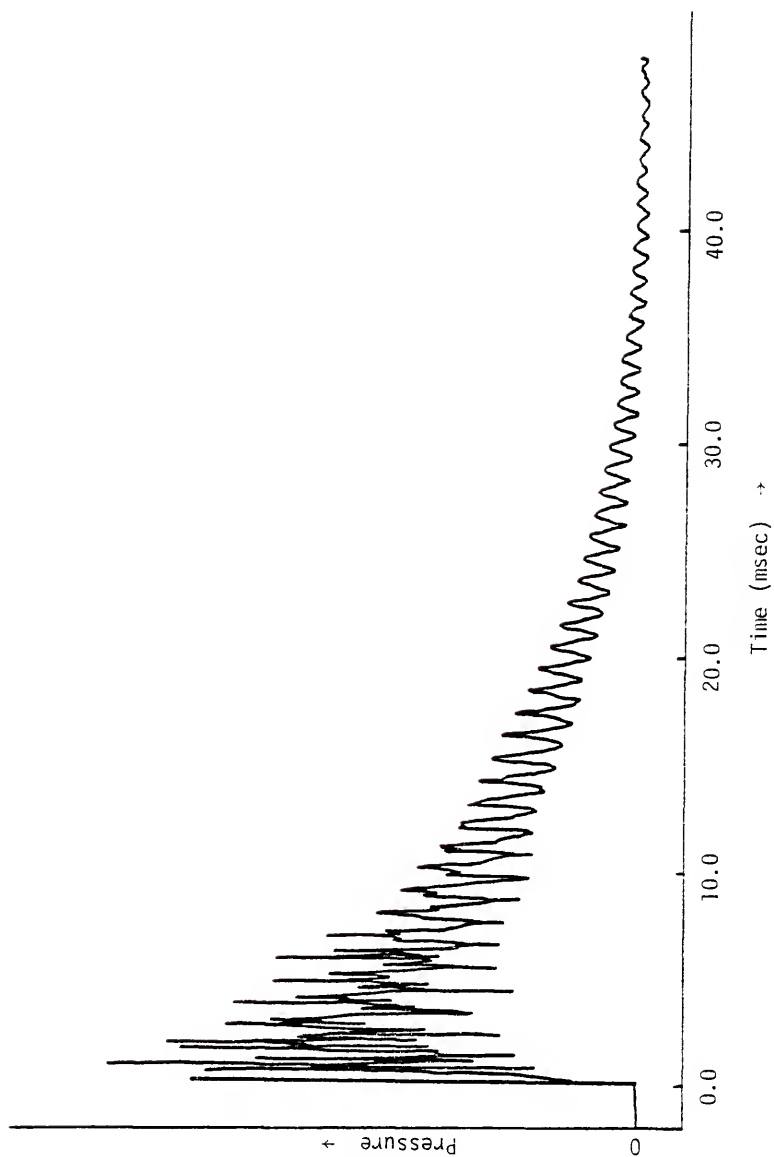


signal averager, false triggering of the signal averager by the Phase-R generated RFI/EMI, and thermal decomposition of the dithione after several hours in the heated cell.

While the Candela laser system was on order, the next attempt was made using an Avco nitrogen laser-pumped dye laser equipped with electronic wavelength scanning drive. No results were obtained because the output pulse energy (200.  $\mu$ J maximum) is insufficient to produce a pressure rise signal greater than the pressure equivalent noise level of about 0.20 mtorr. Therefore, a xenon flashlamp (Vivitar) with wavelength selective filters (Veb Jena<sup>er</sup> Glaswerk Schott & Gen., Jena) was used to provide pulse excitation of the dithione. A typical result is shown in Figure 14. The relatively slow data acquisition rate of the signal averager (20.  $\mu$ sec/channel minimum dwell time) and CM allowed no conclusions to be drawn concerning the crucial initial portion of the spectra; it was decided, therefore, to upgrade the data acquisition system, associated electronics, sample cell, and pressure transducer. In addition, an Ithaco model 1391 low noise, charge preamplifier was purchased to provide amplification for the recently acquired piezoelectric disks and cylinders to be used as fast pressure transducers.

Lack of adequate UV optics and pulse energy measurement equipment led to the decision to use the Candela system only in the visible region. Dithione was once again tried in hopes of improving upon the previous promising results. The piezoelectric transducer (hereafter PT) was used in addition to using the CM. These experiments and the Xe flashlamp ones previously performed were done using sample cell #2. This cell was far easier to load, clean, heat, and mount than cell #1. It could also be pumped down for use with the PT elements. Unfortunately,

Figure 14. The TR0AS spectrum of dithione obtained with a Xe flashlamp (unfiltered) and a capacitance electret microphone. Cell temperature was 55. C.



no significant results were obtained despite modifications to the pre-amplifier circuitry and heating of the sample cell. It was decided, therefore, to conserve the small remaining reserves of dithione for a later attempt.

The next sample substance studied was biacetyl. It was deemed a reasonable candidate for study by TROAS techniques because of the favorable properties listed in Table 7 of the previous chapter. The only anticipated problems were possibly inadequate triplet molar absorption coefficient, possible photochemistry or decomposition, and the definite strong rancid butter odor of biacetyl even in minute concentrations in air. A technical grade sample was repeatedly freeze-pump-thawed (liquid nitrogen and  $10^{-4}$  torr liquid nitrogen-trapped pump) to remove dissolved oxygen and placed in sample cell #2. The biacetyl sample exhibited its characteristic oxygen-free phosphorescence [32]. Several experiments were performed at room temperature using the PT and several different excitation sources. Broadband laser excitation below the triplet ( $T_2$ ) at  $4430 \text{ \AA}$  gave a null result. Broadband ( $70\text{--}100 \text{ \AA}$ ) excitation above  $T_2$  resulted in excitation of the lowest excited singlet with consequent triplet production via intersystem crossing. The result was large amplitude oscillations superposed on a small amplitude exponential pulse. Electronic filtering of the transducer output with an active fourth-order Butterworth filter (equal component Sallen-Key) removed most of the oscillatory features at the expense of the risetime of the buried exponential waveform.

Similar results were obtained when unfiltered broadband Xe flash-lamp excitation was employed. Triplet excitation via intersystem crossing from the easily excited lowest singlet is achieved at light



intensities much lower than those routinely obtained with the Candela system [97]. In fact, triplet-triplet annihilation processes become important at low excitation source intensities [97]. Unfortunately, the resulting TROAS spectrum cannot be interpreted without the direct triplet excitation TROAS result unless the information it supplies is available from other sources.

It was not possible to tune the Candela system to only excite the triplet because it refused to tune or lase narrowband ( $2 \text{ \AA}$ ) just as the Phase-R had. This problem was finally traced to the laser cavity length being too short. Attempts to make the system tune with a laser cavity of about  $2/3 \text{ m}$  were invariably unsuccessful while the system worked perfectly with a cavity of  $2 \text{ m}$ . Alignment did not seem to be at fault though a longer cavity must necessarily emphasize the effects of the dispersion element (diffraction grating) and the alignment is easier.

An unexpected problem with biacetyl was its ability to dissolve ketone-resistant "O"-rings with consequent oxygen contamination of the degassed sample. To avoid these problems, five naphthalene and anthracene derivatives were selected for study. It was hoped that the stability and relative inertness of the compounds would enable the experiment to proceed. The molar absorption coefficient of the 2-chloronaphthalene triplet is approximately  $10^{-3} \text{ l mole}^{-1} \text{ cm}^{-1}$ . The other compounds studied are likely to have similar extremely small values. It is exceptionally difficult to obtain such values by optical means. Unfortunately, this means that the expected pressure rise from these compounds may be below the pressure equivalent noise levels of the system regardless of pressure transducer used. Without the molar absorption coefficients this simply is not known. Nevertheless, the

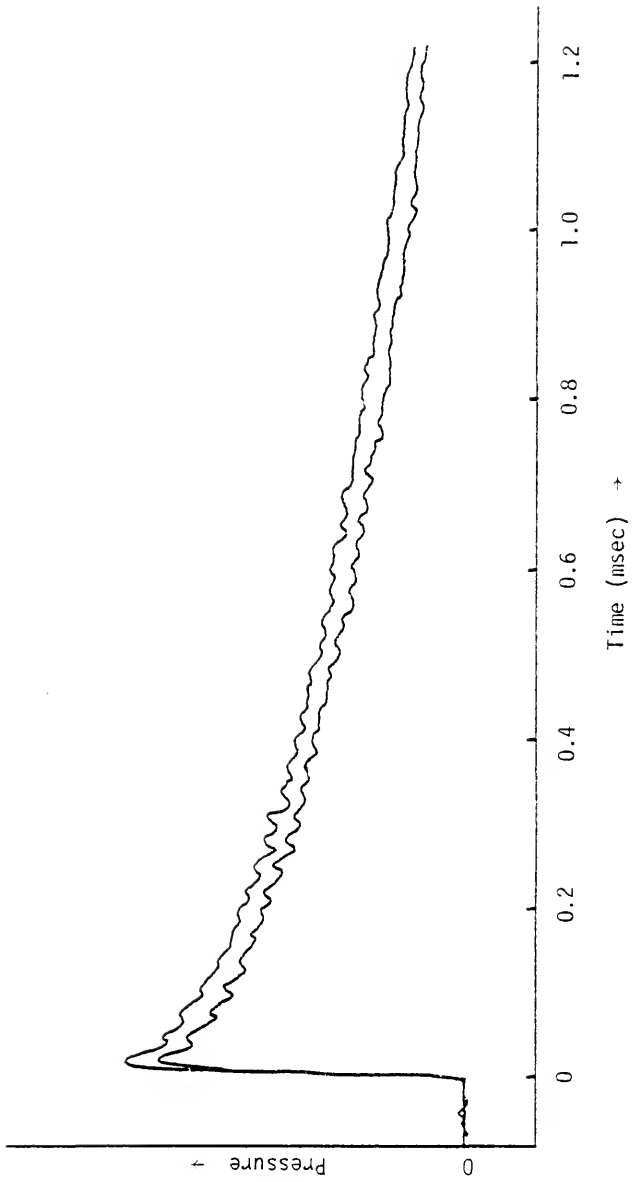
compounds were tried for several reasons: favorable triplet lifetimes, reasonable vapor pressures, photochemical stability, accessible triplet states in the visible, and thermal stability.

Naphthalene was the most studied of the aromatic hydrocarbons. As usual, the initial results were quite encouraging (Figure 15) though incorrect because the exponential decay is independent of carrier gas composition. This cannot be explained if the decay is actually due to thermal reequilibration as it should be. Experiments were done at room temperature and again at approximately 85 C. Experiments were performed with piezoelectric transducers, electret capacitance microphone, and a laboratory-made externally polarized capacitance microphone. Naphthalene was run neat, with air, and with helium at pressures below 760 torr.

Although the triplet wavelengths are known from 77 K glass phase results, they may be shifted in the gas phase. Therefore, the TROAS experiments were carried out by manually scanning the laser from longer wavelengths (below the triplet in energy) to shorter wavelengths (above the triplet). The dye laser was usually scanned over about 500 Å in increments of 10 Å or less.

The effect of wavelength scanning was quite unexpected. Instead of a relatively sharp onset of the pulsed optoacoustic effect, the acquired spectra had maximum amplitude near the dye output energy maximum. The spectra were reduced in amplitude as an extreme in the dye gain curve was approached and invariably the spectra had become no-signal baseline immediately prior to the laser reaching the ends of its tuning range. This was observed with dithione (Rhodamine 6G), naphthalene (Laser Dye 473), and anthracene (Kiton Red S).

Figure 15. The TROAS spectra of naphthalene in helium (upper trace) and in air (lower trace). Carrier gas pressures were 1 atmosphere, cell temperature 85. C, and the Candela dye laser with Laser Dye 473 (broadband) provided excitation.



The behavior strongly suggests that the obtained spectrum is proportional to laser pulse energy but is independent of laser wavelength over several hundred nanometers in the visible. Accordingly, it was tentatively assumed that the obtained spectra were at least partially due to an artifact induced by the laser light pulse or firing sequence.

Anthracene was tried next to see if the same wavelength dependence of the spectrum amplitude would be obtained. As noted above, similar results were obtained. If the cell was carefully cleaned with detergent followed by acetone rinses and then concentrated nitric acid and ethanol, a spectrum could still be obtained. Addition of sample compound caused an increase in signal amplitude and a definite increase in the complexity of the spectrum. This was taken to imply that some part of the spectrum was valid pulsed optoacoustic effect and the remainder was an artifact.

Previous experience with the Phase-R system had shown that significant amounts of RFI/EMI were generated by a laser firing sequence. Shielding was finally effected by constructing an enclosure of brass screen (2 layers), wood, and woven RFI shielding strip. The enclosure was well grounded and an AM/FM radio inside would not play. Therefore, great care was taken to properly ground and shield the Candela system. The Candela laser was mounted on a 1/4" thick aluminum plate and covered with a 1/16" thick solid aluminum enclosure. The laser was run on a separate electrical circuit and computer fired via an optocoupler. These procedures largely eliminated RFI/EMI generated by a laser firing sequence except for an occasional spike produced in the spectrum at the moment of laser firing. With the aid of the microcomputer-controlled transient recorder and a few lines of

assembly language code, it was possible to rule out RFI/EMI as the cause of all but the occasional spike. The spike was found to precede the transducer output of the spectrum by several microseconds and was eventually eliminated by modification of the amplifier circuitry.

To determine whether a real pulsed optoacoustic effect exists, iodine was run in cell #2. Although iodine cannot be modeled with a simple two state model, it does absorb strongly in the visible, has a vapor pressure of 0.53 torr and 300 K, and is capable of exciting the metastable, long-lived (45 minutes) oxygen  $^1\Delta_g$  state [87]. Thus, the behavior of iodine vapor differs in air from its behavior in helium. The reactivity of iodine, especially in the presence of traces of moisture, precluded use of a capacitance microphone largely constructed of aluminum. Although the silver metallization on the PT elements was attacked by the iodine vapor, intermittent operation was not especially troublesome after the silver was gone. An iodine spectrum is shown in Figure 16. The cell was at room temperature (25 C) and spectra were obtained neat, with air at various pressures, and with helium at various pressures. Figure 16 shows that a pulsed optoacoustic effect is indeed observable.

After iodine, the remaining three compounds in the aromatic hydrocarbon series were run. Figure 17 shows a 9-bromoanthracene spectrum obtained using the PT. Similar results were obtained with helium as carrier gas. No results were obtained with 1-chloroanthracene or with 2-chloronaphthalene. Air was used as the carrier gas for the chlorinated aromatic hydrocarbons. The artifact interfered with all of the previous spectra to some extent.

Figure 16.

The TROAS spectrum of iodine at 25. C in air at atmospheric pressure. The pressure transducer was a piezoelectric ceramic disk. Excitation was provided by the Candela laser operating broadband with Coumarin 540 laser dye. The time axis is reversed from the standard "right-handed coordinate system" due to a quirk in the chart recorder design.

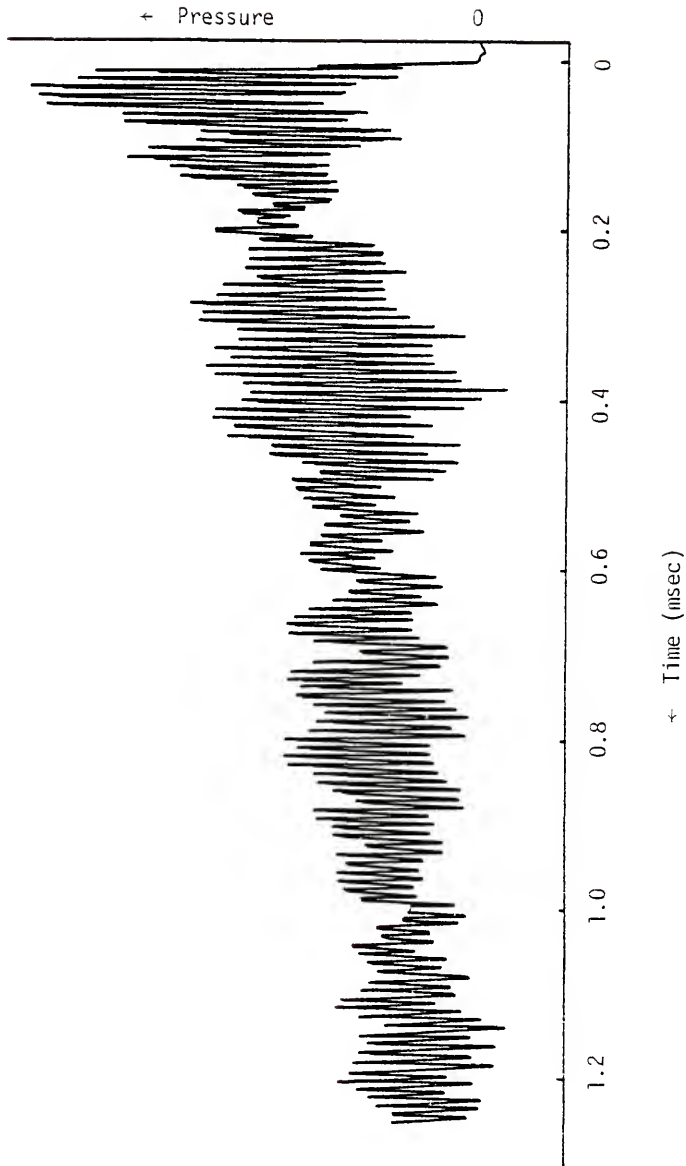




Figure 17. The TROAS spectrum of 9-bromoanthracene in air at atmospheric pressure with the piezoelectric transducer used to detect the signal. The Candela laser was used broadband with Kikon Red S laser dye. Cell temperature was 80. C. The time axis is reversed from the usual convention as in Figure 16.

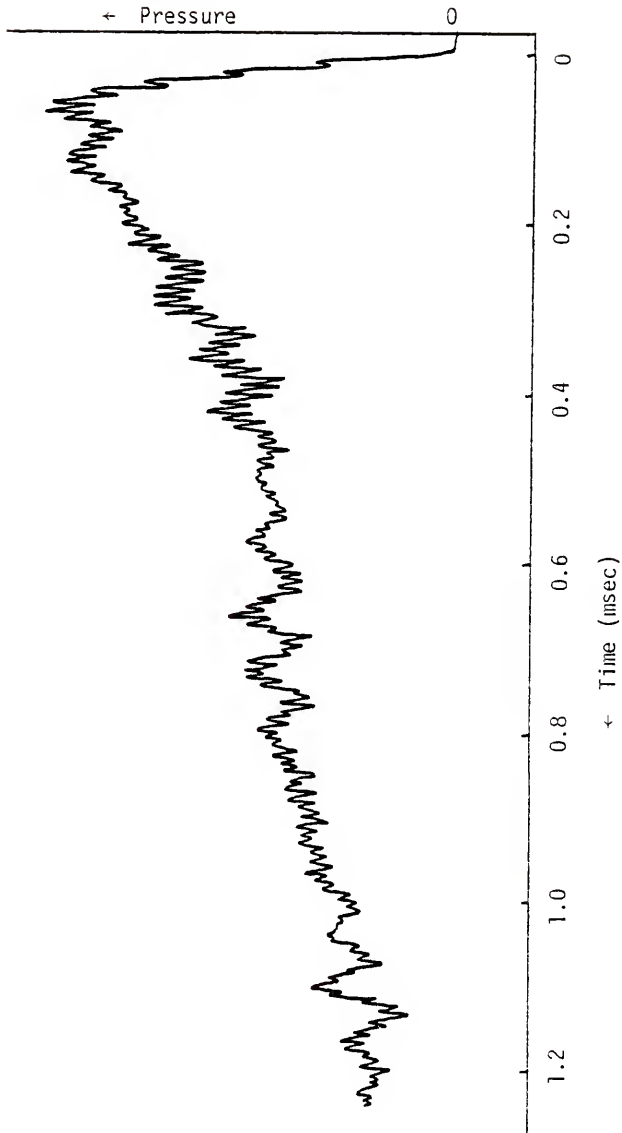
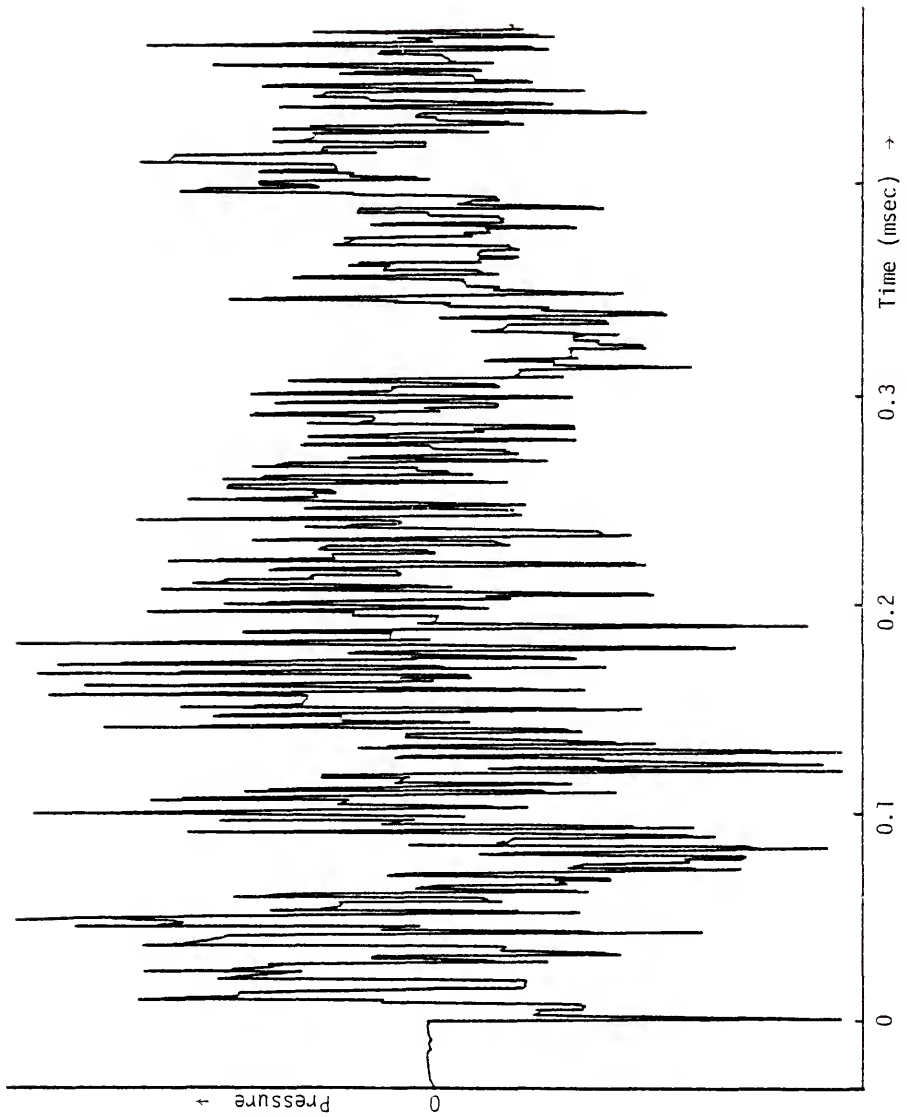


Figure 18 shows a typical TROAS artifact spectrum. To analyze such results, a Fortran Fast Fourier Transform program was converted to Basic and assembly language (on the 6502-based PET microcomputer) [77]. With the aid of this FFT subroutine, many spectra were obtained and processed at various transient recorder sampling rates. The FFT subroutine was tested for accuracy with summed signal generator input, and it was tested on data calculated from an analytic exponential pulse. The transform calculated from the data via the FFT subroutine was essentially identical to the transform calculated from the analytic Fourier transform.

Almost all of the processed spectra showed peaks at about 100. KHz, 204. KHz, 450. KHz, and 750. KHz. In addition, mechanical resonances of the sample cell may be excited by external sounds (whistling or snapping one's fingers) or by external vibrations (light tapping of the cell or nearby equipment). These frequencies were primarily in the range between 2.5 KHz and 8.0 KHz. Even the sound of the laser driver spark gap when triggering occurs can excite the cell mechanical resonances. Fortunately, cell mechanical resonances were of little importance since the transient recorder was usually done acquiring a spectrum before the spark gap sound could reach the cell. Acoustic shielding was not necessary at any time.

In an attempt to avoid the artifact, sample cell #4 was constructed. Despite the switch to (roughly) spherical symmetry, the expected pressure rise should be approximately the same. The acoustic resonances would be expected to occur at different frequencies than in the cylindrical cell. Note that the longitudinal acoustic resonances in the cylindrical cell are harmonically related while the radial modes are

Figure 18. An artifact TROAS spectrum obtained with air at 25. C and atmospheric pressure in the sample cell. A stainless steel disk in front of the piezoelectric transducer prevented light from directly striking the transducer. The axes have been changed to the conventional "right handed coordinate system" by appropriate microcomputer programming (i.e., the 8 bit value to be output to the D/A is subtracted from hexadecimal FF and the result is output).



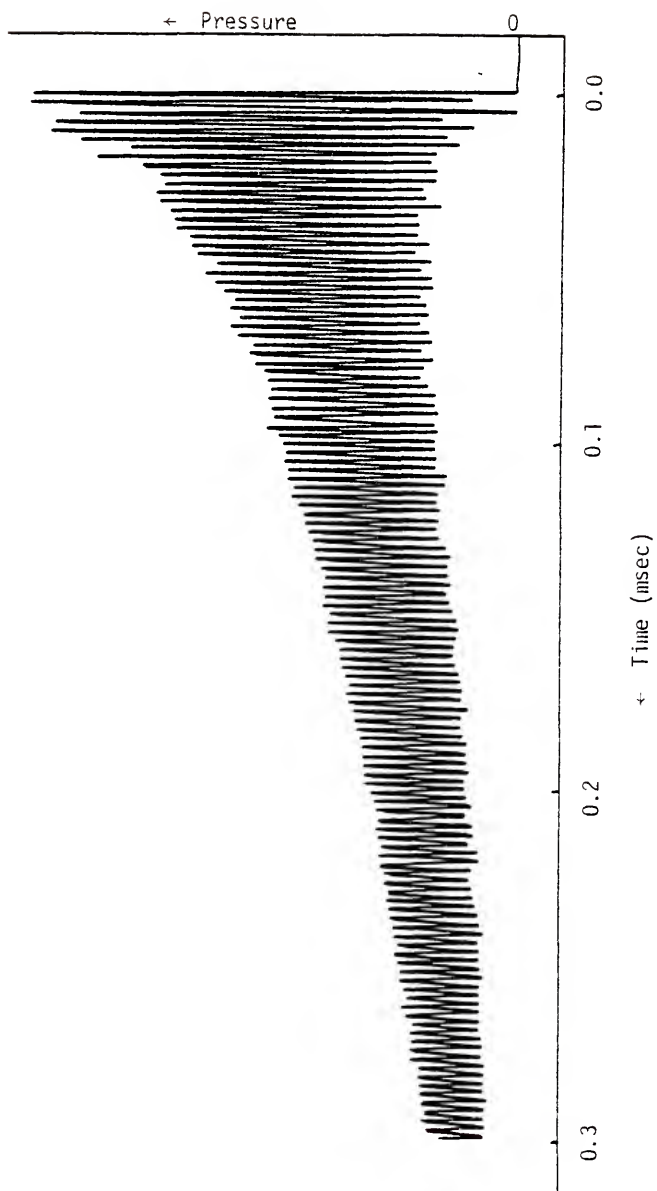
proportional in frequency to the roots of the integral Bessel function  $J_1$ . Thus, the radial resonances are not harmonically related. In a spherical cell, the modes are related to the spherical harmonics and thus the new cell should aid in determining whether the acoustic modes are excited as expected.

Solid anthracene was placed in cell #4 and strongly heated in vacuo. The vapor pressure of anthracene at 25 C is very low (0.38 mtorr) but is 0.57 torr at the approximate temperature used (150. C). Experiments at both temperatures quickly revealed that the PT produces an output signal when struck by light. Experiments with an empty cell and both Candela system and Xe flashlamp gave similar results. The output waveform was found to be an exponential waveform with amplitude approximately proportional to light intensity. Blocking the direct light path from excitation source to transducer by placing a small piece of electrical tape on the outside of cell #4 eliminated the artifact completely.

It was known that piezoelectric transducers are susceptible to light generated artifacts; they may, for example, give a response to the shock front-induced luminescence in shock tube experiments (where the transducers are used for pressure measurements) [62]. The amount of light scattered onto the pressure transducer when installed in cell #2 was found to be small. This was determined by removing the transducer and firing the laser repeatedly, under microcomputer control, while looking into the port. Very little light was scattered from the side walls of the cell out the side port.

Nevertheless, when the piezoelectric transducer is directly exposed to the laser output, the result is shown in Figure 19. The

Figure 19. The output of a piezoelectric transducer directly exposed to a laser light pulse of high intensity. The 204. KHz ringing is evident.





signal is so large no amplification was needed. The FFT of this spectrum has components at 204. KHz (very large), 450. KHz (small), 750. KHz (small), and negligible background. Since the nominal resonant frequency of the particular transducers used is 160. KHz, the 204. KHz peak was tentatively identified as the actual resonant frequency of the transducer. This was verified by direct excitation of the normally mounted PT using an externally mounted PT driven by an audio sine wave generator. No output was obtained until frequencies of 203. KHz, 450. KHz, and 750. KHz were selected on the signal generator.

This was not, however, the only artifact. Sample cell #3 was devised to determine whether the artifact was due in part to an elastic wave in the sample cell. Anthracene was melted in vacuo into intimate contact with the glass cell, and a piezoelectric disk was firmly pressed against the outside of the glass. See Figure 7 for details. The PT was electrically shielded and also shielded from the effects of direct light by the small, snugly fitting aluminum enclosure. Nonreproducible results were obtained with both the laser system and broadband flash-lamp excitation at room temperature (where the vapor pressure is a negligible 0.38 mtorr).

With the aid of nitrogen dioxide, the sensitivity of the PT was compared to that of the CM and found to be a relatively poor 20. mV/mtorr. As with iodine, the study of  $\text{NO}_2$  is not feasible because of the complexity of its spectrum. It does not, however, attack aluminum or stainless steel.

The matter of the acoustic resonances was still not resolved, and the artifact was not solely due to the direct effect of light. To clarify the situation, a very small cell was constructed (cell #5).

With a small cell, the acoustic resonances shift to higher frequencies, and the mechanical resonances are also shifted upwards in frequency because of the size and mass reduction. It was hoped that the rise-time of the pressure rise would be only marginally impaired by the increased importance of wall effects [59].

Sample cell #5 was a modified Cajun Ultratorr 3/8" tee connector. It was machined to accept either a PT disk or a CM. Naphthalene was placed in the unheated cell, and the Candela system was used to try to excite the triplet state. The results were similar to those obtained in the much larger cell #2. To eliminate the light-induced artifact, a stainless steel disk was placed in the pressure transducer port in front of the transducer. The experiments were repeated with and without naphthalene in the cell and with both transducers. The result was an artifact spectrum in each case. Turning the cell so that the laser pulse struck the outside of the cell also gave an exponential pulse artifact spectrum.

This result was also obtained with cell #2. It was completely unexpected since previous experiments with the relatively massive cell #2 (mass greater than 5. kg) had involved the use of a variable aperture between the laser output mirror and the sample cell. It was also noted that only a small amount of incident light struck the cell walls.

With this information, dithione was placed in cell #2 in an attempt to finally get an artifact-free TROAS spectrum. Through the use of multiple irises, the laser pulse was prevented from striking any portion of the cell other than the Suprasil windows. Again, no significant results were obtained regardless of cell, transducer, carrier gas, or beam diameter. A curious result of the use of the irises was the

need for three of them positioned as far apart as possible in the space between the laser output mirror and the sample cell. The approximately 1" diameter laser beam had to be narrowed to slightly less than 1/5" to significantly reduce the effect of the artifact. It was not sufficient to merely eliminate a line of sight path from the laser cavity to the nonwindow portion of the cell. This, naturally, greatly reduces the laser energy incident upon the sample and cell windows. For a TEM<sub>00</sub> Gaussian beam of diameter 1" with an aperture of 1/5" diameter, the ratio of transmitted energy to incident energy is

$$1 - e^{-2(0.2/1.0)^2} = 0.077.$$

For a multimode beam, the result is

$$(0.2/1.0)^2 = 0.040.$$

Thus, between 4% and 8% of the incident energy is passed along to the sample cell.

Consequently, irises were dispensed with and a simple test tube was used as cell #6. The CM was snugly inserted into the test tube mouth after solid dithione was placed in the test tube. The CM was wrapped with Teflon tape to achieve the snug fit required to give immunity to extraneous room noises. The cell was heated with a separately mounted heat gun. No results of a reproducible nature could be obtained.

Since the curved test tube might perhaps reflect light onto the CM, another highly transparent cell was constructed (see Figure 9). The diameter of the cylindrical cell was more than large enough to allow the full laser beam to traverse the cell length without impinging on

the cell walls. Nevertheless, the irises were used to produce a 1/2" diameter beam to be certain scattered light would not be troublesome. Laser firings showed that light scatter and reflections were negligible. Dithione solid was placed in the cell, and the cell was heated by the previously mentioned heat gun. The CM was used as the pressure transducer. Again the only spectra obtained were contaminated by an artifact. The empty cell gave similar results. Turning the cell so that reflected light definitely struck the front of the CM did not increase the artifact amplitude.

Finally, a PT was epoxied to the rear of a small front surface mirror which was then epoxied to a corner of the square glass plate used as the rear window of cell #7. The PT gave a distinct artifact output when a laser pulse traversed the cell whether air or helium was used as carrier gas in the cell. No absorbing substance was placed in the cell.

Several details were neglected in the above rather concise description of the experimental arrangements. First, several substances, for example, iodine and naphthalene, were run at times other than those listed above in addition to the described sequence. Second, the charge preamplifier was replaced with various voltage preamplifiers during the course of the experiments. The charge preamplifier was found to be noisy, did not prove immune to cable microphonics, and did not provide adequate gain.

Another recurring problem was condensation of sample on the cell windows. This was definitely the cause of an artifact signal. Consequently, the cell was heated until any condensed sample vaporized or melted and drained away.

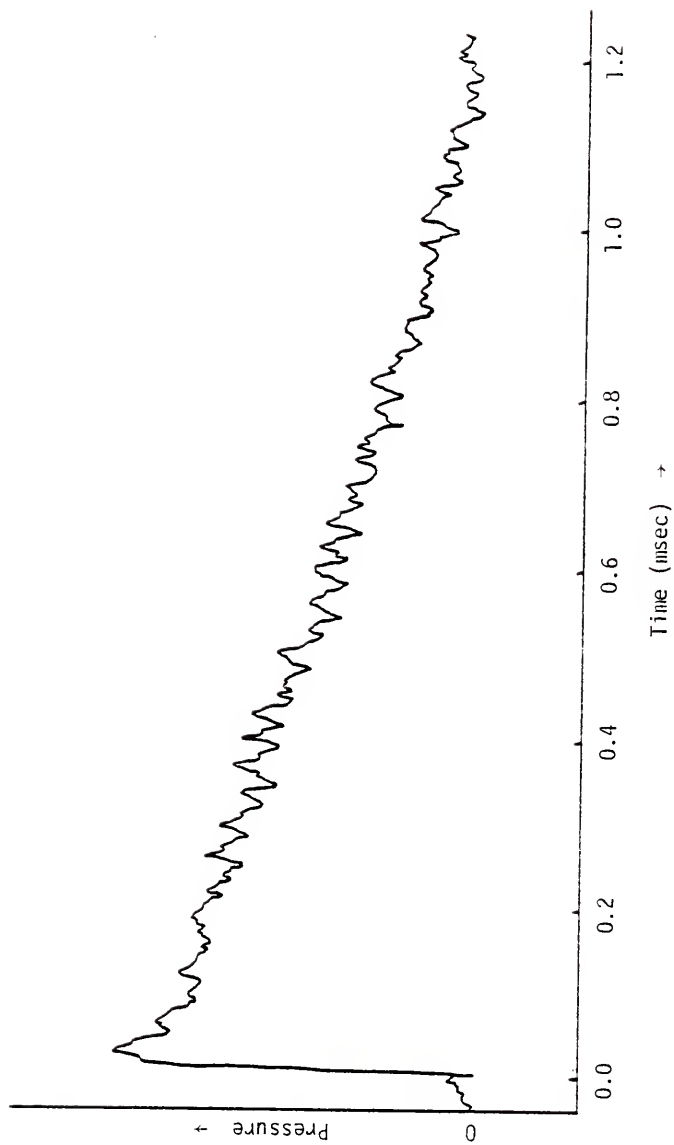
The laser tuning problem was peculiarly difficult to correct because of its unusual nature. Three different diffraction gratings, two rear mirrors, and eight front reflectors (three laser mirrors and five neutral density filters) were used in attempts to achieve narrow-band tuning. Numerous laser dyes failed to tune despite concentration changes, pumping speed variations, and an attempt to modify the solvent pH with acetic acid [56]. A call to the president of Candela Corporation (Dr. Horace Furumoto, one of the developers of the coaxial flashlamp [98-100]) was of little help though his suggestions concerning the addition of a bubble trap/particle filter and the necessity of turbulent dye solution pumping were immediately implemented. Cavity length was simply not suspected since both Candela and Phase-R sell short (about 45 cm) optical benches for use with their systems. Additional steps taken to eliminate the tuning problem, prior to discovering the cause, included use of intracavity irises and even use of a low reflectivity mirror between the grating and flashlamp [101].

## CHAPTER SIX

### RESULTS

That a pulsed optoacoustic signal was observed in these experiments seems established beyond reasonable doubt. On numerous occasions, a blank was run by illuminating a clean, evacuated cell. An additional blank was run with air in the cell and then sample substance was added and allowed to equilibrate. The resultant spectrum was always larger in amplitude and reproducibly more complex. This was especially easy to observe with iodine or nitrogen dioxide as samples but was also observed with dithione, biacetyl, naphthalene, and 9-bromoanthracene. Figure 20 shows the spectrum obtained in a run with a clean, empty ( $10^{-4}$  torr) cell under conditions almost identical to those used to obtain the naphthalene spectra of Figure 15. Although the blank was run with four times higher sensitivity than that used for the naphthalene spectra, the artifact is plainly visible even without the aid of increased sensitivity. Unfortunately, the artifact was not reproducible. It was found to vary in amplitude as much as tenfold from one shot to the next. The laser was not especially stable in output pulse energy (about 10%) but was not directly responsible for the gross variations in artifact amplitude. Furthermore, the waveform of the artifact is only roughly an exponential pulse and varies from shot to shot. This rules out any possibility of signal averaging or subtraction of the artifact from the artifact-containing spectrum.

Figure 20. The TROAS spectrum obtained with an empty ( $10^{-4}$  torr) cell. Except for increased transient recorder input sensitivity (4X), the experimental conditions were precisely the same as those used to obtain the naphthalene spectra of Figure 15. No light struck the piezoelectric transducer because a stainless steel disk was positioned in front of the transducer in the pressure port.





Although differential mode operation with two sample cells is possible, it will not eliminate the artifact. If the cells are arranged coaxially, the second cell will receive less light than the first and will also receive more scattered light. In addition, the second cell cannot present exactly the same environment as the first because it does not contain an absorbing sample. Furthermore, the cells must thermally track to avoid thermal drift in the transducer outputs and any buildup with time of absorbing or scattering films (due to decomposition of sample, for example) must be identical in the cells.

Similar restrictions apply to the standard dual-beam configuration since alignment becomes difficult, and the cells must be precisely equidistant from external noise sources such as the flashlamp driver unit spark gap. Nevertheless, Deaton et al. have used the series arrangement in low source intensity OAS [102], and Hordvik and Schlossberg [103] have used dual piezoelectric transducers in differential mode with lock-in amplifier detection. Even so, they were limited by the in-phase spurious response of their system.

As stated previously, cell mechanical resonances were not especially troublesome though the vacuum system did have to be disconnected from the cell to avoid pickup of the rotary oil pump noises. Condensation of sample on the cell windows definitely produced an artifact. Both of these artifacts may be easily avoided by proper design.

This is not true of the acoustic resonances. It would be best to avoid, as much as possible, putting energy into the acoustic modes since this reduces energy available to produce the concomitant pressure rise. This means that the excitation beam should have a diameter equal to

the cell diameter. But an artifact is produced if any portion of the cell is illuminated. Hence, the acoustic modes are not easily minimized. Electronic filtering is possible, but cumbersome, since six or more sharp notch filters may be needed, and they must be readily tunable since the acoustic mode frequencies are dependent on the speed of sound in the sample. In addition, signal risetime may be degraded unless care is taken.

For this reason, an attempt was made to employ the technique of mathematical (or digital) filtering. Briefly stated, this technique involves transforming a time domain spectrum to the frequency domain via the FFT algorithm, removing or modifying selected frequencies and transforming back to the time domain. The advantage of digital filtering is that perfect filters can be rapidly implemented. Any desired transfer function and phase shift can be easily implemented even if they are physically impossible to realize. Thus, the acoustic resonances and cell mechanical resonances could be eliminated without degrading either the low or high frequency response of the acquired signal.

This attempt came to naught because the 8 K of RAM on the PET microcomputer proved insufficient to contain the main program and the necessary array storage needed by the FFT algorithm. It should be noted that the FFT subroutine in Appendix Four cannot be used directly to back transform since it computes the 128 point power spectrum of 256 real input spectrum points. Nevertheless, the subroutine contains the complex Cooley-Tukey algorithm needed to perform the back transform. In fact, the necessary modifications were made and even a 128 point input spectrum caused memory overflow problems.

The corrected mode amplitude equation (A1.20) and the signal amplitude equation (A2.1) may be used to compute the ratio of the amplitudes of the lowest radial mode and the pressure rise. The result is

$$A_1(\omega_1)/A_0(0) = Q_1/\omega_1 t_T \quad (6.1)$$

where  $\omega_1 = \alpha_{1,1}c/A$  is the lowest radial frequency,  $\alpha_{1,1}$  is the first nontrivial root of  $J_1$  (3.832),  $A$  is the cell radius, and  $c$  is the speed of sound in the sample. For cell #2,  $\omega_1$  is  $99.9 \times 10^3$  radians/sec in air at STP. The amplitude ratio is thus

$$12./(99.9 \times 10^3 \text{ sec}^{-1})(2.7 \text{ sec}) = 4.4 \times 10^{-5}$$

where  $Q_1$  is assumed to be 12. (the approximate measured value for cell #2). The value of  $Q_1$  was obtained using a signal generator, oscilloscope, and small speaker attached to cell #2. Values of  $Q$  as high as 890 have been reported in the literature [23].

Actually, the amplitude of the acoustic modes depends on the sample composition and is definitely larger than the above ratio suggests. The acoustic resonances are of large amplitude in iodine, moderate in 9-bromoanthracene, small in dithione, and very small in naphthalene. Evidence for the existence of the acoustic modes is not as clear-cut as might be hoped since the artifacts, particularly the 204. KHz transducer resonance, obscure the acoustic modes. The longitudinal and radial mode frequencies are given by

$$2\pi f_{1n_z} = \omega_{n_z} = \pi c n_z / L \quad \text{for } n_z = 1, 2, 3, \dots, \text{ and} \quad (6.2)$$

$$2\pi f_{ri} = \omega_i = \alpha_{1,i} c / A \quad \text{for } i = 1, 2, 3, \dots \quad (6.3)$$

If an FFT is performed on a typical spectrum, the obtained frequencies will not generally completely match the acoustic mode frequencies given by the above equations although as many as five matchups may occur. The odd thing about the matches is that the spectrum might contain only the lowest two radial modes and the third and fifth longitudinal modes.

One explanation for this is that sampled acoustic mode frequencies which are not sampled precisely an integer number of times will appear as a rather broad band (6 to 10 or so) of peaks in the FFT spectrum. This phenomenon is called leakage, and it may be minimized by reducing the sampling rate (for better resolution) and by smoothing the raw spectrum before processing (a process called apodization) [104]. In the present case, the program used is quite similar to that of the above reference, and leakage was definitely shown to exist by using a signal generator as the input source.

Reduction of the sampling rate was not feasible in the present case because of the strong 204. KHz piezoelectric transducer resonance. If the 204. KHz signal is not removed and the sampling rate is sufficiently reduced, aliasing will occur. If filtering is employed, care must be taken to avoid distorting the spectrum in other ways. In particular, the risetime must not be limited by the filter.

Whether the acoustic modes are observed is of little significance if the transducer artifacts cannot be eliminated. The experiments outlined in the preceding chapter were not successful in eliminating the artifacts, but they do suggest the causes. Consider first the light generated artifact. Bradley [62], Hordvik and Schlossberg [103], and Farrow et al. [69] note that piezoelectric transducers produce a spurious output signal if exposed to the illumination light source. Bradley

claims the effect is pyroelectric in nature, so presumably the effect is directly proportional to the incident light intensity. This is reasonable if the output voltage is directly proportional to the stress which in turn is proportional to the heat generated in the transducer by absorption. Hordvik and Schlossberg confirm the thermal nature of the effect and the proportionality. It is not possible to baffle the light without possibly setting up new cell resonances (e.g. Helmholtz resonances [105]) and attenuating the acoustic signal. Nevertheless, a small plug of opaque foam (used to protect CMOS or n-MOS integrated circuits normally) was placed in front of the transducer without benefit. The cell (#2) was even lined with brass screen to block the light without greatly impeding the desired pressure rise. This, too, was unsuccessful.

The light-induced artifact is not avoidable even by reducing pulse energy because both signal and artifact are directly proportional to source intensity for given pulse width, and they are commensurate in magnitude. Hordvik and Schlossberg [103] state that "in our experiments the sensitivity was not limited by electronic or environmental noise, but rather by the signal generated by radiation scattered from sample inhomogeneities onto the transducer." The samples used there were large crystals of  $\text{CaF}_2$ ,  $\text{SrF}_2$ , and  $\text{BaF}_2$ . Dual piezoelectric transducers in differential mode were used (as noted previously) to measure absorption coefficients down to  $10^{-5} \text{ cm}^{-1}$ , and they note that  $10^{-6} \text{ cm}^{-1}$  is obtainable with 1 W of laser excitation power if scattering can be avoided. Farrow et al. have performed OAS and pulsed OAS studies on opaque solids using piezoelectric detection of the resultant elastic wave in the solid [69]. They note that signal averaging is necessary

even with opaque solids because of the low signal to noise ratio of individual acoustic transients. The excitation pulses were supplied by an acousto-optic modulator following an argon ion laser and pulse width was 1 msec. The front surface mirror technique for coupling elastic waves from sample to transducer while blocking incident light is due to Farrow et al. It was tried with cell #7 to determine whether the cell itself generates the indirect artifact. It does. In fact, while the lasers used by Farrow et al. had an average output power of 190. mW, the average output power of the Candela system used here was greater than 1. MW. Hence, the transducer and front surface mirror combination did not "block the light" and thereby eliminate an artifact. When the Candela system was fired directly onto the mirror, a large exponential waveform was produced by the transducer. The cause is absorbance by the mirror.

The results of Hordvik and Schlossberg [103] are important in understanding the nature of the indirect artifact. They note that the piezoelectric transducer may be used to measure the strain produced in the solid sample following illumination. The equation they arrive at is [103]

$$e_{rr} = -e_{\theta\theta} = -\alpha P \alpha_0 (1 + \sigma) t / 2\pi C \rho (1 - \sigma) r^2 \quad (6.4)$$

where  $e_{rr}$  and  $e_{\theta\theta}$  are the relevant strains,  $\alpha$  is the absorption coefficient,  $P$  is the total beam power,  $\alpha_0$  is the thermal expansion coefficient,  $\sigma$  is Poisson's ratio,  $C$  is the specific heat,  $\rho$  is the density, and  $r$  is the detector position. Typical values for their experiments were  $\alpha = 10^{-4} \text{ cm}^{-1}$ ,  $P = 0.1 \text{ W}$ ,  $\alpha_0 = 10^{-5} \text{ K}^{-1}$ ,  $t = 5 \times 10^{-3}$ ,  $r = 2 \text{ mm}$ ,  $C = 1 \text{ J g}^{-1} \text{ K}^{-1}$ ,  $\rho = 3 \text{ g cm}^{-3}$ , and  $\sigma = 0.3$ . With these values,

$e_{rr} = -1.23 \times 10^{-12}$  which is sufficient to produce a transducer output of several microvolts. It is important to note that the transducer output is directly proportional to the strain so transducer output is proportional to incident laser power and to sample absorption coefficient. The strain (and signal) will vanish if the thermal expansion coefficient is zero.

The importance of acoustic impedance matching is now apparent. The piezoelectric transducer is well coupled to the sample cell since both are solids, and the reduced pressure in the sample cell would act to force the transducer more tightly against the sample cell. If the above equation is solved for a Suprasil 2 quartz window, the result is

$$e_{rr} = - \frac{(10^{-4} \text{ cm}^{-1})(10^6 \text{ W})(5.5 \times 10^{-7} \text{ K}^{-1})(1 + 0.17)(5 \times 10^{-3} \text{ sec})}{2(0.75 \text{ J g}^{-1} \text{ K}^{-1})(2.20 \text{ g cm}^{-3})(1 - 0.17)(0.2 \text{ cm})^2}$$

$$= -2. \times 10^{-6}$$

where the absorbance of Suprasil 2 is assumed to be  $10^{-4} \text{ cm}^{-1}$ . This is definitely too large, but it indicates, nevertheless, that even a Suprasil 2 window may be expected to produce a signal when illuminated by the high intensities available from the Candela laser system. The production of an artifact signal when sample vapor condensed on a window and was illuminated, is explained by the excellent acoustic impedance coupling obtainable even with liquid droplets on the windows (where  $\alpha_t = 0.2$  typically). This mechanism will be designated the strain artifact.

Parker [40] has also observed an artifact due to optical absorption by borosilicate glass of light of wavelengths shorter than  $2.5 \mu\text{m}$ . He used a conventional OAS apparatus with capacitance microphone pressure

transducer and high pressures (to 35 atmospheres) of nonabsorbing gases such as Ne, N<sub>2</sub>, and O<sub>2</sub>. His experimental results support the predictions of his theoretical model that a thin boundary layer in the window material absorbs light, produces heat, and by thermal diffusion into the carrier gas, periodic pressure fluctuations are produced. These fluctuations take place in a boundary layer of carrier gas proportional to the thermal diffusion length in the gas. This mechanism was independently arrived at by Rosencwaig and Gersho [44], who used it to explain their results on the OAS of solid samples. They elaborated upon the similar results of Parker. Rosencwaig has also noted that "the cyclical expansion and contraction of the solid cannot be the major source of the signal" [106].

The thermal diffusion length is the distance over which a thermal wave is attenuated by  $e^{-1}$ . The Rosencwaig and Gersho model applied to situations where the substrate and carrier gas were thermally thick (i.e., the thermal diffusion length is much less than the thickness of the substance). The sample applies to the model used by Parker. These results were further extended by Aamodt, Murphy, and Parker [107] to allow for thermally thin substrate and gas phase. This extension gives better results but not quite good enough.

Accordingly, McDonald and Wetsel, Jr., [45] extended the solutions further to include precisely the effect Rosencwaig omitted. Acoustic waves in the condensed phase sample result in a mechanical motion of the sample surface. This mechanical piston action couples with the previous thermal piston action in what is dubbed the composite piston model. This model is the basis of standard condensed phase OAS experiments which employ capacitance microphones to detect the heat-flow generated



acoustic waves in the carrier gas. Since acoustic waves are set up in the sample, due to cyclic thermal expansion and contraction of the sample, these may be detected directly by an appropriate transducer. This has been called thermoacoustics [108]. Whatever its name, it is much more efficient than the slow thermal piston type of standard experiments because the carrier gas and slow thermal waves may be dispensed with and the acoustic impedance mismatch corrected.

The results of Hordvik and Schlossberg [103] are based on detection of the strain produced in single absorbing crystals. Farrow et al. [69] have noted that the acoustic waves (elastic waves) in the condensed phase samples can be detected very efficiently with piezoelectric transducers precisely because of the excellent acoustic impedance match. That acoustic waves are indeed generated when a solid absorbs pulsed light was demonstrated by White [15]. Brienza and DeMaria [46] have obtained similar results and attribute the acoustic waves to absorption of light with subsequent thermal generation of acoustic waves.

The significance of these results is that the cell windows generate two types of spurious response via the composite piston model and the efficiency of most transducers in responding to substrate acoustic waves. Note that using a capacitance microphone will not help significantly because though the microphone may be less sensitive to substrate elastic waves, it will be more sensitive to the carrier gas acoustic waves, which are the predominant problem as the accuracy of the relatively simple Rosencwaig and Gersho model shows.

This is also verified by Dewey, Jr., who notes that in conventional OAS "the dominant source of background noise is absorption at the cell

windows" [65]. He remarks that the windows produce an in-phase signal while surface absorption at the cell walls produces an out-of-phase signal. The result of his analysis of the situation is that the thermal piston action will be minimized for windows of high density, high heat capacity, and high thermal conductivity. This minimizes heat flow into the carrier gas. To avoid the strain artifact, window absorbance must be minimized by choice of material and window thickness, and the thermal expansion coefficient must be minimized.

Capacitance microphones are also susceptible to light-induced artifacts as noted by McClelland and Kniseley [109]. They state "microphones are often highly sensitive to scattered light because absorption at the microphone couples efficiently to the microphone diaphragm." The Princeton Applied Research Model 6001 photoacoustic spectrometer uses a capacitance microphone to detect the acoustic signal. It is isolated from the sample chamber via an interconnecting duct with several right-angle bends to trap scattered and reflected light and thereby avoid producing a light-induced artifact.

Since all three of the artifacts are proportional in amplitude to the laser pulse intensity, they may be ameliorated by reducing the laser intensity. This is not possible, however, unless a sample substance is found which is markedly superior to the substances chosen for these studies.

Several additional experiments were attempted during the course of the previous gas phase experiments. A cylindrical piezoelectric transducer was filled with a saturated solution of anthracene in ethanol and illuminated with both the Candela laser and broadband flashlamp excitation. It was not possible to obtain results similar

to those of Callis et al. [20] because of the artifacts. Placing the cylinder inside cell #2 and filling the cell with an acetone solution of dithione gave similar results. The laboratory-made microphone also produced an artifact.

An attempt was made to use cell #4 with solutions of anthracene (saturated) in ethanol and eosin in ethanol. The direct light artifact was apparent, but the decay time constant was four times longer for 200 proof ethanol than for a dilute solution of eosin in ethanol.

An experiment was also performed with the front surface mirror and piezoelectric transducer combination. As previously stated, the laser pulse causes an artifact when the mirror is struck. A ruby boule approximately 1 cm thick was epoxied to the front surface mirror. Pink ruby has an absorbance of about  $3.3 \text{ cm}^{-1}$  at  $5600 \text{ \AA}$  [110]. The absorbance is from approximately  $4900 \text{ \AA}$  to  $6100 \text{ \AA}$ . Consequently, the laser system was operated with Rhodamine 6G broadband. No increase in signal was observed. Note that if the excitation source intensity is low enough to be completely absorbed by the sample on the mirror, signal averaging may be used to improve the S/N ratio of the transducer output, if necessary. In the experiments of Farrow et al. the average source intensity (190. mW) was low enough to require averaging of as many as  $10^3$  acoustic transients.

## CHAPTER SEVEN SINGLET TIME-RESOLVED OPTOACOUSTIC SPECTROSCOPY

If it is difficult, as Eddington has said, to empty the well of Truth with a leaky bucket, then we must content ourselves with the use of a cup. Consider, for example, the results of Callis et al. [20] concerning the triplet yield of anthracene in ethanol solution. Using broadband flash-lamp illumination, capacitance microphone volume change detection, and signal averaging, they obtained average triplet yields of 0.66. This compares favorably with values of 0.72 in ethanol [51] and 0.58 in liquid paraffin [48]. The equation from which their results were obtained is

$$\phi_t = Q_s(h\bar{\nu}_{in} - \phi_f h\bar{\nu}_f) / Q E_t \quad (7.1)$$

where  $Q_s$  is the slow heat,  $Q$  is the total heat ( $= Q_s + Q_f$ ),  $E_t$  is the triplet state energy,  $h\bar{\nu}_{in}$  is the average exciting photon energy,  $h\bar{\nu}_f$  is the average fluorescent photon energy, and the capacitance microphone signal is directly proportional to the released heat. The equation was derived assuming  $\phi_p$  is much less than  $\phi_t$ . The model used is the same as that presented in the introduction with  $k_{T_1}^v$  neglected and  $k_{T_1^v, T_1^0}$  large relative to  $k_p^*$ . Note the similarity with the result obtained by Wrobel [47]

$$\phi_t = P'_s(h\nu_{T_1^v, T_1^0}) / P'_f h\nu_{T_1^0} \quad (7.2)$$

The above equation (7.2) applies to the case of direct excitation from  $S_0$  to  $T_1^V$ . Consider now the case of direct excitation from  $S_0$  to  $S_1^0$ . Since this is a spin-allowed process, much lower incident light intensities should suffice. This means that all of the artifacts will be reduced in intensity proportionately while the desired pressure rise will be  $\phi_t$  of its previously expected value (2.16). It may be possible, therefore, to entirely avoid the artifacts. It must be shown, however, that singlet excitation is capable of producing the desired triplet yield information.

For direct excitation into  $S_1^0$  from  $S_0$ , the normalized expected pressure rise is given by Wrobel [47] as (with  $0 = k_7 = k_8^{nr} = k_8^r$ ):

$$\frac{P'_{0,0}}{(\gamma-1)n_{S_1^0}^0 q_{0,0}} = [\phi + hv_{S_1^0, T_1^0} + \phi_{S_1^0}^{IC} hv_{S_1^0} + \phi_t \phi_{T_1^0}^{ISC} hv_{T_1^0} (1 - e^{-k_p^{*t}})] \quad (7.3)$$

where  $p'_s = \phi_t \phi_{T_1^0}^{ISC} hv_{T_1^0}$ ,  $\phi_{T_1^0}^{ISC} \equiv k_T/k_p^*$ ,  $\phi_{S_1^0}^{IC} \equiv k_s/k_f^*$ , and

$p'_f = \phi_t hv_{S_1^0, T_1^0} + \phi_{S_1^0}^{IC} hv_{S_1^0}$ . Let  $hv_{T_1^0} = E_t$ ,  $hv_{S_1^0} = E_s$ , and

$hv_{S_1^0, T_1^0} = D$ . Then we have the following:

$$P'_s/P'_f = \phi_t \phi_{T_1^0}^{ISC} E_t / (\phi_t D + \phi_{S_1^0}^{IC} E_s) \quad (7.4)$$

Assume, as Callis et al. [20] did, that  $\phi_p$  is much less than  $\phi_t$ . From the definitions (Chapter One), this implies  $k_p$  is much less than  $k_T$ . Hence,  $\phi_{T_1^0}^{ISC}$  is approximately unity. Assume also that  $D$  is much less than  $E_t$ . Then the above equation simplifies to (since  $E_t < E_s$ )

$$P'_S/P'_f = \phi_t E_t / \phi_{S_1}^{IC} E_S . \quad (7.5)$$

But this may be rearranged to the following:

$$\phi_t / \phi_{S_1}^{IC} = (E_S/E_t) P'_S/P'_f . \quad (7.6)$$

Note that  $\phi_t / \phi_{S_1}^{IC}$  is equal to  $k_{ISC}/k_S$ . We are able, therefore, to experimentally determine the ratio of the two unknown quantities in the known observed fluorescence lifetime (i.e.,  $(k_f^*)^{-1}$  and  $\phi_f$  are obtainable by fluorimetry and  $k_f^* = k_S + k_{ISC} + \phi_f k_f^*$ ). The values of  $k_p$  and  $k_T$  are obtainable by phosphorimetry from  $\phi_p$  and  $k_p^*$  (Chapter One) when the triplet yield is known. Hence, all five desired quantities are available and the definition of  $\phi_t$  (Chapter One) directly gives the desired result:

$$\phi_t = k_{ISC} (k_f^*)^{-1} \quad (7.7)$$

The triplet yield equation for singlet TROAS has several immediate consequences. First, because of the approximations made in its derivation, the yield equation is expected to be most accurate when fluorescence yield and particularly phosphorescence yield are small and when their spectral regions heavily overlap (i.e., the singlet-triplet separation is small). Note that this is the most difficult situation to study for phosphorimetry and fluorimetry. Second, despite the approximations, many more compounds are available for study by singlet TROAS than by triplet TROAS, particularly since lower power lasers, such as nitrogen laser-pumped dye lasers, may be employed to excite the singlets. Energies of several millijoules in the near UV would be

especially advantageous, particularly if obtainable at repetition rates concordant with signal averaging. Third, if phosphorimetry data are available, the phosphorescence yield may be used to obtain, via equation (7.4), a more accurate  $\phi_{T0}^{ISC}$  value, which in turn may be used to obtain a more accurate triplet yield value. Despite the lack of results from the triplet TROAS studies, there is every reason to expect, with adequate pressure transducer and associated electronics, that the singlet TROAS technique will prove useful and convenient.

## APPENDIX ONE RELEVANT OAS RESULTS

As previously mentioned, the results obtained by Wrobel [47] in his development of the theory of TROAS are incomplete since the equation he chose as fundamental neglects all dissipative processes external to the model-specific source term. This fundamental equation (A1.1 below) is a consequence of the conservation equations and equation of state of the sample. Precisely the same equation underlies the theory of OAS. However, as Kreuzer has noted "this equation does not include the effects of acoustic loss produced by heat conduction and viscosity. In order to properly discuss the optoacoustic effect, it is necessary to include these mechanisms" [63]. If the mechanisms are not included, it is not possible to avoid such consequences as unrealistically large or infinite acoustic mode amplitudes, undefined mode amplitude ratio expressions, and noise equivalent powers of essentially zero. In TROAS, similar problems occur. In fact, the fundamental pressure rise equation (2.10) is evaluated in the limit as  $t \rightarrow \infty$  since no thermal reequilibration is predicted by the theory of TROAS if the loss mechanisms are neglected.

Consequently, the losses must be readmitted to the theory. This is elegantly done by Kreuzer [63] using Fourier transform techniques. It is not necessary, therefore, to replace equation (A1.1) below by a more complicated system of tensor equations if the losses are small enough to allow them to be considered perturbations of the loss-free equation. That this is usually true may be seen in the work of Kamm [61].



Examination of Kreuzer's results shows that the transition from OAS to TROAS is remarkably simple as indeed it should be. Hence, the remainder of this Appendix will contain a brief resume of Kreuzer's results [63]. Consult the original reference for further details. Note that it would be difficult to obtain similar results if the technique employed by Wrobel [47] were the only means available for solving the equations of state and conservation of mass, energy, and momentum. Conversely, it would be difficult to obtain the radiationless decay rates and quantum yields if only the method of Kreuzer were used.

Let  $p = p(\vec{r}, t)$  be the pressure,  $H = H(\vec{r}, t)$  the source term,  $c$  the speed of sound, and  $\gamma = C_p/C_v$  the heat capacity ratio. Then the fundamental equation describing pressure changes induced by released heat  $H$  in a closed sample cell is [1,2]

$$\nabla^2 p - c^{-2} \frac{\partial^2 p}{\partial t^2} = -[(\gamma - 1)/c^2] \frac{\partial H}{\partial t}. \quad (A1.1)$$

The time Fourier Transform of both sides of (A1.1) yields

$$(\nabla^2 + \omega^2/c^2) p(\vec{r}, \omega) = [(\gamma - 1)/c^2] i\omega H(\vec{r}, \omega) \quad (A1.2)$$

$$\text{where } p(\vec{r}, t) = \int p(\vec{r}, \omega) e^{-i\omega t} d\omega \quad (A1.3)$$

$$\text{and } H(\vec{r}, t) = \int H(\vec{r}, \omega) e^{-i\omega t} d\omega \quad (A1.4)$$

The transform of the acoustic velocity  $\vec{v}(\vec{r}, t)$  is

$$\vec{v}(\vec{r}, \omega) = (i\omega\rho_0)^{-1} \nabla p(\vec{r}, \omega). \quad (A1.5)$$

We now apply the boundary condition that the component of  $\nabla p$  normal to the cell walls vanish at the walls. This condition determines the normal mode solutions  $p_j$  of the homogeneous wave equation (A1.6) corresponding to (A1.2) above

$$(\nabla^2 + k_j^2) p_j(r) = 0 \quad (\text{A1.6})$$

These acoustic modes are orthogonal and normalized by the following equation

$$\int p_i^* p_j dv = V_c \delta_{ij} \quad (\text{A1.7})$$

where  $V_c$  is the cell volume.

For a cylindrical sample cell of length  $L$  and radius  $A$ , the general solution (ignoring azimuthal modes) is

$$p_j(\vec{r}, t) = P_j J_0(k_r r) \cos(k_z z) e^{-i\omega_j t} \quad (\text{A1.8})$$

where  $k_z = \pi n_z / L$  for  $n_z = 1, 2, 3, \dots$ ,

and  $k_r = \alpha_{1,n} / A$  for  $\alpha_{1,n}$  the  $n$ -th root of  $J_1(r)$ .

The acoustic resonant frequency  $\omega_j$  (in radians per second) is

$$\omega_j = c(k_z^2 + k_r^2)^{1/2} \quad (\text{A1.9})$$

Note that  $\omega_j = 2\pi f_j$  where  $f_j$  is the resonant frequency in Hz.

The acoustic pressure  $p(\vec{r}, \omega)$  is thus

$$p(\vec{r}, \omega) = \sum_j A_j(\omega) p_j(\vec{r}, \omega_j) \quad (\text{A1.10})$$

Substitution of (A1.8) and (A1.10) into (A1.1) using (A1.6), (A1.7) yields the acoustic mode amplitudes  $A_j(\omega)$

$$A_j(\omega) = \frac{-i\omega}{\omega_j^2} \frac{[(\gamma-1)/V_c] \int p_j^*(\vec{r}, \omega) H(\vec{r}, \omega) dV}{1 - \omega^2/\omega_j^2} \quad (A1.11)$$

The amplitudes are infinite at  $\omega = \omega_j$  because all energy loss mechanisms were neglected in the derivation of (A1.1); see references [63,111] for details. The two major energy loss processes are viscosity and thermal conductivity [61]. They may be introduced into the theory either at the beginning or much more conveniently as perturbations of the already obtained loss-free solution of (A1.1). This procedure will be outlined below; further details may be found in the original source [63].

The mode quality factor  $Q_j$  is defined as

$$Q_j \equiv \omega_j \frac{E_j}{L_{sj} + L_{vj}} \quad (A1.12)$$

where the mode energy  $E_j$  is

$$E_j = |A_j|^2 V_c / \rho_0 c^2 \quad (A1.13)$$

and  $L_{sj}$ ,  $L_{vj}$  are surface and volumetric losses primarily due to viscosity and thermal conductivity. The volumetric loss of the  $j$ -th mode is

$$L_{vj} = \frac{\omega_j^2}{\rho_0 c^4} [(\gamma-1)(K/2C_p) + (2\eta/3)] V_c |A_j|^2 \quad (A1.14)$$

where  $K$  is the thermal conductivity,  $C_p$  is the heat capacity at constant pressure, and  $\eta$  is the coefficient of viscosity. The volumetric

losses are described in further detail by Morse and Ingard [111] and by Kamm [61]. They are, however, usually small relative to the surface losses. The surface loss may be considered to take place in surface layers of thickness

$$\lambda_v^2 = 2\eta/\omega\rho_0 \quad (\text{A1.15})$$

$$\lambda_h^2 = 2\kappa/\omega \quad (\text{A1.16})$$

where  $\lambda_v$  is the viscosity loss thickness,  $\lambda_h$  is the thermal loss thickness, and the Prandtl number of the sample gas mixture is

$$\text{Prandtl number} = (\lambda_v/\lambda_h)^2. \quad (\text{A1.17})$$

The surface loss is then

$$L_{sj} = |A_j|^2 \int [1/2 R_v |v_{tj}|^2 + 1/2 R_h |p_j|^2] dS \quad (\text{A1.18})$$

where  $R_v \equiv (\eta\omega\rho_0/2)^{1/2},$

and  $R_h \equiv [(\gamma-1)/\rho_0 c^2] (\kappa\omega/2)^{1/2},$

and  $|v_{tj}|$  = the acoustic velocity component tangential to the walls that would exist in the loss-free case. The surface losses may be qualitatively understood as follows. Near the cell walls, gas expansion and contraction are isothermal. Far from the walls, they are approximately adiabatic. Thermal losses occur in the transition region from isothermal to adiabatic behavior. Viscosity losses occur because of the requirement that the acoustic velocity component tangential to the

walls vanish at the walls rather than be as described by equation (A1.5). Further details are given by Kreuzer [63], Kamm [61], and Morse and Ingard [66].

The  $Q_j$  may be measured experimentally with good accuracy by pulse excitation of the  $\omega_j$  acoustic modes noting that the damping is described by [65]

$$\frac{A_j(\omega_j, t)}{A_j(\omega_j, 0)} = e^{-\omega_j t / 2Q_j} \quad (\text{A1.19})$$

The corrected mode amplitudes are thus

$$A_j(\omega) = \frac{-i\omega}{\omega_j^2} \frac{[(\gamma-1)/V_c] \int p_j^*(\bar{r}, \omega) H(\bar{r}, \omega) dV}{[1 - \omega^2/\omega_j^2 - i(\omega/\omega_j Q_j)]} \quad (\text{A1.20})$$

Given the quality factors  $Q_j$ , it is also possible to give an expression for the power spectrum of the noise that results from acoustic mode excitation by the thermal fluctuations in the sample and carrier gases. This is

$$|A_{jn}(\omega)|^2 = \frac{4\rho_0 c^2 k T}{V_c \omega_j Q_j [(1 - \omega^2/\omega_j^2)^2 + (\omega/\omega_j Q_j)^2]} \quad (\text{A1.21})$$

where the average energy per mode is  $kT$  and the noise energy in a frequency band of width  $\Delta\omega$  centered at  $\omega$  is  $|A_{jn}(\omega)|^2 \Delta\omega / \rho c^2$ . Thus, noise energy may be concentrated around the acoustic mode frequencies by increasing the  $Q_j$ . The average energy per mode ( $kT$ ) is independent of  $Q_j$ . This thermal noise determines the fundamental sensitivity limit of OAS and TROAS experiments.

## APPENDIX TWO TROAS NOISE EQUIVALENT POWER

In this appendix an expression for noise equivalent power is derived. The treatment is a simple modification of the derivation of noise equivalent power (NEP) given for conventional optoacoustic spectroscopy by Kreuzer [63].

Let the pulsed light source uniformly illuminate the sample cell such that the assumption  $H = \alpha I$  is satisfied. Then the corrected mode amplitude equation (A1.20) gives the desired signal amplitude  $A_0(\omega)$

$$A_0(\omega) = \frac{i \alpha (\gamma - 1) I}{\omega (1 + (1/\omega \tau_T))} . \quad (A2.1)$$

The light pulse of energy  $E$  and duration  $t_p$  has intensity  $I$  given by

$$I = \frac{L}{V_c} \frac{E}{t_p} \quad (A2.2)$$

where  $L/V_c$  is the cell cross-sectional area. Thus, for TROAS (with  $\omega \tau_T \gg 1$ ), equations (A2.1) and (A2.2) yield the following

$$A_0(\omega) = \frac{i \alpha (\gamma - 1) E L}{\omega V_c t_p} . \quad (A2.3)$$

Define NEP by

$$NEP \equiv \alpha L E / t_p \quad (A2.4)$$

Note that for TROAS,  $\omega > \omega_j$  for most acoustic modes. Thus, the noise power spectrum (A1.21) becomes

$$|A_{jn}(\omega)|^2 = \frac{4\rho_0 c^2 k T \omega_j^3}{v_c Q_j \omega^4} . \quad (\text{A2.5})$$

Then (A2.3), (A2.4), (A2.5) imply

$$(\text{NEP})^2 = \frac{v_c^2 \omega^2}{(\gamma-1)^2} \sum_j \frac{4\rho_0 c^2 k T \omega_j^3}{v_c Q_j \omega^4} . \quad (\text{A2.6})$$

Hence, we obtain

$$(\text{NEP})^2 = \sum_j \frac{4\rho_0 c^2 k T v_c \omega_j^3}{(\gamma-1)^2 Q_j \omega^2} . \quad (\text{A2.7})$$

The units for NEP in (A2.7) above are watts/(radians/sec)<sup>1/2</sup> rather than the conventional watts/(Hz)<sup>1/2</sup>; this is due to use of  $\omega$  rather than  $f$ .

Performing the substitution yields

$$(\text{NEP})^2 = \sum_j \frac{8\pi\rho_0 c^2 k T v_c f_j^3}{(\gamma-1)^2 Q_j f^2} . \quad (\text{A2.8})$$

Note that NEP decreases with increasing frequency  $f$ . Since short pulses have high spectral bandwidth, NEP decreases with decrease in excitation pulse width in a linear fashion. This is in accord with the results of Aamodt and Murphy [112] who found that the signal to noise ratio in a pulsed OAS experiment increased with decreasing pulse width. The authors claim this confirms a suggestion of Reichard [112] that short pulses are preferable to square waves when the S/N ratio of the (lock-in amplifier) detected signal is source-power limited.

### APPENDIX THREE CAPACITANCE MICROPHONE PREAMPLIFIER NOISE MODEL

The most common method of capacitance microphone preamplification is the voltage amplifier circuit. For optimum results, the amplifier should provide gain in the first stage; otherwise, the signal to noise ratio will be degraded. A typical circuit is shown in Figure 21. Noise sources for this circuit are included in Figure 22. The calculation of total noise voltage follows that of Kreuzer [63] closely though several additional sources were used to extend the model as necessary [113], [114], [74], [73].

Noise sources in the circuit are due to microphone acoustic noise, bias resistor thermal noise, input resistor noise, feedback loop resistor noise, amplifier input current noise, and amplifier input voltage noise. The square of the noise voltage is the sum of six terms given by

$$\begin{aligned}
 |V_n|^2 \cong & |e_n|^2 + |i_{n+}|^2 (\omega C_e + R_p^{-1})^{-2} \\
 & + 4 k T R_f + |i_{n-}|^2 R_f \\
 & + (4 k T / R_p) (\omega C_e + R_p^{-1})^{-2} \\
 & + \frac{4 k T C'}{Q_m \omega_m C_e^2} [((\omega / \omega_m)^2 - 1)^2 \\
 & + (\omega / \omega_m Q_m)^2]^{-1}
 \end{aligned} \tag{A3.1}$$



Figure 21. A voltage preamplifier and externally polarized capacitance microphone circuit. This circuit was the basis of the noise model calculations of Appendix Three. Typical values are  $C_m = 40$  pf,  $R_B = 10^{10}$  ohms,  $C = 0.1$   $\mu$ f,  $C_i = 10$  pf,  $R_e = 10^{10}$  ohms,  $R_1 = 10$  K ohms, and  $R_2 = 300$  K ohms.

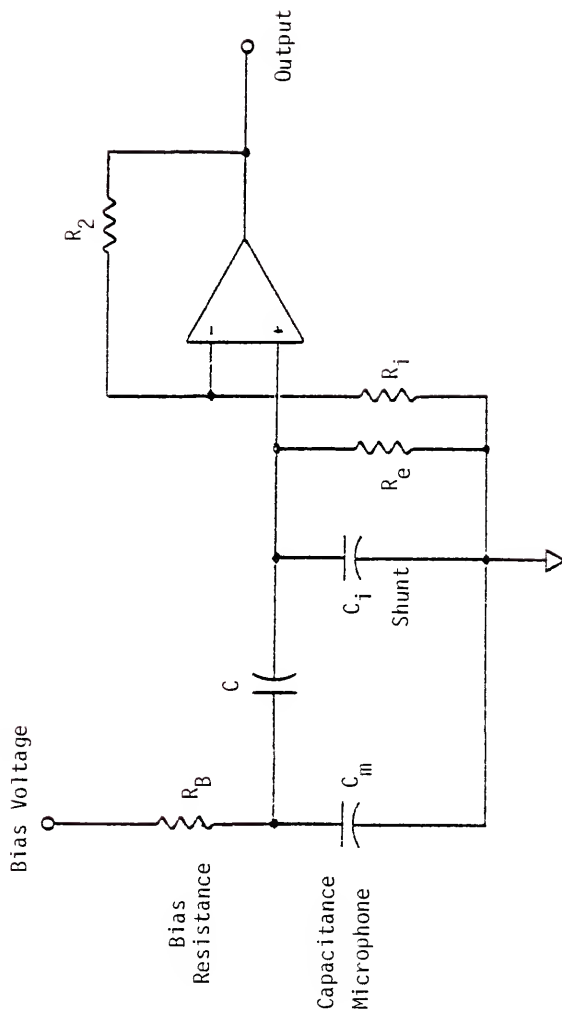
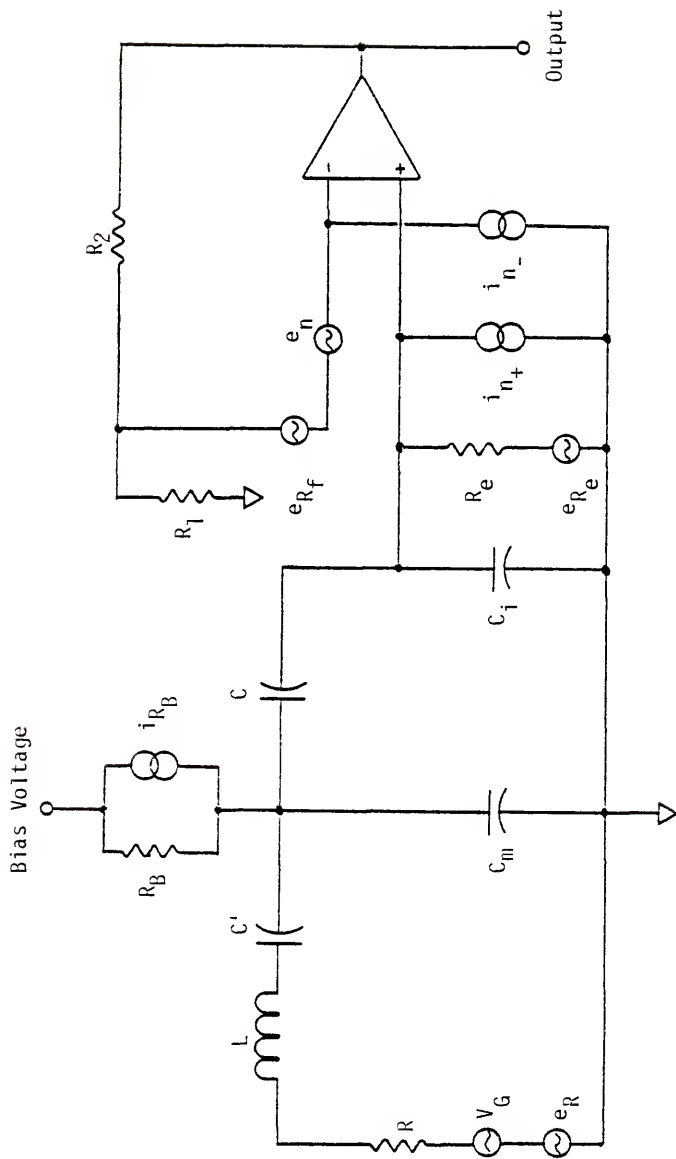


Figure 22. The voltage preamplifier and externally polarized capacitance microphone circuit of Figure 21 with appropriate noise sources added. Typical values are  $R = 5. \text{ M ohms}$ ,  $C' = 5 \text{ pf}$ , and  $L = 70 \text{ H}$ . All other values are as in Figure 21.



The first term is the amplifier input voltage noise. The second is amplifier input current noise while the third is thermal noise due to the feedback resistors. The fourth term is amplifier input current noise at the inverting input. Term five is thermal noise due to the parallel combination of the bias and input resistors. The sixth term is the microphone acoustic noise due to Brownian motion.

The restoring force, mass, damping, and output voltage of a capacitance microphone model are [63]

$$C' = C_m^2 V_B^2 / k_m d^2 \quad (A3.2)$$

$$L = m/k_m C' = 1/\omega_m^2 C' \quad (A3.3)$$

$$R = \delta/k_m C' = 1/Q_m \omega_m C' \quad (A3.4)$$

$$V_G = (Ad/V_B C_m) p_m \quad (A3.5)$$

where  $m$  is the diaphragm mass,  $\delta$  is the damping,  $C_m$  is the microphone capacitance,  $k_m$  is the restoring force,  $V_B$  is the bias voltage,  $d$  is the electrode spacing,  $\omega_m$  is the resonant frequency,  $A$  is the microphone area, and  $p_m$  is the diaphragm acoustic pressure. In addition, the following relations hold

$$R_B \gg (\omega C)^{-1}, \quad \omega_{\lambda} = [R_p (C_m + C_i)]^{-1},$$

$$C_e \equiv C_m + C_i, \quad R_p = R_B R_e / (R_B + R_e),$$

$$R_f \equiv R_1 R_2 / (R_1 + R_2)$$

where  $\omega_1$  is the lower frequency limit. Typical values for  $C_m$ ,  $C'$ ,  $L$ , and  $R$  are 40 pf, 5 pf, 70 H, and 5 Mohm. Realistic values for  $R_e$  and  $R_B$  are  $10^3$  to  $10^{15}$  ohms with  $10^{10}$  ohms a good choice. The input noise values for a typical low noise bipolar input 725 op amp are

$$e_n \cong 8. \times 10^{-9} \text{ V/H}_z^{1/2}, i_{n_+} = i_{n_-} \cong 1.5 \times 10^{-13} \text{ A/H}_z^{1/2}.$$

For the JFET input AD514 op amp the values are

$$e_n \cong 30. \times 10^{-9} \text{ V/H}_z^{1/2}, i_{n_+} = i_{n_-} \cong 10^{-13} - 10^{-15} \text{ A/H}_z^{1/2}.$$

Calculations indicate that the AD514 is much less noisy than the 725 for source impedances above several hundred thousand ohms.

APPENDIX FOUR  
MICROCOMPUTER PROGRAM AND I/O LOCATIONS

The last version of the microcomputer program used in the TROAS research is listed below.

TROAS-7

```
200      DIM A%(256),S(256)
300      DATA A2,07,A9,00,8D,4C,03,4E,4B
310      DATA 03,2E,4C,03,CA,D0,F7,60
312      DATA 00,00,A9,08,8D,00,A0,CE
314      DATA 5B,03,D0,FB,EE,00,A0,60
320      FOR J=826 TO 858:GOSUB 900:POKE J,C:NEXT J
330      POKE 1,58:POKE 2,3
500      ? " ENTER DWELL TIME/CHANNEL IN SECONDS":INPUT U
502      ? " ENTER SENSITIVITY & GAIN":INPUT N5,N3
510      FOR I=1 TO 2:GOSUB 1000:NEXT I
520      ? " SELECT OFFSET,GROUND INPUT,EXT. TRIGGER":INPUT I:GOSUB
2000:OF=T
530      ? "  OFFSET=";OF:~
540      ? " UNGROUND INPUT,SELECT TRIGGER":?:INPUT I:~
610      ? "          INPUT OPTION?"
620      INPUT V:ON V GOSUB 1000,2000,3000,4000,5000,6000,7000,
8000,9000:GOTO 610
700      S=0
710      FOR I=1 TO 256
```

```

720      C=PEEK(4.5E4):IF C<128 GOTO 720
730      A%(I)=PEEK(4.4E4):S=S+A%(I)
740      POKE 4.5E4,54:POKE 4.5E4,62:NEXT I
750      T=S/256:RETURN
800      FOR I=1 TO 256
810          IF A%(I)>255 THEN A%(I)=0
820          IF A%(I)<0 THEN A%(I)=0
830          POKE 4.8E4,255-A%(I)
840          GOSUB 890:NEXT I:RETURN
850      FOR I=1 TO 255 STEP 2
860          IF A%(I)>255 THEN A%(I)=255
865          IF A%(I)<0 THEN A%(I)=0
870          POKE 4.8E4,255-A%(I)
880          GOSUB 890:POKE 4.8E4,255:GOSUB 890:GOSUB 890:GOSUB 890
          NEXT I:RETURN
890      FOR J=1 TO 600:NEXT J:RETURN
900      READ G$:C=0
910      FOR I=1 TO 2
920          F$=MIDS(G$,I,1):A=ASC(F$)-64
930          IF A>0 THEN A=A+9
940          IF A<0 THEN A=VAL(F$)
950          C=C+A*(31-15*I):NEXT I:RETURN
1000     ?:" "      PIA I/O PORT STATUS":?
1010     ?:"PIA$#","$9","$A","$B":?::??
1020     POKE 4.0E4,0:POKE 4.5E4,0:POKE 4.9E4,0
1030     POKE 3.9E4,127:POKE 4.4E4,0:POKE 4.8E4,255
1040     POKE 4.0E4,4:POKE 4.5E4,62:POKE 4.9E4,4

```



```

1050      POKE 3.9E4,127:POKE 4.8E4,0
1060      ? "CRB",PEEK(4.0E4),PEEK(4.5E4),PEEK(4.9E4):?::?
1070      ?,"TR & SM","TR DATA","D/A":?
1080      ? " B",PEEK(3.9E4),PEEK(4.4E4),PEEK(4.8E4):?::?
1090      POKE 3.8E4,0:POKE 4.2E4,0:POKE 4.7E4,0
1100      POKE 3.7E4,0:POKE 4.1E4,255:POKE 4.6E4,0
1110      POKE 3.8E4,4:POKE 4.2E4,4:POKE 4.7E4,4:POKE 4.7E4,14
1120      ? "CRA",PEEK(3.8E4),PEEK(4.2E4),PEEK(4.7E4):?::?
1130      ?,"A/D","SYS-CONT","FREE":?
1140      ? " A",PEEK(3.7E4),PEEK(4.1E4),PEEK(4.6E4):?::?:RETURN
2000      POKE 3.9E4,63:POKE 3.9E4,127:A=PEEK(4.1E4):POKE 4.1E4,A-5:
        POKE 4.1E4,A-4
2005      GOSUB 3030
2010      B=PEEK(3.9E4):IF B>127 GOTO 2010
2020      POKE 4.1E4,2:LP=PEEK(3.7E4)-128
2024      IF LP<10 THEN LP=1
2026      ?::? " LASER PULSE=";LP:~
2030      POKE 4.1E4,A:POKE 3.9E4,111:~? " ACQUIRE?":~
2040      INPUT N::~?IF N=0 GOTO 2060
2050      GOSUB 700:GOSUB 2070
2060      POKE 3.9E4,127:RETURN
2070      06=255:07=0
2080      FOR I=1 TO 256
2090      IF A%(I)>07 THEN 07=A%(I)
2100      IF A%(I)<06 THEN 06=A%(I)
2110      NEXT I:08=07-06:N4=(08/255)*N5/N3
2120      ? " SIGNAL VOLTAGE=";INT(.5+1E6*N4);"MICROVOLTS":?

```

```

2130      ? " NORMED SIGNAL=";INT(.5+(1E6*N4/LP));"MICROVOLTS":
      ?:RETURN
3000      POKE 4.8E4,0:GOSUB 3030:POKE 4.8E4,255:GOSUB 3030
3010      GOSUB 800
3020      POKE 4.8E4,255:GOSUB 3030:POKE 4.8E4,0:GOSUB 3030:RETURN
3030      FOR I=1 TO 3000:NEXT I:RETURN
4000      FOR I=1 TO 4
4010      OPEN I,1,1,"TROAS DATA"
4020      FOR J=1 TO 64:Z=J+64*(I-1)
4030      PRINT#I,A%(Z)
4040      NEXT J
4050      CLOSE I:NEXT I:RETURN
5000      ?:" AVERAGE SUBTRACTED?":?:INPUT W:X=T-OF
5005      FOR J=1 TO 128:J2=2*J:M=J-1:POKE843,M:X=USR(0):I=PEEK(844):
      L=2*I
5010      S(J2-1)=A%(L+1)-OF-W*X:S(J2)=A%(L+2)-OF-W*X:NEXT J
5020      N=128:N2=7:IL=2:LE=1:JE=N/2
5030      FOR K=1 TO N2:AR= $\pi$ /LE
5040      FOR J=1 TO JE:J1=J-1
5050      FOR L=1 TO LE:L1=L-1:JP=2*(IL*J1+L1)+1:JQ=JP+IL:AX=L1*AR
5060      WR=COS(AX):WI=-SIN(AX)
5070      RE=S(JQ)*WR-S(JQ+1)*WI:FI=S(JQ)*WI+S(JQ+L)*WR
5080      S(JQ)=S(JP)=RE:S(JQ+L)=S(JP+1)-FI:S(JP)=S(JP)+RE:S(JP+1)=
      S(JP+1)+FI:NEXT L
5090      NEXT J
5100      LE=2*LE:JE=JE/2:IL=2*IL:NEXT K
5110      N1=N/2

```

```

5120   FOR M=2 TO N1:M1=2*(N-M)+3:M2=2*M-1:MB=M1+1:MC=M2+1
5130   DR=(S(MC)+S(MB))/2:DI=(S(M1)-S(M2))/2
5140   CR=(S(M2)+S(M1))/2:CI=(S(MC)-S(MB))/2
5150   S(M1)=DR:S(MB)=DI:S(M2)=CR:S(MC)=CI:NEXT M:AR=π/N
5160   FOR K=2 TO N1:AX=AR*(K-1):WR=COS(AX):WI=-SIN(AX):KN=2*
      (N-K)+3:KI=2*K-1
5170   RE=S(KN)*WR-S(KN+1)*WI:FI=S(KN)*WI+S(KN+1)*WR
5180   BR=S(KI)+RE:BI=S(KI+1)+FI:H1=SQR(BR*BR+BI*BI):
      BR=S(KI)-RE:BI=S(KI+1)-FI
5190   S(KI)=H1:S(KN)=SQR(BR*BR+BI*BI):NEXT K
5200   S(129)=SQR(S(129)*S(129)+S(130)*S(130)):O1=1E4:O2=-1E4
5210   FOR I=1 to 255 STEP 2
5220   IF S(I)<O1 THEN O1=S(I)
5230   IF S(I)>O2 THEN O2=S(I)
5240   NEXT I:O3=O2-O1
5250   FOR I=1 TO 255 STEP 2
5260   A%(I)=INT(.5+255*(S(I)-O1)/O3):NEXT I
5270   ??: " MAX. AMPLITUDE=";INT(.5+O3):?:RETURN
6000   ??: " ENTER LOWER THRESHOLD IN %":?:INPUT Z:
6010   ? " FREQUENCIES ABOVE THRESHOLD":?
6020   ? TAB(3);"HERTZ";TAB(18);"INTENSITY";TAB(33);"POWER"
6030   Z1=2.55*Z:U1=1/(510*U):G1=0
6035   FOR I=1 TO 255 STEP 2:G1=G1+A%(I):NEXT I
6040   FOR I=1 TO 255 STEP 2
6050   IF A%(I)>Z1 THEN GOSUB 6070
6060   NEXT I:RETURN

```

```

6070      U2=INT(.5+I*U1):Z2=.1*INT(A%(I)*3.922):Z3=.1*INT(.5+1E3*
      A%(I)/G1)
6080      ? : TAB(3);U2;TAB(18);Z2;TAB(33);Z3;RETURN
7000      POKE 4.8E4,0:GOSUB 3030:POKE 4.8E4,255:GOSUB 3030
7010      GOSUB 850
7020      POKE 4.8E4,255:GOSUB 3030:POKE 4.8E4,0:GOSUB 3030:RETURN
8000      POKE 1,77:POKE 2,3:POKE 3.9E4,63:POKE 3.9E4,127:A=PEEK(4.1E4)
8010      ? " INPUT TR DELAY":INPUT I:POKE 859,I:J=USR(0):POKE 1,58:
      POKE 2,3
8020      POKE 4.1E4,A-4:GOTO 2010
9000      ? "INPUT # OF POINTS TO OMIT":INPUT NN:SC=256-NN
9005      S1=0:S2=0:S3=0:S4=0:S5=0
9010      FOR I=NN+1 TO 256
9020      S1=S1+I*U:S2=S2+I*U*I*U:S3=S3+LOG(A%(I)):S4=S4+LOG(A%(I))*
      LOG(A%(I))
9030      S5=S5+I*U*LOG(A%(I))
9040      NEXT I
9050      SA=S5-S1*S1/SC:SB=S2-S1*S1/SC
9060      S6=SA/SB
9070      SA=S3/SC:SB=S6*S1/SC:S7=EXP(SA-SB)
9080      SA=(S5-S1*S3/SC)+2:SB=S2=S1*S1/SC:SD=S4-S3*S3/SC
9090      S8=SA/(SB+SD)
9100      ? "Y=A EXP(BX)"
9110      ? " A=";S7
9120      ? " B=";S6;"SECONDS"
9130      ? " R 2";S8
9140      RETURN

```

Remarks have been omitted from the above program to conserve RAM memory space which was at a premium. Several points of nomenclature: semicolons separate lines; question marks are seen as abbreviations of the print command; and dollar signs denote hexadecimal notation. The main program and utility subroutines lie below line number 1000. The nine main subroutines are positioned in blocks of 1000 line numbers starting at line number 1000. In lieu of remarks, a brief description of the program is presented.

The data statements (300-314) contain simple assembly language subroutines used by the FFT subroutine and the transient recorder trigger subroutine. Lines 320 and 330 place the assembly language program in memory (in the PET's unused, protected, second tape buffer RAM), while lines 500-620 request information concerning transient recorder settings, et cetera, and request the input (main subroutine) option. Lines 700-750 acquire 256 data points from the transient recorder and also average them. Lines 800-840 check for illegal data and then output to the D/A driving the chart recorder. Lines 850-880 output the FFT spectrum as a line spectrum while line 890 is a delay subroutine. Lines 900-950 convert the hexadecimal op codes in the data statements to decimal (required by the POKE command).

The locations in memory space of the D/A, A/D, transient recorder control lines, et cetera are shown in Table 9. Subroutine 1, at lines 1000-1140 initializes the PIA chips and thereby initializes the transient recorder, chart recorder output, et cetera. The status of the various initialized subsystems is displayed on the built-in video monitor. Subroutine 2, at lines 2000-2130, triggers the laser and transient recorder, reads the photodetector peak output, determines whether the

Table 9. Peripheral systems memory locations

Decimal address	PIA number (4 K select)	Function
3.7E4	\$9	8-bit A/D (msb-PA7)
3.8E4	\$9	Control register for 3.7E4
3.9E4	\$9	PA0 - stepping motor drive pulses PA1 - stepping motor direction PA2 - choice of stepping motor PA3 - computer override of manual default PA4 - transient recorder plot command PA5 - transient recorder PA6 - transient recorder PA7 - transient recorder
4.0E4	\$9	Control register for 3.9E4
4.1E4	\$A	PA0 - transient recorder trigger PA1 - laser trigger pulse line PA2 - peak detector reset PA3 & 4 - multiplexer channel select PA5 & 6 - amplifier gain select PA7 - active filter bypass select
4.2E4	\$A	Control register for 4.1E4
4.4E4	\$A	Transient recorder data (msb-PB7)
4.5E4	\$A	Control register for 4.4E4
4.6E4	\$B	Unused
4.7E4	\$B	Control register for 4.6E4
4.8E4	\$B	8-bit D/A (msb-PB7)

Defaults are as follows: manual control of the monochrometer, peak detector reset, amplifier gain of unity, pressure detector multiplexer input, active filter (-24 db/octave, -3 db @ 1.8 KHz) bypassed.

data need be acquired, and outputs the peak-to-peak voltage of any acquired signal. The integer array A% is used throughout the program as a shared array. Subroutine 3, at lines 3000-3030, outputs chart recorder data.

Subroutine 4, at lines 4000-4050, allows data to be stored as named files on cassette tape. Subroutine 5, at lines 5000-5270, is the FFT routine. Lines 5000-5010 perform the necessary binary bit inversion required by the Cooley-Tukey algorithm. Lines 5020-5100 compute the complex transform of the sorted real data. Lines 5110-5190 correct the result for the real nature of the data, while line 5200 computes a point missed in the clash of indices. Lines 5210-5270 scale the floating point FFT so that it may be output to the chart recorder and also output the unscaled maximum peak-to-peak amplitude. Further details may be found in [77].

Subroutine 6, at lines 6000-6080, displays the frequencies, normalized intensities, and powers of spectral peaks in the FFT above a specified intensity. Subroutine 7, at lines 7000-7020, outputs the FFT spectrum to the chart recorder. Subroutine 8, at lines 8000-8020, calls the assembly language routine that triggers the transient recorder. Because of delays in the optocoupled laser trigger, the transient recorder, at dwell times per channel of 5  $\mu$ sec or less, may finish recording before the laser has fired. Therefore, the laser is triggered first, then a delay loop is entered, and finally the transient recorder is triggered (immediately prior to the actual firing of the laser).

Subroutine 9, at 9000-9140, is a simple least squares fit to an exponential curve with provision for omitting an arbitrary initial number of points (the expected step-rise, for example). The subroutine outputs the decay time in seconds.

## REFERENCES

1. A. G. Bell, *Philos. Mag.*, 11, 510(1881)
2. E. Mercadier, *C. R. Acad. Sci.*, 91, 929(1880)
3. W. H. Preece, *Proc. Roy. Soc. (London)*, 31, 506(1881)
4. W. C. Rontgen, *Ann. Phys. Chem.*, 12, 155(1881)
5. J. Tyndall, *Proc. Roy. Soc. (London)*, 31, 307(1881)
6. M. L. Veingerov, *Dokl. Akad. Nauk. SSSR*, 19, 687(1938)
7. A. H. Pfund, *Science*, 90, 326(1939)
8. K. F. Luft, *Z. Tech. Phys.*, 24, 97(1943)
9. M. J. E. Golay, *Rev. Sci. Instrum.*, 20, 816(1949)
10. W. D. Hersberger, E. T. Bush, and G. W. Leck, *RCA Rev.*, 7, 442(1946)
11. G. Gorelik, *Dokl. Akad. Nauk. SSSR*, 54, 779(1946)
12. R. Kaiser, *Can. J. Phys.*, 37, 1499(1959)
13. M. E. Delaney, *Sci. Prog. (Oxford)*, 47, 459(1959)
14. Y. I. Gerlovin, *Opt. Spectry.*, 7, 352(1959)
15. R. M. White, *J. Appl. Phys.*, 34, 2123 & 3559(1963)
16. C. M. Percival, *J. Appl. Phys.*, 38, 5313(1967)
17. J. C. Bushnell and D. J. McCloskey, *J. Appl. Phys.*, 39, 554(1968)
18. E. Hey, Ph.D. Thesis, University of Heidelberg (1967)
19. P. G. Seybold, M. Gouterman, and J. Callis, *Photochem. Photobiol.*, 9, 229(1969)
20. J. B. Callis, M. Gouterman, and J. D. S. Danielson, *Rev. Sci. Instrum.*, 40, 1599(1969)
21. L. B. Kreuzer, *J. Appl. Phys.*, 42, 2934(1971)



22. L. B. Kreuzer, N. D. Kenyon, and C. K. N. Patel, *Science*, 177, 347(1972)
23. E. Max. and L.-G. Rosengren, *Opt. Commun.*, 11, 422(1974)
24. C. F. Dewey Jr., *Opt. Eng.*, 13, 483(1974)
25. C. W. Bruce and R. G. Pinnick, *Appl. Optics*, 16(7), 1762(1977)
26. M. S. De Groot, C. A. Emeis, I. A. M. Hesselman, E. Drent, and E. Farenhorst, *Chem. Phys. Letters*, 17(3), 332(1972)
27. C. A. Emeis, E. Drent, E. Farenhorst, I. A. M. Hesselman, and M. S. De Groot, *Chem. Phys. Letters*, 27(1), 17(1974)
28. C. K. N. Patel and R. J. Kerl, *Appl. Phys. Letters*, 30(11), 578(1977)
29. G. Stella, J. Gelfand, and W. H. Smith, *Chem. Phys. Letters*, 39(1), 146(1976)
30. W. R. Harshbarger and M. B. Robin, *Accounts Chem. Research*, 6, 329(1973)
31. W. R. Harshbarger and M. B. Robin, *Chem. Phys. Letters*, 21, 462(1973)
32. K. Kaya, W. R. Harshbarger, and M. B. Robin, *J. Chem. Phys.*, 60, 4231(1974)
33. K. Kaya, C. L. Chatelain, M. B. Robin, and N. A. Kuebler, *J. Am. Chem. Soc.*, 97, 2153(1975)
34. J. G. Parker and D. N. Ritke, *J. Chem. Phys.*, 59, 3713(1973) & 61, 3408(1974)
35. J. G. Parker, *J. Chem. Phys.*, 62, 2235(1975)
36. T. F. Hunter, D. Rumbles, and M. G. Stock, *J. Chem. Soc. Faraday Trans. 2*, 70, 1010(1974)
37. T. F. Hunter and M. G. Stock, *J. Chem. Soc. Faraday Trans. 2*, 70, 1022 & 1028(1974); *Chem. Phys. Letters*, 22, 368(1973)
38. M. G. Rockley and J. P. Devlin, *Appl. Phys. Letters*, 31(1), 24(1977)
39. J. D. Stettler and N. M. Witriol, in Optoacoustic Spectroscopy and Detection, Academic Press, Inc., N. Y., 1977
40. J. G. Parker, *Applied Optics*, 12(12), 2974(1973)
41. A. Rosencwaig, *Opt. Commun.*, 7, 305(1973)

42. A. Rosencwaig, *Science*, 181, 657(1975)
43. A. Rosencwaig, *Anal. Chem.*, 47, 592A(1975)
44. A. Rosencwaig and A. Gersho, *J. Appl. Phys.*, 47, 64(1976)
45. F. A. McDonald and G. C. Wetsel, Jr., *J. Appl. Phys.*, 49(4), 2313(1978)
46. M. J. Brienza and A. J. DeMaria, *Appl. Phys. Letters*, 11, 44(1967)
47. J. J. Wrobel, Ph.D. Dissertation, University of Florida, 1976
48. P. G. Bowers and G. Porter, *Proc. Roy. Soc. (London)*, 299A, 348(1967)
49. A. A. Lamola and G. S. Hammond, *J. Chem. Phys.*, 43, 2129(1965)
50. C. A. Parker and T. A. Joyce, *Trans. Faraday Soc.*, 62, 2785(1966)
51. A. R. Horrocks and F. Wilkinson, *Proc. Roy. Soc. (London)*, 306A, 257(1968)
52. M. Gueron, J. Eisinger, and R. G. Shulman, *Mol. Phys.*, 14, 111(1968)
53. C. A. Parker, Photoluminescence of Solutions, Elsevier, Amsterdam, 1968
54. J. Birks, Photophysics of Aromatic Molecules, Wiley-Interscience, 1970
55. B. Soep, A. Kellmann, M. Martin, and L. Lindqvist, *Chem. Phys. Letters*, 13, 241(1972)
56. K. H. Drexhage, in Dye Lasers (Topics in Applied Physics, Vol. 1), Springer-Verlag, N. Y., Berlin, Heidelberg, 1973
57. S. P. McGlynn, T. Azumi, and M. Kinoshita, Molecular Spectroscopy of the Triplet State, Prentice Hall, Inc., Englewood Cliffs, N. J., 1969
58. Optoacoustic Spectroscopy and Detection, Y.-H. Pao, editor, Academic Press, Inc., N. Y., 1977
59. T. Aoki and M. Katayama, *Japan. J. Appl. Phys.*, 10, 1303(1971)
60. F. R. Grabiner, D. R. Siebert, and G. W. Flynn, *Chem. Phys. Letters*, 17(2), 189(1972)
61. R. D. Kamm, *J. Appl. Phys.*, 47(8), 3550(1976)
62. J. N. Bradley, Shock Waves in Chemistry and Physics, J. Wiley and Sons, Inc., N. Y., London, 1962

63. L. Kreuzer, in Optoacoustic Spectroscopy and Detection, Academic Press, Inc., N. Y., 1977
64. A. B. Carlson, Communication Systems, McGraw-Hill, Inc., N. Y., 1975
65. C. F. Dewey, Jr., in Optoacoustic Spectroscopy and Detection, Academic Press, Inc., N. Y., 1977
66. P. M. Morse and K. V. Ingard, Theoretical Acoustics, McGraw-Hill, Inc., N. Y., 1968
67. F. W. Fraim and P. V. Murphy, J. Acous. Soc. of Am., 53(6), 1601(1973)
68. G. M. Sessler and J. E. West, J. Acous. Soc. Am., 53, 1589(1973)
69. M. M. Farrow, R. K. Burnham, M. Auzanneau, S. L. Olsen, N. Purdie, and E. M. Eyring, Applied Optics, 17(7), 1093(1978)
70. Low noise preamplifiers selection guide, Ithaco, Inc., Ithaca, N. Y., Publication number IPS 112 9/76
71. J. J. Zaalberg van Zelst, Philips Tech. Rev., 9(12), 357(1947/48)
72. Precision condenser microphone data sheets, Dynasciences Corp., Chatsworth, Calif., Models 404, 414, 504, 514, 814.
73. FET design ideas and selection guide, Texas Instruments, Inc., Houston, Texas
74. H. W. Ott, Noise Reduction Techniques in Electronic Systems, Wiley-Interscience, N. Y., 1976
75. S. M. Sze, Physics of Semiconductor Devices, Wiley-Interscience, N. Y., 1969
76. Radio Shack capacitance electret microphone #33-1056 data sheet
77. J. R. Bell, Introductory Fourier Transform Spectroscopy, Academic Press, Inc., N. Y., 1972
78. R. Spafford, J. Baiardo, J. Wrobel, and M. Vala, J. Am. Chem. Soc. 98, 5217(1976)
79. J. Baiardo, R. Spafford, and M. Vala, J. Am. Chem. Soc. 98, 5225(1976)
80. J. P. Baiardo, private communication
81. D. H. Powell, private communication
82. J. Herst, private communication

83. E. U. Elam and H. E. Davis, *J. Organic Chem.*, 32, 1562(1967)
84. W. Siebrand, in The Triplet State, Beirut Symposium 1967, Cambridge U. Press, Cambridge, England, 1967
85. CRC Handbook of Chemistry and Physics, 44th Edition, 1961
86. J. Calvert and J. Pitts, Jr., Photochemistry, J. Wiley and Sons, Inc., N. Y., 1966
87. M. B. Robin, in Optoacoustic Spectroscopy and Detection, Academic Press, Inc., N. Y., 1977
88. H. W. Sidebottom, C. C. Badcock, J. C. Calvert, B. R. Rabe, and E. K. Damon, *J. Am. Chem. Soc.*, 94(1), 13(1972)
89. E. Drent, R. P. van der Werf, and J. Kommandeur, *J. Chem. Phys.*, 59, 2061(1973)
90. W. A. Noyes, Jr., G. B. Porter, and J. E. Jolly, *Chem. Rev.*, 56, 49(1956)
91. R. B. Cundall and A. S. Davies, *Progr. React. Kinet.*, 4, 149(1967)
92. F. C. Henriques, Jr., and W. A. Noyes, Jr., *J. Am. Chem. Soc.*, 62, 1038(1940)
93. H. Okabe and W. A. Noyes, Jr., *J. Am. Chem. Soc.*, 79, 801(1957)
94. H. Ishikawa and W. A. Noyes, Jr., *J. Chem. Phys.*, 37, 583(1962)
95. C. S. Parmenter and B. L. Ring, *J. Chem. Phys.*, 46, 1998(1967)
96. C. S. Parmenter and H. M. Poland, *J. Chem. Phys.*, 51(4), 1551(1969)
97. C. C. Badcock, H. W. Sidebottom, J. C. Calvert, B. R. Rabe, and E. K. Damon, *J. Am. Chem. Soc.*, 94(1), 19(1972)
98. H. W. Furumoto and H. L. Ceccon, *Appl. Optics*, 8, 1613(1969)
99. H. W. Furumoto and H. L. Ceccon, *J. Appl. Phys.*, 40, 4204(1969)
100. H. W. Furumoto and H. L. Ceccon, *IEEE J. Quant. Electr.* QE-6, 262(1970)
101. F. P. Schafer, in Dye Lasers (Topics in Applied Physics, Vol. 1), Springer-Verlag, N. Y., Berlin, Heidelberg, 1973
102. T. F. Deaton, D. A. Depatie, and T. W. Walker, *A-pl. Phys. Letters*, 26, 300(1975)
103. A. Hordvik and H. Schlossberg, *Applied Optics*, 16(1), 101(1977)

104. W. D. Stanley and S. J. Peterson, *Byte*, 3(12), 14(1978)
105. D. M. Munroe and H. S. Reichard, *American Laboratory*, 119, 2/77
106. A. Rosencwaig, *Physics Today*, 23(9/75)
107. L. C. Aamodt, J. C. Murphy, and J. G. Parker, *J. Appl. Phys.*, 48, 927(1977)
108. T. G. Muir, C. R. Culbertson, and J. R. Clynch, *J. Acous. Soc. Am.*, 59, 735(1976)
109. J. F. McClelland and R. N. Kniseley, *Applied Optics*, 15(12), 2967(1976)
110. H. H. Theising and P. J. Caplan, *Spectroscopic Calculations for a Multielectron Ion*, Interscience Publishers, N. Y., 1966
111. P. M. Morse and K. U. Ingard, in *Encyclopedia of Physics* (S. Flugge, editor), Vol. X1/1, Springer-Verlag, Berlin, N. Y., 1961
112. L. C. Aamodt and J. C. Murphy, *J. Appl. Phys.*, 49(6), 3036(1978)
113. W. G. Jung, *IC Op-amp Cookbook*, H. W. Sams and Co., Inc., Indianapolis, Ind., 1974
114. J. Sherwin, in *National Semiconductor's Linear Applications Handbook 2*, N. S., Santa Clara, Calif., 1976

## BIOGRAPHICAL SKETCH

Edward G. Voigtman, Jr., was born on December 26, 1949, in St. Louis, Missouri. Family instabilities led to his attending nine schools before graduating from Parsippany High School in June 1968. In September 1968 he entered Rensselaer Polytechnic Institute with the intention of majoring in inorganic chemistry. In 1970, he realized that, in order to take up the slack, he would have to intensify his self-teaching efforts, and he also realized that specialization is usually a quick route to stultification. In June 1972, he graduated from R. P. I. with a B. S. degree in chemistry. In September 1972, not knowing any better, he accepted a Graduate School Fellowship to the University of Florida. He has been pursuing his studies at the University of Florida since then.

In June 1973, while visiting his friend Richard Lawrence in South Bend, Indiana, he met Janiece Lee Leach. They were married on May 31, 1975.

I certify that I have read this study and that in my opinion it conforms to acceptable standards of scholarly presentation and is fully adequate, in scope and quality, as a dissertation for the degree of Doctor of Philosophy.



---

M. T. Vala, Chairman  
Professor of Chemistry

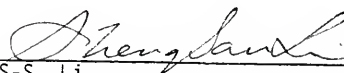
I certify that I have read this study and that in my opinion it conforms to acceptable standards of scholarly presentation and is fully adequate, in scope and quality, as a dissertation for the degree of Doctor of Philosophy.



---

E. D. Adams  
Professor of Physics

I certify that I have read this study and that in my opinion it conforms to acceptable standards of scholarly presentation and is fully adequate, in scope and quality, as a dissertation for the degree of Doctor of Philosophy.



---

S-S. Li  
Professor of Electrical Engineering

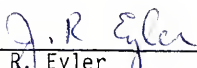
I certify that I have read this study and that in my opinion it conforms to acceptable standards of scholarly presentation and is fully adequate, in scope and quality, as a dissertation for the degree of Doctor of Philosophy.



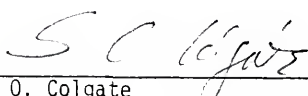
---

D. C. Wilson  
Associate Professor of Mathematics

I certify that I have read this study and that in my opinion it conforms to acceptable standards of scholarly presentation and is fully adequate, in scope and quality, as a dissertation for the degree of Doctor of Philosophy.

  
\_\_\_\_\_  
J. R. Eyler  
Assistant Professor of Chemistry

I certify that I have read this study and that in my opinion it conforms to acceptable standards of scholarly presentation and is fully adequate, in scope and quality, as a dissertation for the degree of Doctor of Philosophy.

  
\_\_\_\_\_  
S. O. Colgate  
Associate Professor of Chemistry

This dissertation was submitted to the Graduate Faculty of the Department of Chemistry in the College of Liberal Arts and Sciences and to the Graduate Council, and was accepted as partial fulfillment of the requirements for the degree of Doctor of Philosophy.

March 1979

\_\_\_\_\_  
Dean, Graduate School



UNIVERSITY OF FLORIDA



3 1262 08553 1084